Aus der Klinik und Poliklinik für Zahn-, Mund-

und Kieferkrankheiten der Universität Würzburg

Lehrstuhl für Funktionswerkstoffe für Medizin und Zahnmedizin

Direktor: Professor Dr. rer. nat. Jürgen Groll

Biomimetic calcium phosphate modification of 3D-printed tissue engineering scaffolds using reactive star-shaped macromers

Inaugural - Dissertation

zur Erlangung der Doktorwürde der

Medizinischen Fakultät

der

Julius-Maximilians-Universität Würzburg

vorgelegt von

Jean Nicolas Behets

aus Nörvenich, Deutschland

Würzburg, August 2017

Referent: Prof. Paul Dalton, Ph.D.

Koreferent: Prof. Dr. med. Torsten Blunk

Dekan: Prof. Dr. Matthias Frosch

Tag der mündlichen Prüfung:

12.11.2018

Der Promovend ist Zahnarzt.

I dedicate this thesis to my grandfather Stanislaus Gisa.

Ich widme diese Arbeit meinem Großvater Stanislaus Gisa.

Table of Contents:

IV

List of Abbreviations

2-AEP	2-Aminoethylphosphonic acid
$CaCl_2 \cdot 2H_2O$	Calcium chloride dihydrate
CaP	Calcium phosphate
E	Young's modulus
ECM	Extracellular matrix
g	Gram
G	Gauge
GBR	Guided Bone Regeneration
HA	Hydroxyapatite
HCl 25%	Hydrochloric acid
KCl	Potassium chloride
MEW	Melt electrospinning writing
mg	Milligram
$MgCl_2 \cdot 6H_2O$	Magnesium chloride hexahydrate
ml	Milliliter
MSCs	Mesenchymal stem cells
NaCl	Sodium chloride
$Na_2HPO_4 \cdot 2H_2O$	Di-sodium hydrogen phosphate dihydrate
$NaHCO_3$	Sodium hydrogen carbonate
NaOH	Sodium hydroxide
PBS	Phosphate buffered saline
PCL	Poly(ε-caprolactone), PURASORB PC 12
RT	Room temperature
S	sample
SBF 10x	Simulated body fluid 10x
sPEG, star PEG	Six-armed polyethylene glycol
TE	Tissue-engineering, tissue-engineered
water	Distilled and filtered water

1 Introduction

1.1 Etiology of bone defects and current treatment

The treatment of large bone defects remains a serious problem in the field of surgery [1, 2]. Bone damage is usually due to trauma, iatrogenic resection made necessary by a tumor or an infection, or skeletal abnormalities [3, 4]. The patient's quality of life is often compromised, and involves both acute and chronic pain, and a lowered mechanical function of the bone with the risk of fracturing [5, 6]. There are also aesthetic reasons for treating bone tissue [7].

The afore-mentioned issues often last over a long period of time, for example, when dealing with chronic osteomyelitis. In this case the bone initially becomes exposed to a source of infection [8, 9]. This is a common occurrence; for example after a simple tooth extraction surgery, and usually does not lead to a chronic infection as bone is very resistant against infection [10]. However, certain bacterial strains, most commonly *Staphylococcus aureus*, which is highly persistent, can cause osteomyelitis even with the patient's immune system being intact [11]. In this case, the body's inflammatory response, due to bacterial virulence factors, causes several cytokines to be released which promote local osteolysis [6]. Also, the risk of osteomyelitis increases as soon as the patient's local or systemic immune defense is compromised and, therefore, unable to fight bacterial invasion sufficiently [12]. The main causes for a lowered activity of the immune system are iatrogenic, such as radiation, bisphosphonate or immunosuppressive medication [13, 14]. Large bone defects are the consequences as the patient's bone will be destroyed consecutively and the risk of bone fractures increases [8]. Apart from bacterial infection being the crucial initiating factor for osteomyelitis, there are some cases where no clear etiology is found, referred to as primary chronic osteomyelitis [15]. Conservative treatment options show only very limited success. This often leads on to a last resort procedure, which is an extensive decortication and (sometimes even full) resection of the bone and a following reconstruction surgery using bone grafts [15, 16].

Malignant tumors often make bone grafting surgeries necessary as well, for the tumor constantly infiltrates the surrounding tissues. This makes a safety margin mandatory when resecting the infiltrated tissues [17] which could result in surgical removal of bone tissue with a resulting defect, even when the tumor is not a primary bone tumor.

Approximately 2.2 million bone grafting surgeries are performed annually [18]. Bone grafts fill out the defect and contribute to its healing [19]. They can be qualified as osteogenic, osteoinductive and/or osteoconductive. If a graft holds a certain amount of multipotent mesenchymal cells, it is termed osteogenic [20, 21]. Osteoinductivity is defined as the ability of a given material to differentiate mesenchymal cells into chondroblasts or osteoblasts by releasing certain growth factors [22, 23]. Osteoconductivity, on the other hand, is the ability of a graft to conduct ingrowth of new bone tissue into the transplant by providing a porous structure, acting as a scaffold for new bone formation [20, 24]. It is desirable to incorporate both of these properties within an implant, for example by mimicking trabecular bone's surface, which mainly consists of calcium phosphate (CaP). CaP is known to be osteoconductive, supports attachment, proliferation and migration of cells (osteoblasts/osteoclasts) onto the scaffold, especially when being present as hydroxyapatite (HA) [25-28].

Currently most reconstruction surgeries for bone defects are treated by using autologous bone grafts which are obtained from another region of the patient's skeleton [4] where bone tissue can be expended, for example iliac crest or fibula [15, 29]. Materials from other sources such as allogenic [30], xenogeneic [31, 32] or synthetic grafts [32, 33] are also frequently used especially for smaller defects. Decellularized tissue can serve as a scaffold as well [34]. Allogenic and xenogenic materials, however, have the inherent risk of an exacerbated immune response [35, 36] during which the transplant is rejected and attacked by the host's immune system. They have also been linked to a potentially higher risk of graft infection [37].

Apart from many obvious advantages of autologous bone grafts such as instantaneous elimination of the defect and an improved immune response, there

are still drawbacks. A second operating area has to be set, which increases the patient's risk for pathogen transfer and wound infection [38]. Also the amount of autologous graft material is limited to some degree as the donor site should not get overly compromised [34]. It is, therefore, desired to investigate new methods to improve current treatment of bone defects. The rapidly emerging field of tissue engineering combined with stem cell therapy is showing promising results [39] and may provide new ways on how to deal with bone traumata in the future.

1.2 Bone healing

An exceptional characteristic of bone tissue is its ability to repair without any formation of scar tissue [40]. Instead, new bony tissue is produced which undergoes steady remodeling processes until its original stability is achieved [41]. Therefore, it can be considered as a regeneration of tissue.

Bone fractures heal by either direct or indirect bone healing. Direct bone healing requires surgical fixation and stabilization to occur, and its biological pathways are then able to produce mature bone tissue including lamellar bone and the Harversian system [40]. Afterwards cutting cones from nearby osteons emerge to start further remodeling processes [42].

Indirect bone healing is more common in nature and does not require surgical intervention and rigid conditions. However, too much movement or load can result in delayed or non-union of the fragments. The initial hematoma coagulates due to an early inflammatory response to form granulation tissue which acts as a base of early endochondral formation and the generation of a soft callus [43]. Meanwhile, a central hard callus forms between the fracture sites by intramembranous ossification. This provides a semi-stable condition [44]. Precondition is the migration of mesenchymal stem cells (MSCs) to the fracture site [40]. After angiogenesis and vascularization, the cartilaginous callus mineralizes and gets partially resorbed to restore the original anatomic structure. Subsequent remodeling processes further increase the bones mechanical properties. Similar processes occur for the healing of a bony defect. Premise for this to happen is an exclusion of epithelial and connective tissue from the defect, which is one of the main principles of Guided Bone Regeneration (GBR) [45].

1.3 Guided Bone Regeneration

Dental implants represent a high-quality treatment option to replace missing teeth that is frequently performed in dental practice. It requires sufficient amounts of bone tissue, horizontally and vertically, to ensure successful implantation. If this requirement is not met, augmentation techniques become mandatory. GBR describes one of these techniques.

GBR is a surgical augmentation procedure that uses membranes as a barrier between defect and surrounding connective tissue. Optionally, a deposit of grafting material can be put into the defect before it is covered by the membrane and the wound is closed. This physical hindrance prevents the connective tissue from impending osseous regeneration. At the same time, it creates space long enough for pluripotent and osteogenic cells from surrounding tissues as well as from the circulating blood flow to enhance osseous regeneration [46-48]. GBR is often used after tooth extraction to prevent loss of alveolar bone due to resorption [49]. It has been described that four parameters need to be fulfilled to guarantee successful GBR: lack of connective tissue in the defect, a stable fibrin coagulum, space preservation by the membrane and primary wound treatment [45]. After surgery, the coagulum releases growth factors that attract macrophages and neutrophils which lead to its resorption. It gets replaced by highly vascularized granulation tissue. MSCs and osteogenic cells migrate to the defect, differentiate to become osteoblasts and start to produce osteoid. This bone matrix then gets mineralized to act as a template for the generation of lamellar bone [50, 51]. Further remodeling steps result in the formation of mature bone tissue composed of both compact and trabecular bone. The healing phase after a GBR surgery accounts for 3 – 4 months [47].

Researchers working within the field of tissue engineering are currently investigating ways to further improve GBR such as cell modulating factors [52] as well as the optimization of the scaffolds' mechanical and morphological properties [53, 54] and the use of CaP coatings to improve cellular response [55].

1.4 Tissue engineering

1.4.1 History

Although already known before, the term "tissue engineering" (TE) was first officially used for a meeting in 1987 [56, 57]. Over the following three decades the field of TE has steadily grown in popularity mostly due to the development of various methods to produce biocompatible scaffolds and due to the massive developments in additive manufacturing and nanotechnology [58].

1.4.2 Background

TE can be seen as an umbrella term for the artificial manufacturing of biological tissue through directed cultivation of cells to replace or regenerate diseased tissue in a patient. It uses a combination of matrices/scaffolds, cells, and certain biochemical and physicochemical factors to overcome long-known limitations of current treatment options, mainly autologous or allogenic grafts [59]. Biomedical materials are therefore of importance to provide an advanced treatment option for patients in the future.

The concept of a scaffold represents one of the key elements in TE [60]. The scaffold acts as a cell carrier, provides mechanical stability as well as a large surface area for cell attachment, reserves the possibility of surface functionalization and conducts cell arrangement and ingrowth [61, 62]. Furthermore, its design influences the biological interactions with cells significantly [59]. Optionally, scaffolds can be seeded with cells *in vitro* before implantation. Apart from geometry and shape of the scaffold [63, 64], seeded cells can be influenced in terms of differentiation, proliferation and cell attachment by incubating them with certain media and growth factors [65, 66]. Recent results in the field of TE are very promising. For instance, decellularization of a rat's limb to produce a complex extracellular matrix (ECM) scaffold followed by recellularization with different multipotent cell lines has been performed and shows that full organ synthesis could be a viable concept in the future [67]. Another example is the introduction of human induced pluripotent stem cells [68] to the field, which nowadays can be reproducibly derived from various tissues with no ethical dilemma as for embryotic stem cells [69-71]. Increased bone

formation of seeded cells due to osteogenic culture conditions has been shown *in vitro* and *in vivo* compared to non-osteogenic conditions [65]. More related to topics of this thesis, TE scaffolds are frequently used to cover up periodontal defects and enhance bone tissue regeneration, mainly by preventing other tissues from infiltrating [72] also referred to as GBR above.

All in all, it can be summarized that the field of TE already provides attractive alternative options to treat some sorts of tissue defects today and it will be exciting to see what future accomplishments will achieve.

1.5 Electrospinning

1.5.1 Principles of electrospinning

Electrospinning is a procedure to manufacture continuous ultrafine filaments from liquids in the micro- and nano-scale range [73]. There are two main techniques for producing fibers by electrospinning: solution electrospinning and melt electrospinning. An essential element of electrospinning is the application of a high voltage between a spinneret that is ejecting polymer solution/melt and the collector, thus creating an electrical potential. The polymer solution/melt is constantly being delivered to the spinneret, via some output of force (e.g. air pressure, plunger). It is necessary to electrostatically force the surface tension of the molten polymer droplet at the spinneret tip to become unstable and, therefore, produce a thin continuous and electrified jet. Once ejection of the liquid occurs from the spinneret, it is exposed to the electrical field and two main forces start competing with each other: the surface tension of the droplet versus the repulsion of Coulomb forces [74]. Additionally, the electrical force applied causes the liquid polymer to be drawn to the collecting zone. As soon as repulsion forces start to exceed the surface tension of the droplet, the formation of a cone, termed Taylor cone, is observed [75]. When the applied voltage is further increased, at a certain point it reaches critical value which allows an electrically charged jet to be formed from the Taylor cone and be drawn towards the charged collecting surface, thus creating a fine filament [76, 77].

1.5.2 Melt electrospinning

Compared to solution electrospinning, the devices required for melt electrospinning are more complex. A continuous and controllable heating system as well as a method to deliver the molten polymer, which is more viscous than a polymer solution, to the spinneret tip needs to be integrated into the machine.

Different heating mechanisms have been investigated [78] using electricity [79], air [80] or circulating fluids [81, 82]. Furthermore, laser heating systems have been used to melt electrospin from a solid polymer rod and therefore function without a spinneret as well [83, 84].

Most melt electrospinning devices make use of a spinneret with circular diameter that is flat-tipped [85]. The purpose of the spinneret is to constantly deliver polymer melt to the tip and to ensure a relatively constant fiber diameter. However, other types of spinnerets can be found in literature, for example having a triangular or cruciform shape [86].

Since voltage is applied between the spinneret tip and the collector, they should be made of conductive material. Commonly used materials are copper [87, 88], aluminum [80] or brass [82]. The collector can have different shapes such as a simple plain surface, rotating cylinders [89], spheres [90], discs [91] or spirals [92] of various diameters depending on what the purposes of the electrospun fibers are.

1.6 Biomedical materials

1.6.1 Poly(ε-caprolactone)

Poly(ε-caprolactone) (PCL) (structure and corresponding monomer is shown in Figure 1) is a polyester that has been extensively studied in regards to the fields of tissue engineering and drug delivery in recent years [93-98]. It was found to contain very attractive mechanical and chemical properties for the usage as a biomaterial [96, 97, 99].

For example, clinical trials have already demonstrated its good biocompatibility [100, 101]. PCL is flexible [102], which is important for surgical handling and also biodegradable [103, 104]. However, it degrades slower than

most biopolymers [103, 105], which is due to its crystallinity and its higher hydrophobicity caused by five methylene groups in each repeating unit. There are two mechanisms involved in the biodegradation of PCL: non-enzymatic cleavage, which is catalyzed by carbonyl end groups and accounts for most of the early PCL degradation; and enzymatic fragmentation, which requires small fragments to diffuse into the media [96, 106-108]. To enhance its mechanical and chemical properties or to decrease its long degradation time, it has been modified with other polymers or inorganic molecules in the past, such as starch [99], polyethylene glycol [109, 110], chitosan [111] polyvinyl alcohol [112] or aluminum oxide [113]. CaP coated PCL fiber meshes have shown promising blood vessel ingrowth and bone formation *in vivo* [55]. For melt electrospinning, PCL has a suitable, low, melting temperature of 55-65°C [102]. Therefore, it is a very good candidate to produce scaffolds using MEW for potential application in bone healing, since thermal degradation of the polymer is minimized. This assists the ultimate goal of translating the manufacturing process for clinical devices.
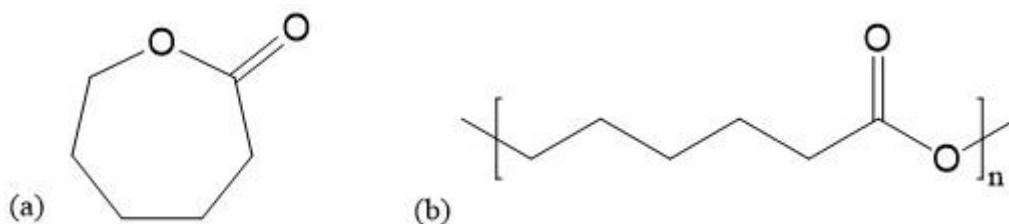

Figure 1: Structural formula of (a) the monomer ε-Caprolactone and (b) poly- ε-Caprolactone (PCL)

Other polymers have also been successfully used to produce fibers via melt electrospinning, for example, polylactic acid [114, 115], polyethylene [116], poly(ethylene-co-vinyl alcohol) [117], or poly(methyl methacrylate) [118].

1.6.2 Star-shaped poly(ethylene glycol) (sPEG)

One challenge with synthetic implants is that they are rapidly coated with biomolecules when they get in contact with bodily fluids, mainly proteins, by the process of adsorption. This leads to a loss of control on how the biomaterial interacts with its new environment, since these proteins can denature and affect wound healing via activation of the immune defense [119].

Polyethylene glycol (PEG) is a synthetic polymer that has shown good results for achieving non-adsorptive surfaces on biomaterials via coatings and is approved by the United States Food and Drug Administration (FDA) for application in humans [120]. Furthermore, star-shaped molecules, whose arms are based on PEG (80% PEG, 20% propylene oxide), provide a higher PEG density on the surface, thus minimizing protein adsorption even more [121, 122]. Also, the size of the star-polymer affects grafting density. Smaller star-polymers seem to be able to pack more closely together and therefore cover the surface more densely and even prevent diffusion of small proteins through the layer [119, 121, 123].

Crosslinking between isocyanate groups via urea bridges occurs after dissolving sPEG in water and takes at least 12 hours to complete. This means that the final sPEG film is a covalently bound 3D-network [119]. For that reason, sPEG has to be utilized as soon as it has dissolved in water.

1.6.3 2-Aminoethylphosphonic acid (2-AEP)
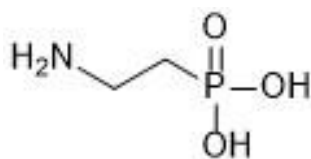
Figure 2: Structural formula of 2-AEP

2-Aminoethylphosphonic acid (2-AEP, synonyms in literature: AEP, ciliatine; structure shown in Figure 2) is a natural occurring phosphonate. During the 1960s and 70s numerous publications showed its relatively high concentrations in human and animal tissues [124-130]. Another study suggested that 2-AEP does not occur as a free molecule as it was only found bound to lipids or proteins [131]. However, little to nothing is known about the actual function of 2-AEP in the body. For medical purposes, phosphonates are mainly used to inhibit enzymes that have an active site for phosphate groups, as they compete with the phosphates [132].

1.7 Calcium phosphate coating

Multiple investigations [133-138] have attempted to optimize the ability of

biomaterials to orchestrate bone regeneration for the use in bone defects by coating them with CaP layer, more precise, a HA layer, hence imitating the surface of the trabecular bone structure. It is generally accepted [139] that the HA percentage of any CaP coating should be as high as possible (>95%) [140]. It has also been stated that HA has a calcium to phosphate ratio of 1.67 [140].

Broadly, two groups of techniques can be distinguished for depositing a CaP layer onto a biomaterial: physical deposition techniques; and wet-chemical techniques [139]. A wet-chemical technique using supersaturated simulated body fluid (SBF 10x) was performed for this thesis. This biomimetic process requires a pretreatment to increase the surface roughness of the base material, which has been reported to have great beneficial effect on bone apposition [141]. Afterwards the sample is immersed in SBF 10x to produce a homogenous coating, typically composed of low-crystalline apatite [142]. The protocol was initially described by Kokubo [143] and further developed by Yang [144]. Vaquette *et al.* adapted this protocol to coat PCL scaffolds more homogenously [145].

One feature of this coating process is the possibility to incorporate proteins [146-148], DNA [149], vitamins [148] and pharmaceuticals, for example hormones [150], antibiotics [151] or bisphosphonates [152] within the CaP layer.

Other biomaterials have also been coated successfully using SBF 10x [150, 153, 154]. CaP coatings provide osteoconductive properties and were found to enhance bone cell attachment and also increase their proliferation and ECM production compared to non-coated samples *in vitro* [26-28], *in vivo* [136, 155, 156] and in clinical trials [157, 158]. A theory of its osteoconductive process was described by Rahbek *et al.* (represented by Figure 3). It hypothesizes the partial dissolution of the CaP layer due to lowered local pH followed by reprecipitation with embedment of proteins. Calcium and phosphate ion concentrations increase and induce chemotaxis of osteoblasts [159].

Alkaline phosphatase, which is the main marker characteristic of osteoblasts and indicates their early differentiation stages [139], has shown increased activity in CaP-based films and coatings, among increased osteocalcin levels [160-162]. Osteocalcin is produced by osteoblasts and comprises a binding
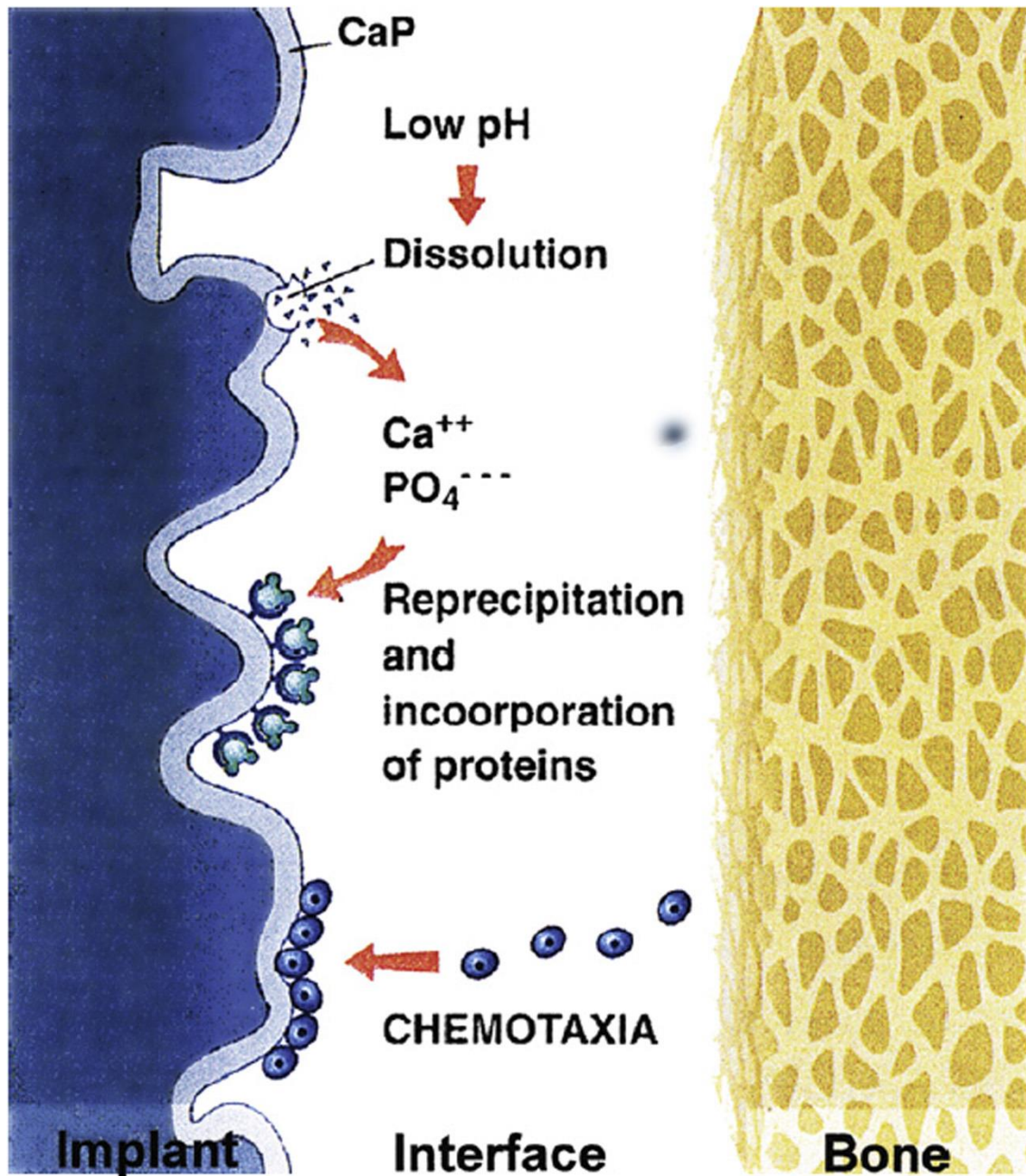
Figure 3: Schematic depiction of Rahbek et al.'s hypothesis of how CaP-coatings induce osteoconduction. CaP gets partially dissolved due to low local pH and incorporate proteins during reprecipitation which induce migration of osteoblasts by chemotaxis. Reprinted from [139] with permission from Elsevier

site for calcium ions to further accumulate local quantities [163].

A study on rabbits showed that HA coatings accelerate osseointegration and enhance tissue quality around the implant [164]. Others report that early bone fixation was significantly improved by HA coatings [137, 165, 166]. CaP coatings have also shown enhancement in bone-implant contact and integration [158].

Furthermore, an accelerated post-operative period due to CaP coatings has been reported [157]. In contrast, there are recent studies that show no significant advantage of HA-coated implants to non-coated ones or even slight negative results [167-170]. Therefore, the beneficial utility of CaP coatings is not definitely proven yet. There rather seem to be multiple factors that positively affect bone ingrowth and healing of an implant, such as surface roughness [141], surface topography and charge of the coating [171-173], its solubility [24] and crystallinity [174, 175]. All these factors affect the adsorption of body proteins in terms of conformation, alignment and quantity [173, 176, 177], which is considered a key element in early osseointegration and occurs within a few minutes after implantation [176, 178, 179]. Further investigations are needed to determine the optimal parameters for each attribute of the coating and a standardized procedure must be developed.

Literature has also described a problem, namely the risk of delamination of the calcium phosphate layer when the scaffold is mechanically stressed [180-182], which may often happen during an implantation surgery. Even though described as an issue, it was not resolved yet. It is understandable that the relevance of this problem intensifies when the construct to be coated is desired to have flexible properties, for example a membrane to cover up osseous defects. This phenomenon is likely due to two reasons: first, the absence of a chemical bond between the carrier and CaP; and second, their large difference in Young's modulus (E). It is comprehensible that little can be done about the variation in E without altering the mechanical properties of the scaffold. Hence, a reproducible method to establish a chemical linkage is a way to enhance the persistence of CaP coatings on flexible carriers.

1.8 Aim of this study

The aim of this thesis is to improve resistance of current CaP coatings to mechanical stress. The research focuses on the possibility of a chemical linkage between PCL and CaP using both sPEG and 2-AEP. A sPEG coating will be applied on the previously etched PCL scaffolds. Apart from prevention of protein adsorption, sPEG fulfills a second very important function. It is the first molecule

in a hypothesized chemical chain linkage between previously functionalized PCL and CaP, as it should react with the carboxylic acid group on the one hand as well as with the amine group from 2-AEP on the other. Furthermore, 2-AEP was chosen for its chemical composition: a molecule was needed that binds to isocyanate groups from sPEG on the one side, and binds to calcium ions from the CaP-layer on the other as well. Also, 2-AEP is a small molecule with a simple structure and its natural occurrence suggests biocompatibility. Hypothetically, the coating will be able to be torn by overstraining of the scaffold, however, it should not be able to flake off due to the covalent linkage. The coating procedure should be economically reasonable and time efficient. It must be reproducible and should provide a homogenous coating among the entire scaffold.

2 Materials and Methods

2.1 Materials

2.1.1 Chemicals

Chemical:	Company:
$NaHCO_3$	Merck KGaA; Darmstadt, Germany
$Na_2HPO_4 \cdot 2H_2O$	Merck KGaA; Darmstadt, Germany
NaCl	Carl Roth GmbH+Co.KG; Karlsruhe, Germany
$MgCl_2 \cdot 6H_2O$	Carl Roth GmbH+Co.KG; Karlsruhe, Germany
KCl	Carl Roth GmbH+Co.KG; Karlsruhe, Germany
$CaCl_2 \cdot 2H_2O$	SIGMA-ALDRICH CHEMIE GmbH; Steinheim, Germany
NaOH	Merck KGaA; Darmstadt, Germany
PBS	Thermo Fisher Scientific; Waltham, Massachusetts, USA
2-AEP	SIGMA-ALDRICH CHEMIE GmbH; Steinheim, Germany
sPEG	DWI – Leibniz Institut für Interaktive Materialien e.V.; Aachen, Germany
PCL	Corbion Inc.; Gorinchem, Netherlands PURASORB PC 12, Lot# 1412000249, 03/2015,
HCl 25%, diluted from 37%	Merck KGaA; Darmstadt, Germany

2.1.2 Consumables

Detailed name of consumable:	Company:	Will be referred to as:/ Will be used as:
Urine beaker with screw top REF: 06.065.4103	MedChrom GmbH; Flörsheim-Dalsheim, Germany	Specimen cups
Pasteur pipettes	A.Hartenstein GmbH; Würzburg, Germany	Plastic pipettes
CELLSTAR serological pipette 10 ml/25 ml	Greiner bio-one; Kremsmünster, Austria	Pipettes

BD Discardit™ II (20 ml)	Becton Dickinson; Fraga, Huesca, Spain	20 ml syringe
rolled-edge glass 15 ml	A.Hartenstein GmbH; Würzburg, Germany	Snap cap vial
Supra single-use cannula with lancet cut	Vivomed GmbH; Geißlingen, Germany	sPEG weighing tool
Nunclon™ Delta Surface	Thermo Fischer; Roskilde, Denmark	Petri dishes, well plates
PELCO® 10 Hitachi SEM Mount Storage Holder and Box	Ted Pella, Inc.	Specimen storage holder boxes
12.7 mm Sample Stub w/ 3.2 mm pin	Ted Pella, Inc.	Specimen pin stub

2.1.3 Devices

Device:	Company:	Will be referred to as:/ Will be used as:
CB340	Zeiss	SEM
CB340 (attachment)	Oxford Instruments	EDX
Accu-jet	Brand; Wertheim, Germany	Measurements between 1 ml and 25 ml
arium pro	Sartorius; Goettingen, Germany	Producing Mili-Q water
Vortex-Genie 2	Scientific Industries; New York, U.S.A.	Vortex
MR 3001	Heidolph; Schwabach, Germany	Stiring device for SBF 10x and PBS 10x
Sonorex, Typ: RK 103 H	BANDELIN; Berlin, Germany	Sonication
Mini Rocker MR-1	BioSan; Riga, Latvia	Shaking device, rocking device

Water bath type 1083	GFL; Burgwedel, Germany	Water bath; incubated at 37 °C
inoLab pH Level 1	WTW; Weilheim, Germany	pH measurements
Premium BioFresh NoFrost	Liebherr; Bulle, Switzerland	Stored at 4 °C
N 022 AN.18	KNF Neuberger; Freiburg, Germany	Vacuum
KB 500-2	Kern & Sohn GmbH; Ballingen, Germany	Weighing system
ABT 320-4M	Kern & Sohn GmbH; Ballingen, Germany	Electronic balance for weighing sPEG
ABT 100-5M	Kern & Sohn GmbH; Ballingen, Germany	Electronic balance for weighing 2-AEP
GS Glovebox Dimension	GS GLOVEBOX Systemtechnik GmbH; Malsch, Germany	Glovebox
EM ACE 600	Leica	Sputter coating device

2.2 Methods

2.2.1 Scaffold fabrication

PCL scaffolds were 3D-printed and provided by Mr Almoatazbellah Youssef. 0.5 – 1 ml of PCL was placed in a disposable plastic syringe and heated up to 85 °C using an electric heating system in a custom-built melt electrospinning writing printer [183]. A 22 G needle (length: 12.5 mm; 0.5 mm protrusion out of high voltage electrode) was used throughout the printing process. After heating the polymer for 30 minutes, printing was done with the following settings:

Pressure: 1.2 bar (digitally controlled air pressure system)

Syringe temperature: 85 °C

Nozzle temperature: 85 °C

Distance from nozzle to collector: 4 mm

Voltage: -1.5 kV for the collector and 4.5 kV for the nozzle

Fiber spacing: 250 µm

Number of layers: 5 layers of 0°/90° fiber orientation

Polymer was used for up to 5 days in the printer.

2.2.2 Group 1: CaP coating for non sPEG coated scaffolds

Fundamentals

The following experiments will be summarized as subgroups of group 1. CaP coating was performed following a protocol from Vaquette *et al.* [145] and modified by Almoatazbellah Youssef. At all times scaffolds were handled carefully with forceps only, holding them from the margin by the turn loops. When adding a liquid to the scaffolds, the containers were slightly tilted to allow liquids to run down the wall, hence not causing unnecessary mechanical stress. All glassware was rinsed with water before usage. After an experiment finished, samples were dried overnight and then stored in plastic petri dishes. Scaffolds treated with sPEG were stored on glass slides.

Preparation

Milli-Q water, from herein referred to as "water", is used for the washing steps and preparation of solutions. First, 1 liter of simulated body fluid 10x (SBF 10x) was prepared by putting 58.430 g of NaCl, 0.373 g of KCl, 3.675 g of $CaCl_2 \cdot 2H_2O$ and 1.016 g of $MgCl_2 \cdot 6H_2O$ under stirring in approximately 600 ml of water until fully dissolved (solution 1). Separately 1.420 g of Na_2HPO_4 was dissolved in approximately 30 ml of water (solution 2). Solution 2 was then added to solution 1 dropwise always making sure the pH did not exceed a value of 4 by adding a few drops of 20% HCl solution as otherwise precipitates would have formed. Afterwards, the beaker was rinsed with 10 ml of water which were then also added to solution 1 dropwise.

Box 1

Group 1: CaP coating procedure

- Remove entrapped air from scaffolds

- Incubate scaffolds in 2 M NaOH*

- Washing 5 x 5 minutes

- Use $NaHCO_3$ to set SBF 10x to pH 6 and filter it into a fresh specimen cup

- Incubate scaffolds for 30 minutes at 37 °C

- Repeat the two above steps twice**

- Perform a 5-minute vacuum treatment prior to the first SBF 10x incubation

- Incubation in 0.5 M NaOH for 30 minutes at 37 °C

- Washing 5 x 5 minutes

- Dry overnight in vacuum desiccator

* 1a: 90 minutes at 37 °C, 1b: 90 minutes at room temperature, 1c: 45 minutes at 37 °C, 1d: 45 minutes at room temperature.

** This refers to 1g. 1e: no repetitions, 1f: one repetition.

Finally, water was added to give a total volume of 1 liter and the pH value was verified to be around 4. When not in use the SBF 10x solution was kept at 4°C and was used within 2-3 weeks. Also, 0.5 M and a 2 M NaOH solutions were prepared by dissolving 1 g and 4 g of NaOH in 50 ml of water in a specimen cup, respectively.

Prewetting and etching of PCL scaffolds

MEW scaffolds were put into a 12-well plate and 2 ml of water were added to each well. Using a syringe, the water was extracted and afterwards poured onto the scaffolds again until entrapped air was completely removed. The 2 M NaOH solution was then preheated to 37 °C in a water bath for a couple of minutes. Afterwards the samples were put in 25 ml of 2 M NaOH solution for 90 minutes at 37 °C (group 1a). After 90 minutes, NaOH solution was extracted and a washing procedure was performed five times (25 ml of water each time) for five minutes (5 x 5 min) each on the scaffolds using a shaking device for mild continuous stirring. Specimen cups were not changed for this procedure. The experiment was repeated using different parameters for the etching procedure: 90 minutes at room temperature (group 1b), 45 minutes at 37 °C (group 1c) and 45 minutes at room temperature (group 1d).

Incubation with SBF 10x

In the meantime, 50 ml of SBF 10x solution were given into a clean beaker which was previously rinsed with SBF 10x as well. Tiny amounts of $NaHCO_3$ were added to increase the pH to 6 (Note: the reaction triggered takes a few minutes to complete). Using a 0.22 μm filter and a syringe the solution was then filtered into a fresh specimen cup. Scaffolds were put in the pH-modified SBF 10x solution, placed in vacuum for 5 minutes and incubated at 37°C for 30 minutes. The steps in this paragraph were repeated twice but without placement in vacuum (group 1g). Also, the experiment was repeated incubating the samples only once (group 1e) or twice (group 1f) in SBF 10x. For group1 e-g etching parameters were set to 90 minutes and 37 °C.

Post-treatment

After the third incubation with SBF 10x, the scaffolds were post treated in 0.5 M NaOH solution for 30 minutes at 37°C then washed with water for 5 x 5 minutes using a shaking device for consistent movement of the liquid. Afterwards the pH was verified to be around the same as for water. Finally, the scaffolds were moved into a glass petri dish and were left to dry overnight in a vacuum desiccator with silica.

2.2.3 Group 2: SPEG coating

Fundamentals

This approach was originally based on a sPEG-coating protocol originally developed by Ms Sarah Bertlein, also from the Department of Functional Materials in Medicine and Dentistry, as part of her doctoral thesis. It will be referred to as group 2 of this thesis. In general, liquids were added to wells using a 10 ml pipette and removed from wells using a 20 ml syringe with a 19 G needle. The molecule used in this thesis consists of a sorbitol core on which six arms of a copolymer of ethylene glycol and propylene glycol in a 4:1 ratio were attached to (2 kDa/arm). Terminal ends of the arms were functionalized using isophorone diisocyanate to give terminal isocyanate groups [184]. This star-molecule will be referred to as Star-PEG or sPEG in this thesis. SPEG was stored at and obtained from a glovebox under argon atmosphere. Transportation out of the glovebox occurred via a closed snap cap vial. sPEG was then used within 30 minutes. The entire experiment was performed at room temperature (RT).

Preparation, prewetting and etching

The 1 M NaOH solution was prepared by dissolving 1 g of NaOH in 25 ml of water. PCL scaffolds were put in a 12-well plate with 2 ml of water per scaffold for 5 minutes. It was ensured that scaffolds did not contain any trapped air bubbles before water was removed. NaOH solution was added to each scaffold (2 ml per scaffold) and left on a shaking device for 5 minutes. Meanwhile, instruments necessary for obtaining sPEG were put in vacuum airlock of the

---

Box 2

Group 2: sPEG coating procedure

- Remove entrapped air from scaffolds

- In a 12-well plate incubate in 1 M NaOH for 5 minutes

- Washing 5 x 5 minutes

- Produce 2% sPEG solution by alternately vortexing and sonicating sPEG and
water for 5 minutes

- Incubate scaffolds in sPEG solution for 10 minutes

- Washing 3 x 5 minutes

- Dry overnight on glass slide

---

glovebox. NaOH solution was removed and the scaffolds were washed 5 times for 5 minutes (5 x 5 minutes) each also using a shaking device. sPEG was then obtained from the glovebox.

SPEG coating

Water from the last washing step was removed. sPEG was then dissolved for 5 minutes with the help of a vortex device and sonication to produce a 2% sPEG solution (e.g. 200 mg sPEG in 10 ml water). Each scaffold was incubated in 1 ml of sPEG solution for 10 minutes. When no further coatings were planned for the samples, they were washed for 3 x 5 minutes and left to dry overnight. Otherwise, a 2 x 30 seconds washing step was performed and the experiment immediately proceeded to the next planned step.

2.2.4 Group 3: Incubation of sPEG coated scaffolds in solutions of different 2-AEP concentrations

Four subgroups were investigated, each group contained three scaffolds. 2-AEP was weighed to give 0.1% (4 mg, group 3 (0.1%)), 1% (40 mg, group 3 (1%)), 5% (200 mg, group 3 (5%)), and 10% (400 mg, group 3 (10%)) solutions

with 4 ml of water. All scaffolds were pretreated and incubated with sPEG according to 2.2.3 with exception to the last washing step which was left out. Instead, after 10 minutes of sPEG incubation a quick washing procedure was performed (2 x 30 s). 1 ml of 2-AEP solution was then added to each scaffold respective to its subgroup and left for 30 minutes on a shaking device. Afterwards the scaffolds were moved in specimen cups (one per group) and incubated in pH-altered SBF 10x according to 2.2.2 (section: Incubation with SBF 10x). Finally, each group was post-treated with 0.5 M NaOH and washed as described in 2.2.2 (section: Post-treatment). This experiment was repeated using two different batches of sPEG. These will be labeled as group 3a (batch #5) and group 3b (batch #6).

Box 3

Group 3: Incubation in different concentrations of 2-AEP

- Treat scaffolds according to **Box 2** (page 23) except final washing and drying step
- Extract sPEG solution
- Quick washing 2 x 30 s
- Incubate scaffold in 1 ml of 0.1% (group 3 (0.1%)), 1% (group 3 (1%)), 5% (group3 (5%)) or 10% (group 3 (10%)) 2-AEP solution for 30 minutes
- Use $NaHCO_3$ to set SBF 10x to pH 6 and filter it into a fresh specimen cup
- Incubate scaffolds for 30 minutes at 37 °C
- Repeat the two above steps twice; perform 5-minute vacuum treatment prior to the first SBF 10x incubation
- Incubation in 0.5 M NaOH for 30 minutes at 37 °C
- Washing 5 x 5 minutes
- Dry overnight on glass slide in a vacuum desiccator

2.2.5 Group 4: Simultaneous incubation of sPEG/ 2-AEP followed by SBF 10x

Group 4a: PBS/water set to pH 8.1 before addition of AEPA

SBF 10x solution, was prepared as in 2.2.2 (section: Preparation). PCL scaffolds were treated as in 2.2.3 (sections: Fundamentals; Preparation, prewetting and etching). sPEG and 2-AEP were obtained in separate snap cap vials in different molar ratios: either 1:1 (i), 1:2 (ii), 1:3 (iii), 1:4 (iv) or 1:6 (v). A 0.2 M and 0.05 M NaOH solution were prepared by adding 0.4 g and 0.1 g of NaOH to 50 ml of water, respectively. Few drops of these solutions were added to 5 ml of PBS to increase its pH to 8.1. Additionally, a 1 M and a 0.5 M NaOH solution were prepared. Four groups were set up for this experiment, which differ in their sPEG to 2-AEP ratio and, also whether phosphate buffered saline (PBS) or water was used as a solvent. For example: 1:1 ratio in PBS with SBF 10x treatment, 1:1 ratio in PBS without SBF 10x treatment, 1:1 ratio in water with SBF 10x treatment, 1:1 ratio in water without SBF 10x treatment. If not labeled otherwise, commercially available PBS (Dulbecco's phosphate buffered saline) was used for the following experiments and will be referred to as PBS. Each group contained two scaffolds. For four scaffolds (e.g. 2 scaffolds for 1:1 ratio in PBS with SBF 10x treatment, and two scaffolds for 1:1 ratio in PBS without SBF 10x treatment), 5 ml of water or 5 ml of PBS (pH 8.1) were added to the snap cap vial containing 2-AEP and briefly mixed until 2-AEP dissolved completely. The pH value of the PBS solution was measured. The resulting solution was then added to the snap cap vial containing sPEG and dissolved for 5 minutes. A mixing cycle of 30 seconds vortex, 60 seconds sonication, 30 seconds vortex, 60 seconds sonication, 30 seconds vortex was performed within the dissolving time. Then each scaffold was incubated in 1 ml of the resulting mixture for 10 minutes using a shaking device. Scaffolds were then quickly washed twice for 30 seconds (2 ml water/scaffold). Scaffolds were carefully moved into a specimen cup and incubated in pH-modified SBF 10x three times and post-treated as in 2.2.2 (sections: Incubation with SBF 10x; Post-treatment). Samples from these experiments will be referred to as subsections of Group 4a (e.g. group 4a (1:1, PBS)).

Box 4

Group 4a: PBS/water set to pH 8.1 before addition of 2-AEP

- Remove entrapped air from scaffolds

- In a 12 well plate incubate scaffolds in 1 M NaOH for 5 minutes

- Washing 5 x 5 minutes

- Use 0.2 M and 0.05 M NaOH to set PBS to pH 8.1

- Add PBS (pH 8.1) to 2-AEP and mix briefly

- Dissolve sPEG in resulting 2-AEP solution using vortex and sonication

- Incubate scaffolds in sPEG – 2-AEP mixture for 10 minutes

- Quick washing (2 x 30 s)

- In a specimen cup incubate scaffolds in pH-altered and filtered SBF 10x for 30 minutes at 37 °C

- Repeat SBF 10x incubation twice; perform 5-minute vacuum treatment prior to the first one

- Treat with 0.5 M NaOH for 30 minutes at 37 °C

- Washing 5 x 5 minutes

- Dry overnight on glass slide in a vacuum desiccator

Group 4b: Different pH values of 2-AEP solutions

Three groups were set up, each containing three scaffolds. Pretreatment according to 2.2.3 (sections: Fundamentals; Preparation, prewetting and etching) was performed. sPEG and 2-AEP were weighed and stored in separate snap cap vials in molar ratios of 1:2. 5 ml of PBS were added in each 2-AEP-containing snap cap vial. One by one the 2-AEP solutions were then set to a certain pH (pH 7 for group 1, pH 7.5 for group 2, pH 8.1 for group 3) using a few drops of 0.2 M and 0.05 M NaOH. 3 ml of each solution was then added to 60 mg of sPEG. The experiment was then proceeded as in 2.2.3 (section: sPEG coating) and 2.2.2 (sections: Incubation with SBF 10x; Post-treatment). These samples were labeled as group 4b.

Box 5

Group 4b: Different pH values of 2-AEP solution

- Treat scaffolds as in **Box 4** (page 26) with exceptions:

    - add PBS to 2-AEP first and then adjust to pH 7 (4b(i)), pH 7.5
     (4b(ii)), pH 8.1 (4b(iii)) using 0.2 M and 0.05 M NaOH

Group 4c: Reduced dissolving and incubation time

An experiment was set up following the protocol from group 4a with two alterations: First the dissolving time of sPEG was reduced from 5 minutes to 2.5 minutes, second the incubation time of scaffolds in sPEG was reduced from 10 minutes to 3 minutes. This experiment was performed for a molar sPEG to 2-AEP ratio of 1:2 with three scaffolds and will be referred to as group 4c.

Box 6

Group 4c: Reduced dissolving and incubation time of sPEG

- Treat scaffolds as in **Box 4** (page 26) with exceptions:

    - reduce dissolving time of sPEG from 5 minutes to 2.5 minutes

    - reduce incubation time of sPEG from 10 minutes to 3 minutes

Group 4d: Samples left in water for 60 minutes after sPEG incubation

The approach of this experiment is leaning on the one of group 4c. The dissolving time of sPEG accounted for 2.5 minutes, incubation time was set to 10 minutes. After incubation of PCL-scaffolds in sPEG and the following 2 x 30 seconds washing procedure, the sample were again put in 2 ml of water per well and left for 60 minutes on a shaking device before the experiment was proceeded as in group 4c. sPEG and 2-AEP were weighed to give a molar ratio of 1:2. This experiment will be referred to as group 4d.

Box 7

Group 4d: 60-minute incubation in water after sPEG incubation

- Treat scaffolds as in **Box 4** (page 26) with exceptions:

    - reduce dissolving time from 5 minutes to 2.5 minutes

    - after the quick washing step, leave samples in water for 60 minutes

---

Group 4e: Effect of 0.5x PBS on CaP coating

This experiment is following instructions from group 4c and shall be named group 4e. sPEG was dissolved in 2-AEP solution for 2.5 minutes. sPEG and 2-AEP were weighed to give a molar ratio of 1:2. Three scaffolds were set up in this group. PBS was diluted to give 0.5x concentrated PBS, which was used to dissolve to 2-AEP and sPEG instead of 1x PBS.

Box 8

Group 4e&f: Effect of PBS 0.5x and self-made PBS

- Treat scaffolds as in **Box 4** (page 26) with exceptions:

    - reduce dissolving time of sPEG from 5 minutes to 2.5 minutes

    - for group 4e: PBS 0.5x was used instead of PBS (1x)

    - for group 4f: self-made PBS was used instead of commercial one

---

Group 4f: Effect of self-made PBS on CaP coating

This group shall be labeled group 4f. Again, the protocol was similar to group 4c with the exception that freshly prepared PBS was used instead of Dulbecco's PBS. It was produced as a 10x stock solution following a protocol from Dr Katrin Schlegelmilch. For preparation of a 10x PBS stock solution 80 g of NaCl, 2 g of KCl, 28 g of $Na_2HPO_4.2\ H_2O$ and 2 g of KH_2PO_4 were dissolved in 800 ml of water. Afterwards the volume was topped off to 1 liter with a final pH of 6.8. When PBS 10x was dissolved to give a 1x solution its pH went up to 7.4.

sPEG was dissolved for 2.5 minutes. Self-made PBS was set to pH 8.1 before addition of sPEG and 2-AEP. The molar ratio of sPEG and 2-AEP remained 1:2. Three samples were produced in this group.

2.2.6 Calculations

Molar calculations were used to figure out the correct amount of 2-AEP needed for each sPEG to 2-AEP ratio. These are illustrated below.

For a 1:1 ratio:

5 ml of PBS/water require 100 mg (0.1 g) of sPEG to produce a 2% solution.

Molar mass of sPEG: 12.000 g/mol^{-1}

Using the formula:

Number of moles (mol) = mass (g) **/** molar mass (g/mol^{-1})

$\rightarrow$ Number of moles (sPEG) = 0.1 g **/** 12000 g/mol^{-1} = 8.3×10^{-6} mol

Therefore, 8.3×10^{-6} moles of 2-AEP are needed to give a 1:1 ratio.

Molar mass of 2-AEP: 125 g/mol^{-1}

Rearranging the formula:

Mass (g) = number of moles (mol) **x** molar mass (g/mol^{-1})

$\rightarrow$ Mass (g) = 8.3×10^{-6} mol **x** 125 g/mol^{-1} = 0.00103 g = 1.03 mg

Hence, 1.03 mg of 2-AEP are needed to give a 1:1 ratio with 100 mg of sPEG.

$\rightarrow$ 2.06 mg for 1:2;   3.09 mg for 1:3;   4.12 mg for 1:4;   6.18 mg for 1:6

2.2.7 Sample analysis

Sample pretreatment

Samples were at first mounted on a carbon adhesive disk which was previously glued onto a specimen pin stub. Using a sputter coating device the mounted samples were then sputter coated with 4 nm of platinum. The settings were set to: Pt, 4 nm. Afterwards samples were stored in specimen storage holder boxes until SEM investigation and each sample was labelled onto the plastic of the boxes.

Scanning electron microscopy

Scanning electron microscopy (SEM) utilizes a beam of electrons which is rasterized on a sample to give an image of its topography. Electrons are derived from a thermionic cathode and focused with the aid of magnetic coils. The bundled beam of these primary electrons then hits the sample's surface. Depending on the objects' surface, the interactions between electrons and object generate a secondary electron pattern which is then detected to give an image. This process takes place under high vacuum to avoid interactions with air molecules.

SEM was performed with the technical assistance of Carina Blum M.Sc. and Judith Friedlein. First of all, samples were carefully taken out of their storage boxes and put onto a specimen holder plate from Zeiss CB340 (up to 5 samples at a time). The plate was then put into the intermediate chamber of the device, where high vacuum was achieved. Using CB340 software, samples were viewed on a monitor screen. Before further investigations, contrast settings and image definition were adjusted precisely. The first sample was then investigated. First a brief overview of the sample was given by hovering the lens over it at 50 – 100 x magnification. Afterwards, diverse structures and coating-patterns were zoomed into at 500 x and 1.500 – 4.000 x depending on structure or surface qualities. It was the aim to ensure that the images' sum gives a representation of all the coating entities of a given sample. The lens was then hovered to the next sample and the imaging started again at 50 – 100 x magnification. At the end samples were unloaded and placed back in their storage boxes.

Energy dispersive X-ray spectroscopy

Energy dispersive X-ray spectroscopy (EDX) is a method to analyze the elemental composition of a samples surface. The principles of EDX are similar to the ones of SEM. Electron-object interactions generate not only electron but also characteristic X-ray patterns which are specific for each element. The X-rays are detected using a second detector and the data are then superimposed on the SEM image.

EDX spectroscopy was performed during SEM investigation. At a higher

magnification (500 x or higher) EDX software was run on the current lens settings to give elemental evaluation of the shown surface. It was ensured that standard deviation was 0.1 or lower for all present elements.

2.2.8 Mechanical testing

Scaffolds, which were already mounted for examination under the SEM, were used. Samples were chosen as follows: one untreated PCL scaffold, one scaffold from group 1 which showed a CaP coating with the least number of flakes and finally, one scaffold that utilized sPEG and 2-AEP to provide a homogenous, mature coating. The samples were looked at using SEM first and then unloaded. Using forceps, the scaffolds were grasped by the overhanging loops and half of the scaffold was peeled off its sticky subsurface. Without readjustment of forceps, the scaffold was then bent so that the line of loops that was grasped met its opposite equivalent.
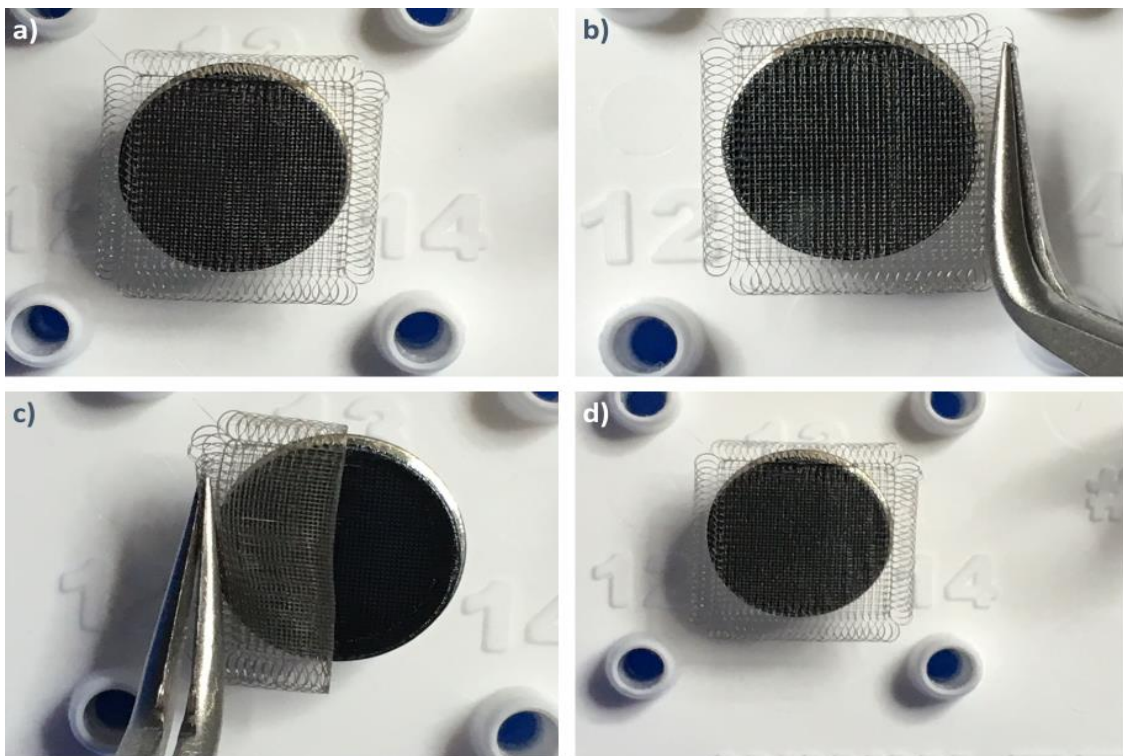
Figure 4: Illustration of the mechanical testing: mounted samples (a) were grasped (b), peeled of the mounted surface and bent (c), before readjusting (d)

3 Results

3.1 Group 1: CaP coating for non sPEG coated scaffolds

3.1.1 Group 1a-d: Variable etching parameters

PCL scaffolds were etched with 2 M NaOH for 90 minutes at 37 °C (group 1a), 90 minutes at RT (group 1b), 45 minutes at 37 °C (group 1c) or 45 minutes at RT (group 1d). Afterwards, they were treated according to Box 1. Before SEM examination, scaffolds were sputter-coated with 4 nm of platinum.
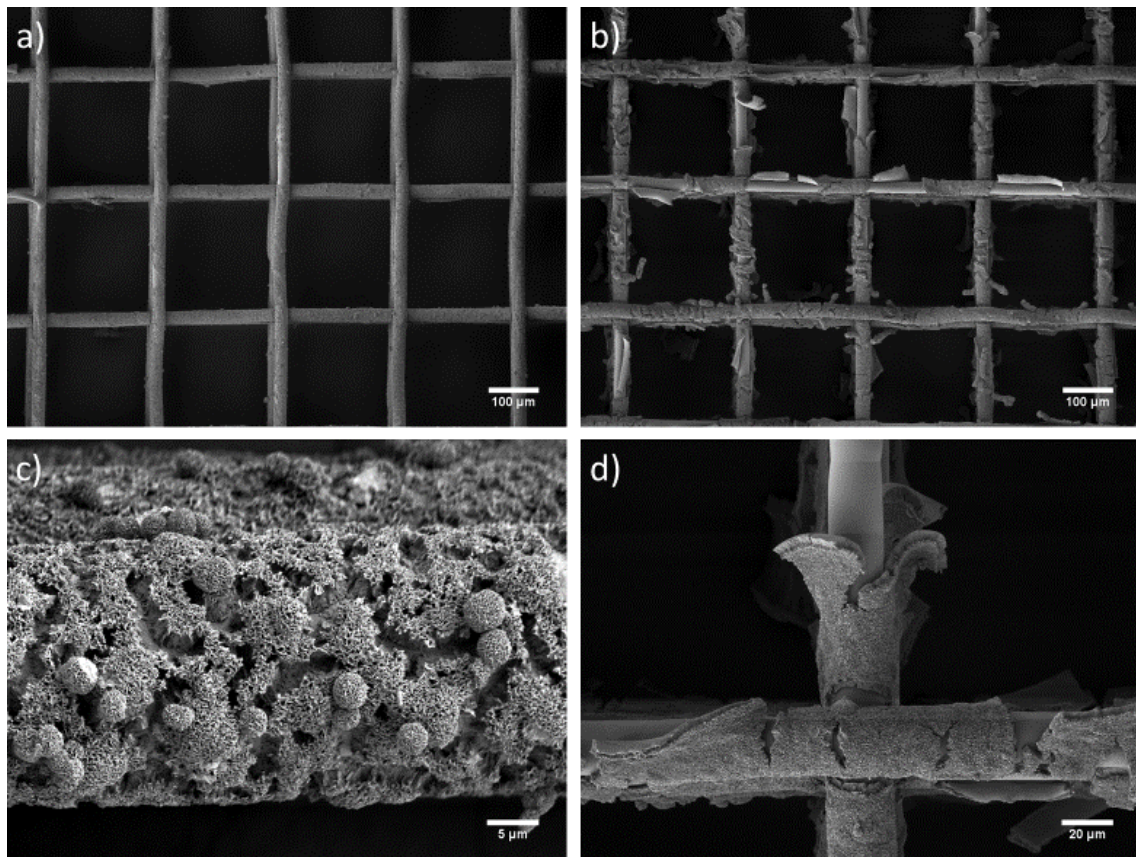
Figure 5: Group 1a (90 minutes, 37 °C) (2.2.2 Group 1: CaP coating for non sPEG coated scaffolds, page 19); magnifications: a), b): 100x; c): 2000x; Id): 500x

Samples from Group 1a (Figure 5) showed CaP-coated fiber-constructs. Some areas (b) on the scaffolds showed accumulation of partially peeled off coating-fragments. The coating itself appears thicker than coatings from group 3 and 4 (see Figure 11 and Figure 19) and Figure 5 (d) suggests that it consists of multiple layers of maturity. The outer layer exhibits a coralline crystal-structure while the inner layer's one appears more densely. Accumulations of spherical

elevations were found on top of the outer layer. The overall coating was coined with cracks (c, d) that were found across the entire samples.
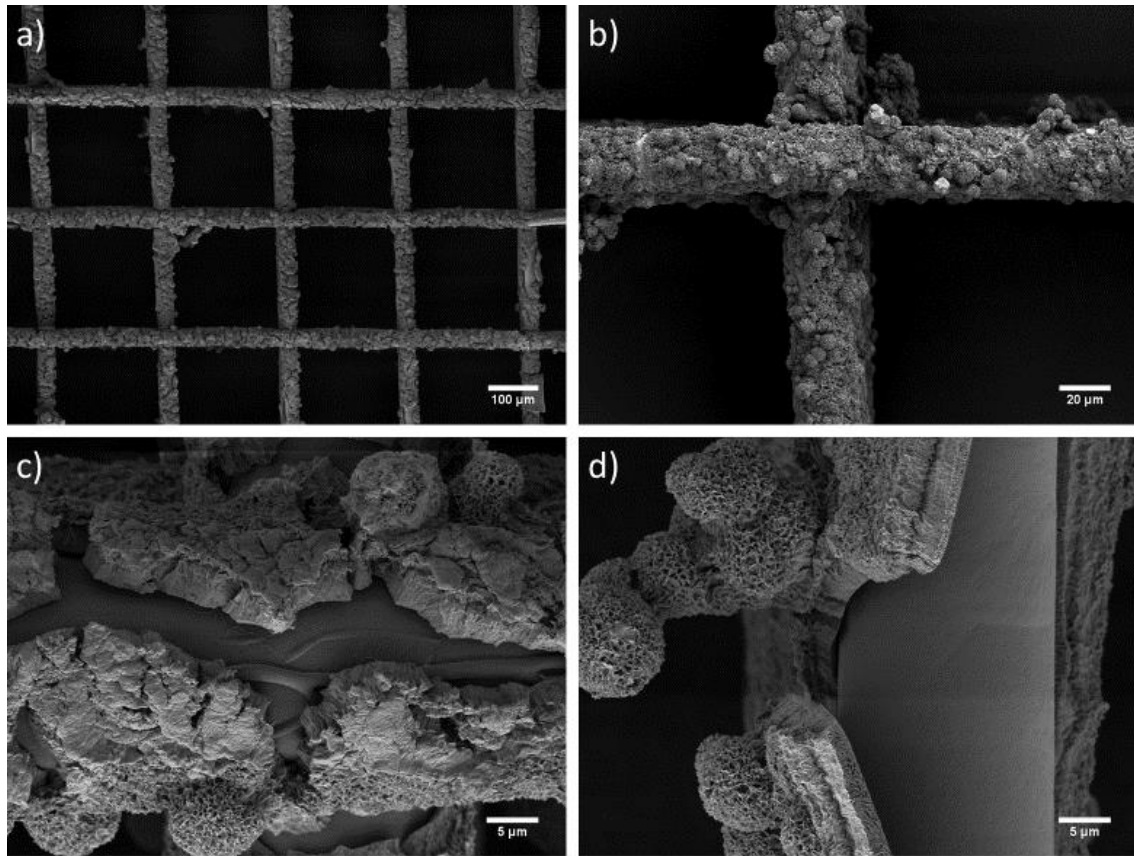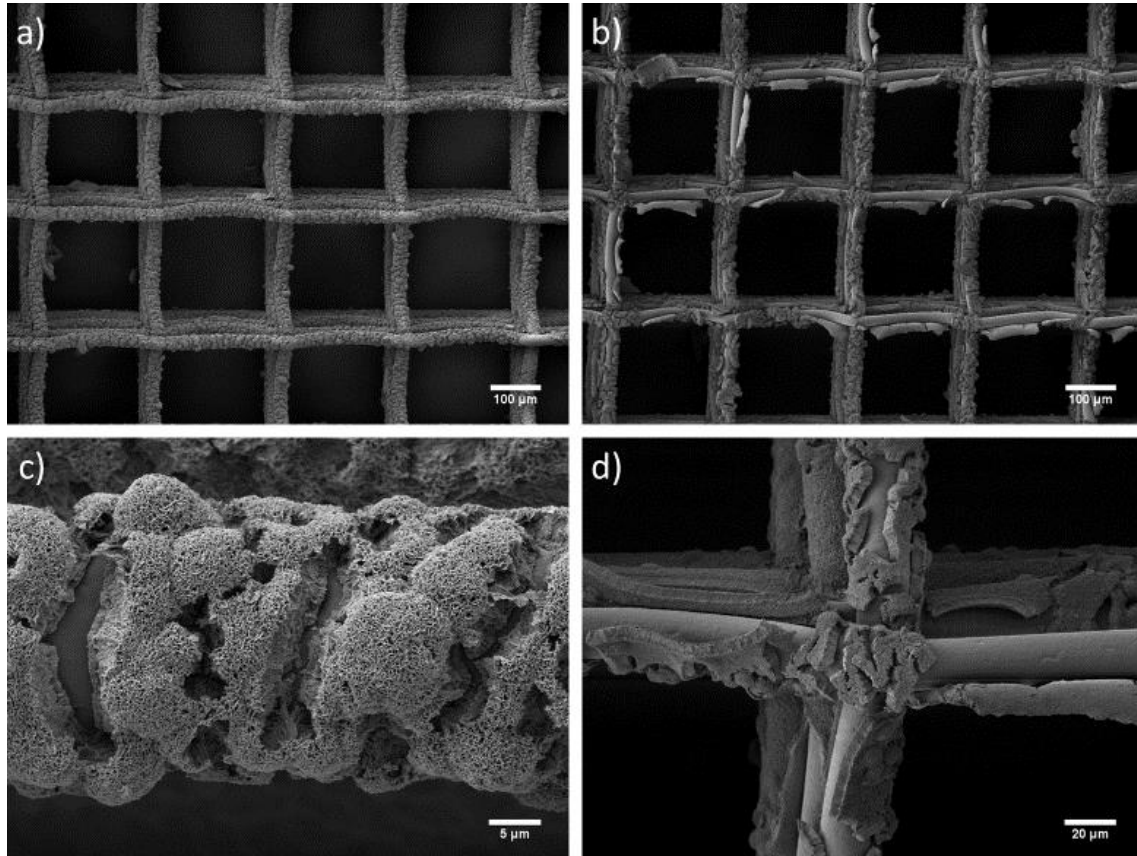

Figure 6: Group 1b (90 minutes, RT (2.2.2 Group 1: CaP coating for non sPEG coated scaffolds, page 19) magnifications: a): 100x; b): 500x; c), d): 2000x

Group 1b is represented by pictures from Figure 6. Samples from group 1b presented similar coatings to samples from group 1a as the coating consisted of more than one layer and their optical appearance (d) in terms of crystallinity showed no significant difference. Cracks (c) were present on all samples, however their quantity staggered between individual samples. Sporadically, delaminated fiber-areas (d) were found on all samples.

Figure 7 displays selected pictures from group 1c at various magnifications. It can be stated that a general CaP coating was present on all samples. Continuous, cracked and delaminated coatings were found on each sample. Coating properties like thickness and crystalline structure are comparable to group 1a and 1b.
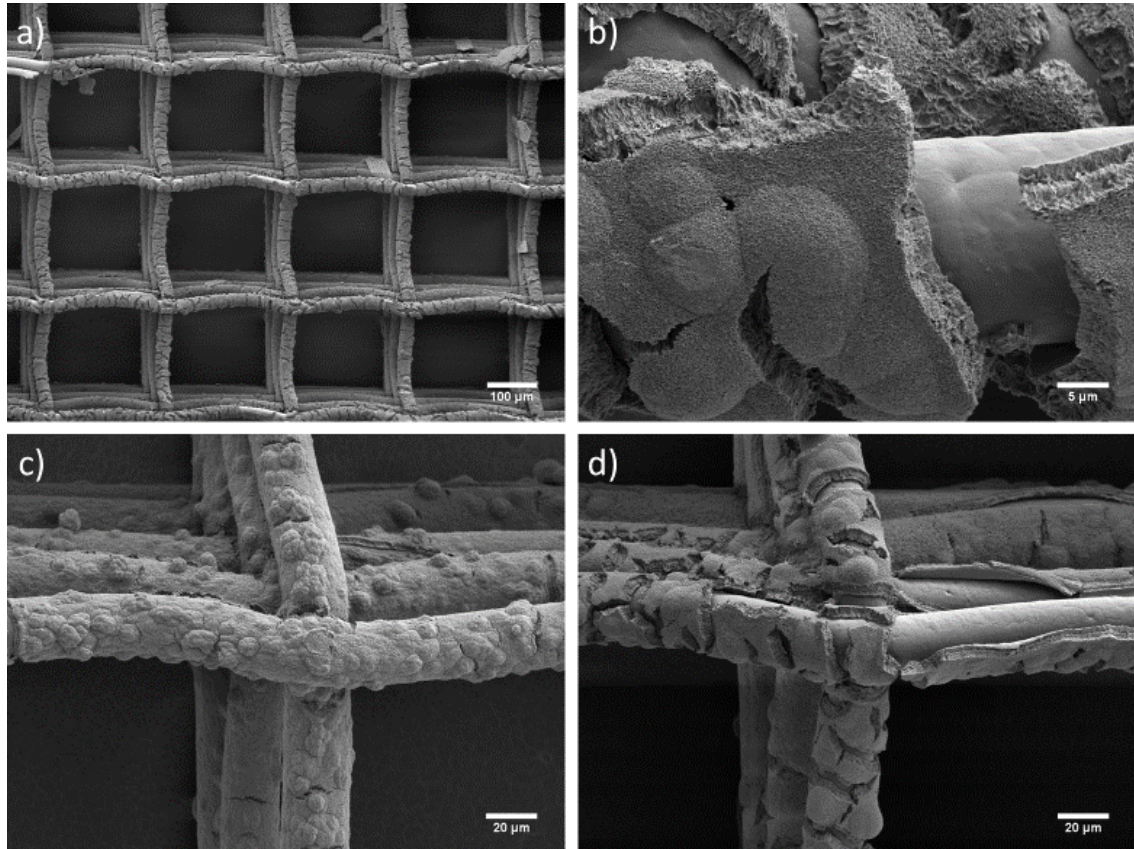
Figure 7: Group 1c (45 minutes, 37 °C) (2.2.2 Group 1: CaP coating for non sPEG coated scaffolds, page 19); magnifications: a): 100x; b): 2000x; c), d): 500x

Scaffolds from group 1d also showed CaP coated PCL fibers as presented in Figure 8. Again, there were areas which were found to be more cracked or delaminated than others (a, b). In comparison to group 1c, samples from group 1d showed a less uniform coating (c), although areas of continuous coating were found as well. Different optical CaP coating layers can be distinguished. The top layer shows a ferny, coralline structure.

3.1.2 Group 1e-g: The effect of multiple SBF 10x incubations

The effect of single and multiple SBF 10x incubations was investigated. First, PCL scaffolds were disposed of air entrapments and etched with a 2 M NaOH solution for 90 minutes at 37 °C. They were then incubated in filtered SBF 10x for 30 minutes once (group 1e), twice (group 1f) or three times (group 1g) at 37 °C. After SBF 10x incubation(s), scaffolds were post-treated with 0.5 M NaOH solution for 30 minutes at 37 °C and washed. Figure 9 shows representable pictures of groups 1e, 1f and 1g.

Figure 8: Group 1d (45 minutes, RT) (2.2.2 Group 1: CaP coating for non sPEG coated scaffolds, page 19); magnifications: a), b): 100x; c): 2000x; d): 500x

Samples from group 1e display fibers with plane, non-continuous deposits on the surface. Also, singular, rock-shaped structures of different sizes can be seen on the fibers (c). Other parts appear non-coated, which display the original surface pattern of an untreated PCL scaffold.

As Figure 9 suggests, samples from group 1f appear coated. The crystalline structure is more distinct than in group 1e and converges to coatings from group 1a as signs of coralline textures can be seen. Cracked coatings and delaminated fiber surfaces were found with a lower frequency than in group 1a-d. Half-spherical elevations of the coating were present (c).

The coating of group 1g presented itself thicker and more mature than group 1e and 1f. As can be seen in Figure 9, it was mostly continuous and homogenous. Still some fiber parts were found to be non-laminated. Fissures were seen at lower frequency than in group 1a. Half-spherical elevations were present on top of the coating. Sporadically, acinus structures containing this type
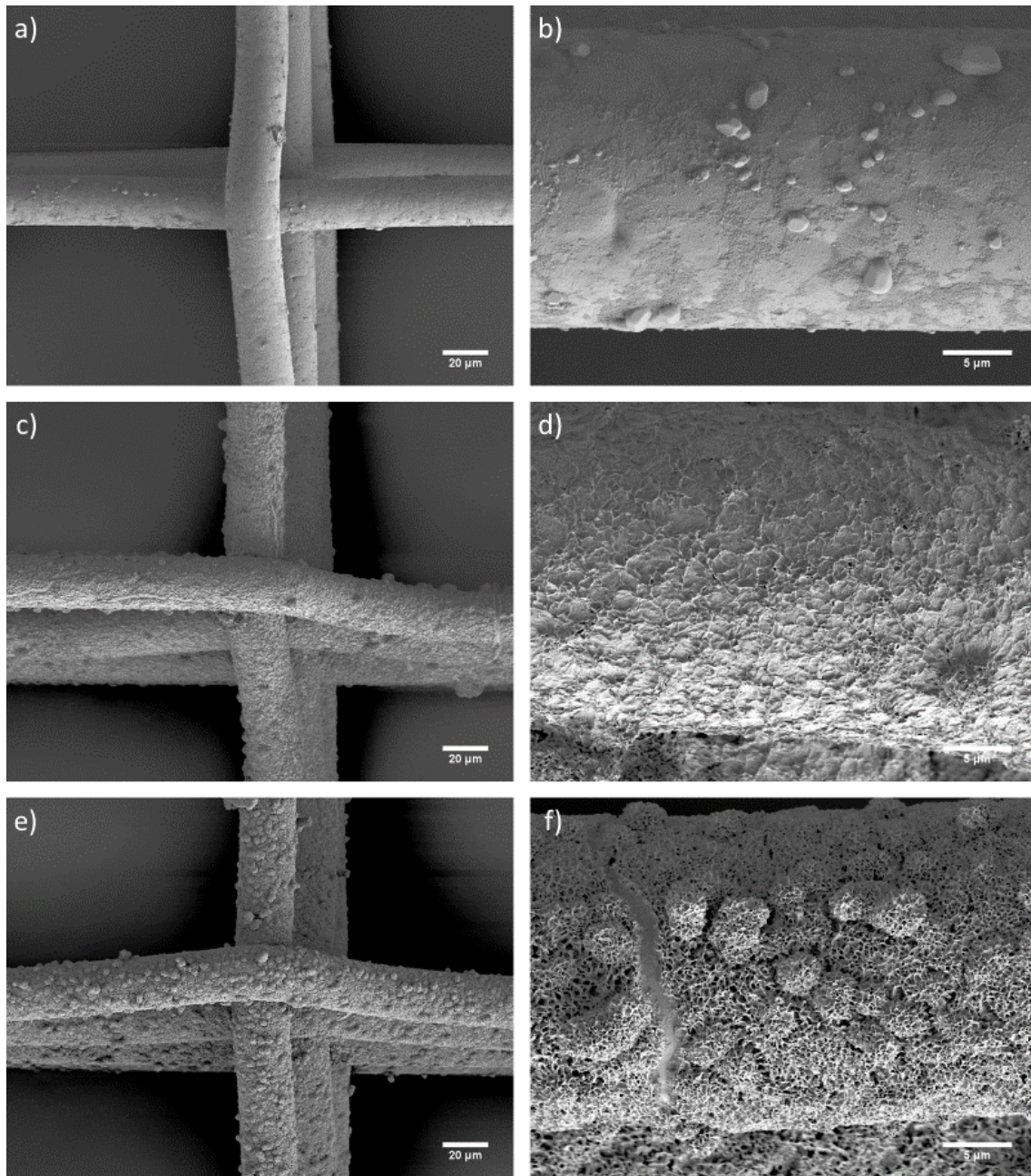
Figure 9: Group 1e-g (2.2.2 Group 1: CaP coating for non sPEG coated scaffolds, page 19); shown in 500x (a,c,e)and 3000x (b,d,f) magnification; group 1e: a), b); group 1f: c) ,d); group 1g: e),f)

of elevation as its unit, can be found.

In summary for group 1, a CaP coating could be deposited onto the PCL scaffolds, however all samples had extensive cracking. This demonstrates the challenge in making a uniform CaP coating onto the PCL substrate. Solving such coating defects is a major aim of this thesis.

3.2 Group 2: Star polyethylene glycol coating

PCL scaffolds have been pre-wetted and etched in 1 M NaOH for 5 minutes. After a washing procedure of 5 x 5 minutes, they were incubated in 1 ml of aqueous sPEG solution for 10 minutes. Afterwards, samples were washed 3 x 5 minutes and left to dry on a glass slide overnight. Figure 10 shows a representable selection of pictures from group 2.
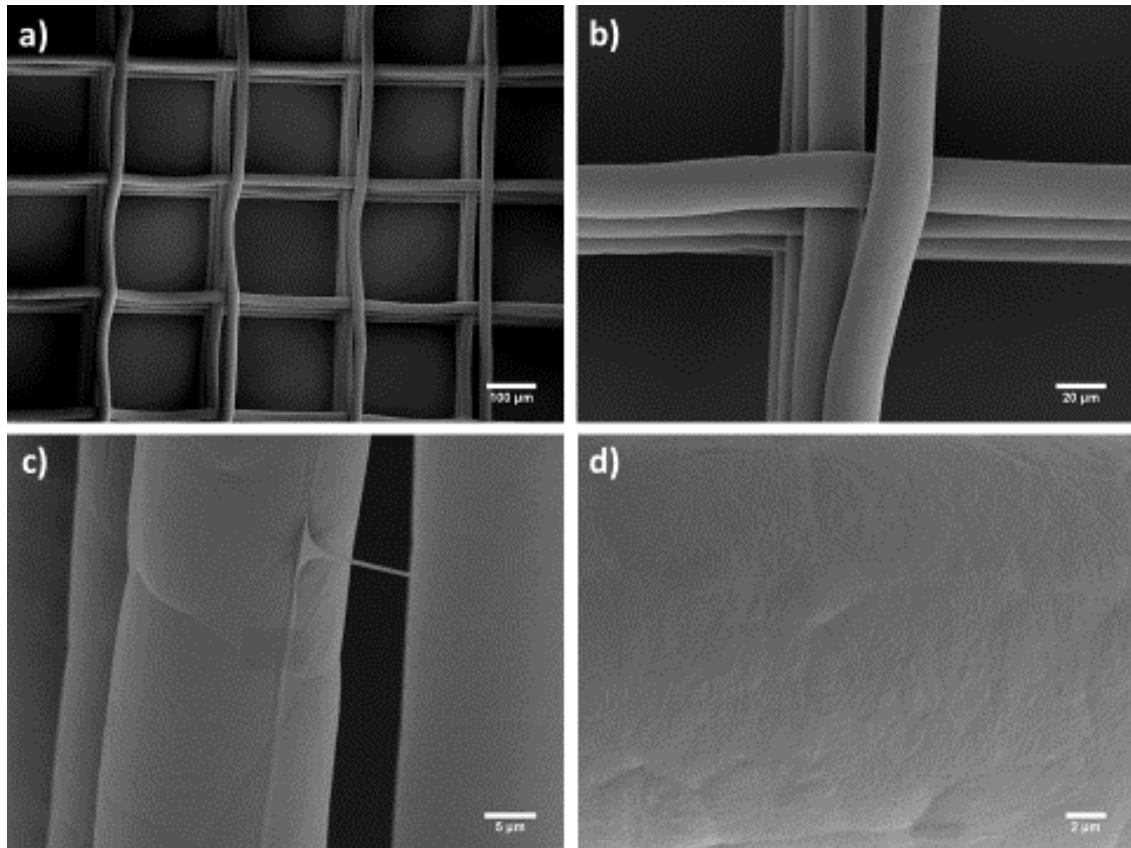
Figure 10: Group 2, sPEG coated PCL scaffold (2.2.3 Group 2: SPEG coating; page 22); magnifications: a) 100x, b) 500x, c) 2000x, d) 4000x

Stacked up PCL fibers of consistent diameter (approximately 25 µm) which are arranged in square boxes can be seen in different magnifications. The fibers of the entire samples appear uncoated as the typical surface patterns (Figure 10 d) of untreated fibers can be seen throughout. Figure 10 c shows a thin filamentous connection between two stacked PCL fibers, which can be found sporadically.

3.3 Group 3: Incubation of sPEG coated scaffolds in 2-AEP different solutions

PCL scaffolds were treated according to the sPEG (batch #5 refers to group 3a; batch #6 refers to group 3b) coating protocol. Afterwards, they were incubated in 2-AEP of different concentrations for 30 minutes. Finally, SBF 10x treatment plus subsequent posttreatment occurred.

3.3.1 Group 3a: sPEG batch #5

SEM pictures of samples of group 3a are shown in Figure 11 and Figure 12. All samples that were incubated in 0.1%, 1% or 5% 2-AEP solution (Figure 12) showed uncoated fibers across the entire scaffold. Patterns similar to non-treated PCL scaffolds can be seen at 2000x magnification. Very rarely, a single CaP deposit onto a fiber was found.

Scaffolds that were treated with 10% 2-AEP solution (Figure 11) were
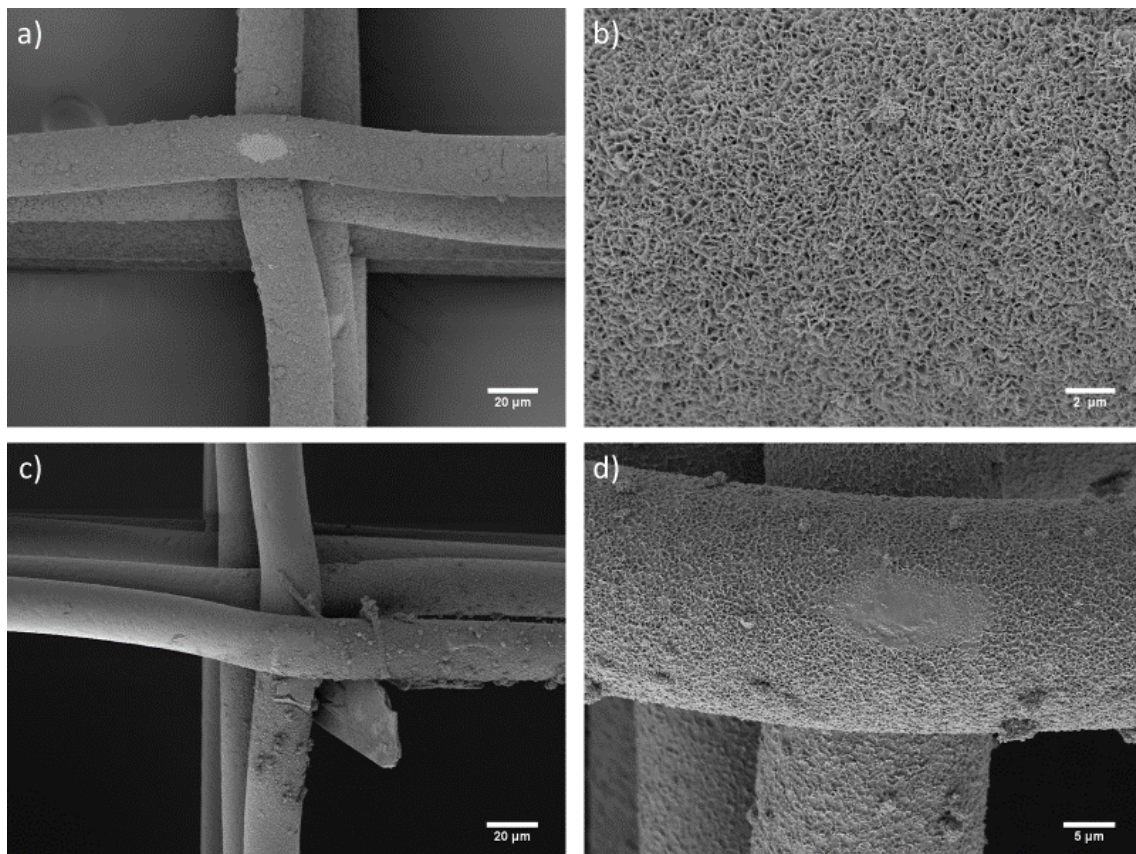
Figure 11: Group 3a (10%) (2.2.4 Group 3: Incubation of sPEG coated scaffolds in solutions of different 2-AEP concentrations; page 23); magnifications: a), c): 500x; b): 5000x; d): 2000x
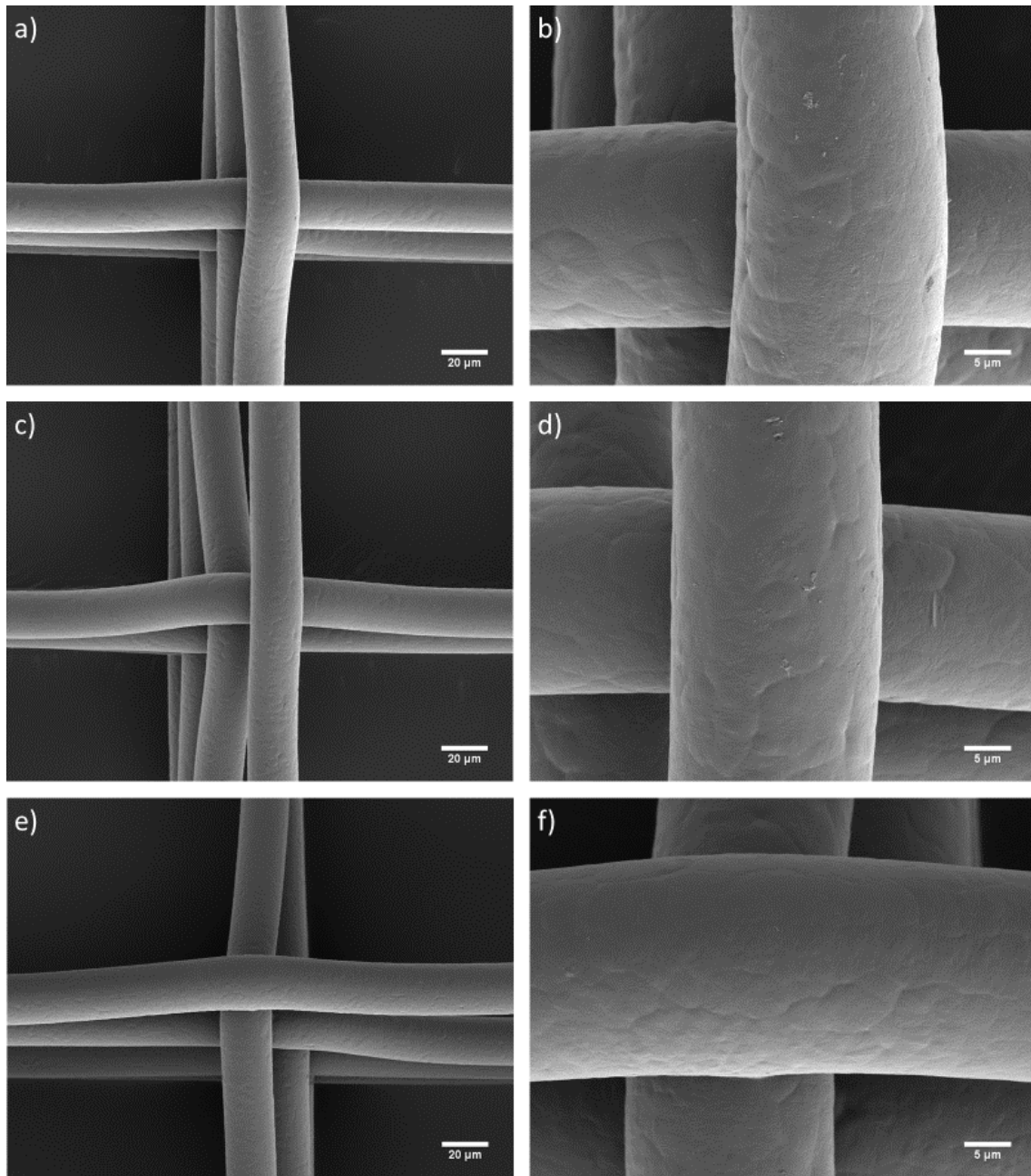
Figure 12: Group 3a 0.1% (a, b), 1% (c, d), 5% (e,f) (2.2.4 Group 3: Incubation of sPEG coated scaffolds in solutions of different 2-AEP concentrations; page 23); magnifications a), c), e): 500x; b), d), f) 2000x;

found to be homogenously laminated with CaP. Coralline-structured crystals of high density and half-spherical elevations can be seen upon the fibers. One of the samples showed areas of non-coated fibers (c).

3.3.2 Group 3b: sPEG batch #6

Figure 13 shows expressible pictures of three samples (S) of group 3b (0.1%). A vast difference in coating quality between S 1, S 2 and 3 can be seen. The coating of S 1 appears to be shallow and can only be seen at higher magnifications (b). It is not evenly distributed among the fibers. Crystals appear immature and sandy. The examination of S 2 showed a homogenous coating among the entire scaffold. The crystals are larger than in S 1 and of granular structure. S 3 presents a CaP coating with different types of crystalline maturity. The crystalline structure seen in b) is coralline shaped. Other areas of the sample were partially covered with evenly distributed spiny crystals. Both, S 2 and S 3, show papilliform elevations of CaP arising on top of the general coating.

A representable selection of pictures from group 3b (1%) can be seen in Figure 14. b) shows partially coated fibers with a coralline crystal structure. The same sample also showed regions of more uniform coatings. Pictures of S 2 and 3 presented a fully homogenous CaP lamination of fibers with the addition of papilliform eminences, which were seen among the whole scaffold.

A big difference of coatings in Group 3b (5%) is represented by Figure 15. S 1 presented itself as entirely uncoated. Patterns of untreated PCL fibers can be seen in a) and b). S 2 showed areas of uncoated fibers or fiber parts. Areas with CaP depositions of variable crystalline shapes (spiny and granular) have also been spotted as seen in d). The third sample displays a homogenous coralline CaP coating with elevations, which coated the entirety of the scaffold.

Finally, Figure 16 represents group 3b (10%). All scaffolds predominantly showed CaP coatings on the fiber surfaces except for a few patches of uncoated fiber. The coating's crystal structure for all three samples can be described as coralline and ferny. S 1 and 2 show a larger quantity of papilliform elevations than S 3.
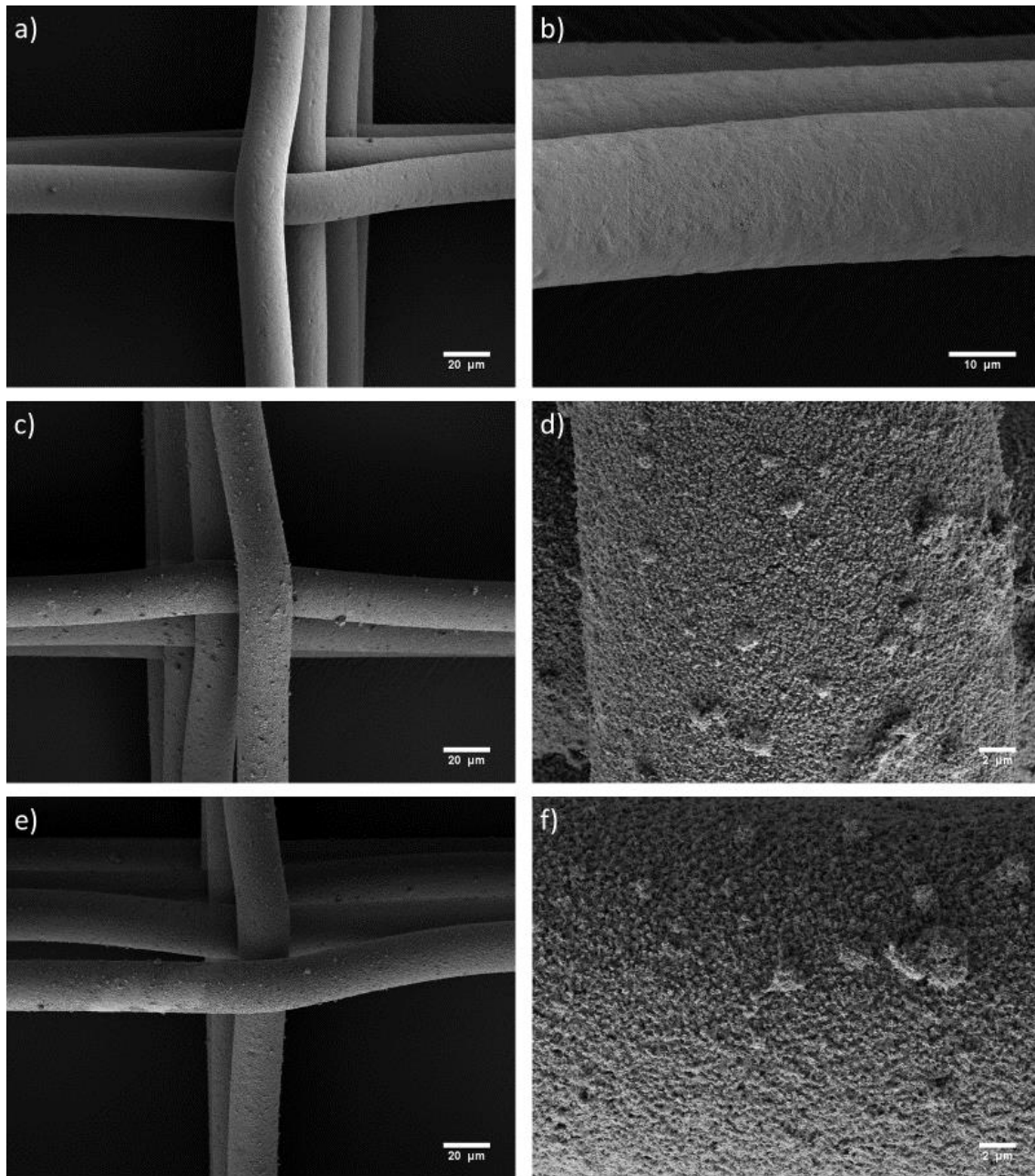
Figure 13: Group 3b (0.1%) (2.2.4 Group 3: Incubation of sPEG coated scaffolds in solutions of different 2-AEP concentrations; page 23); sample 1: a) 500x, b) 1500x; sample 2: c) 500x, d) 1500x; sample 3: e) 500x, f) 4000x
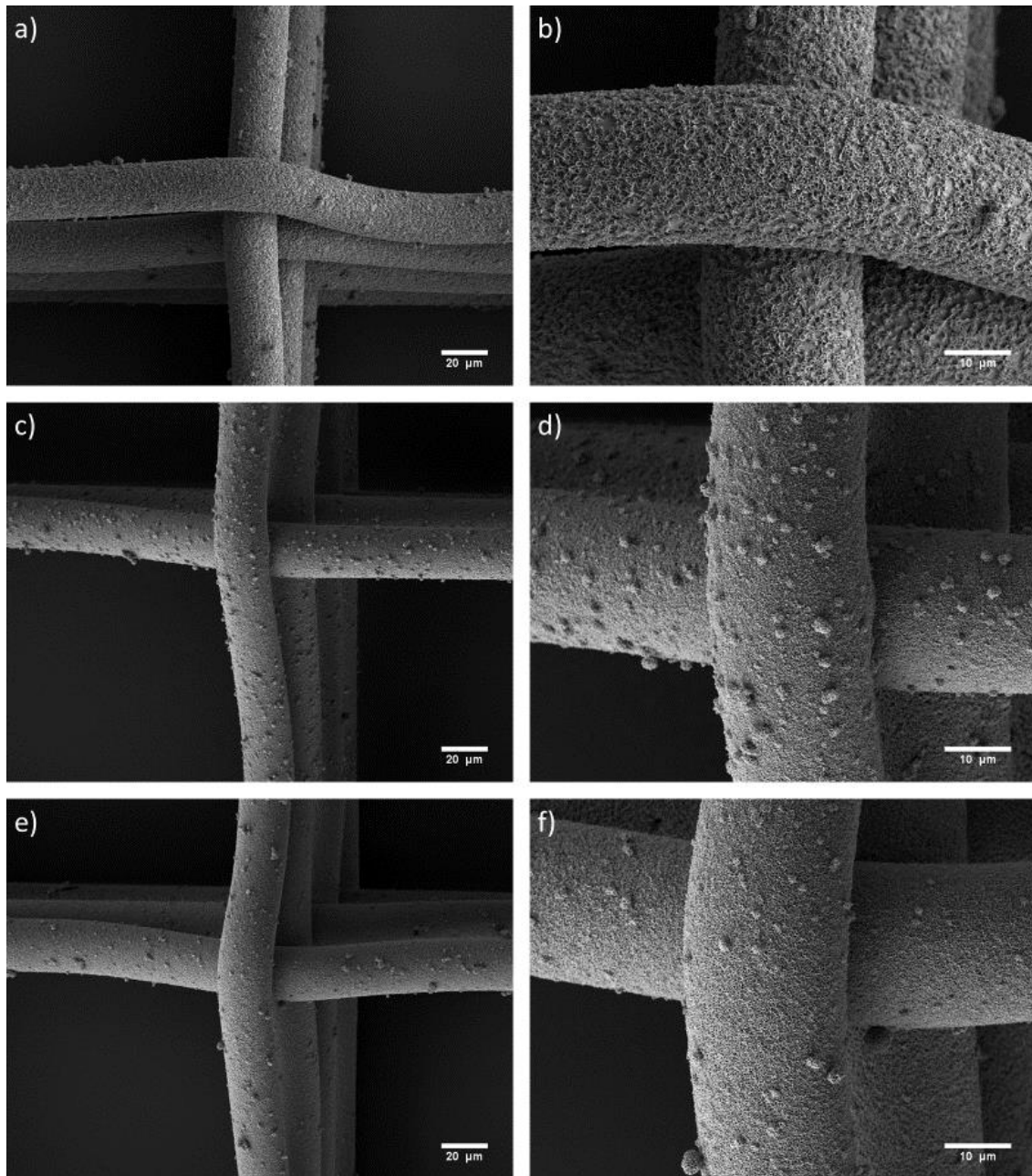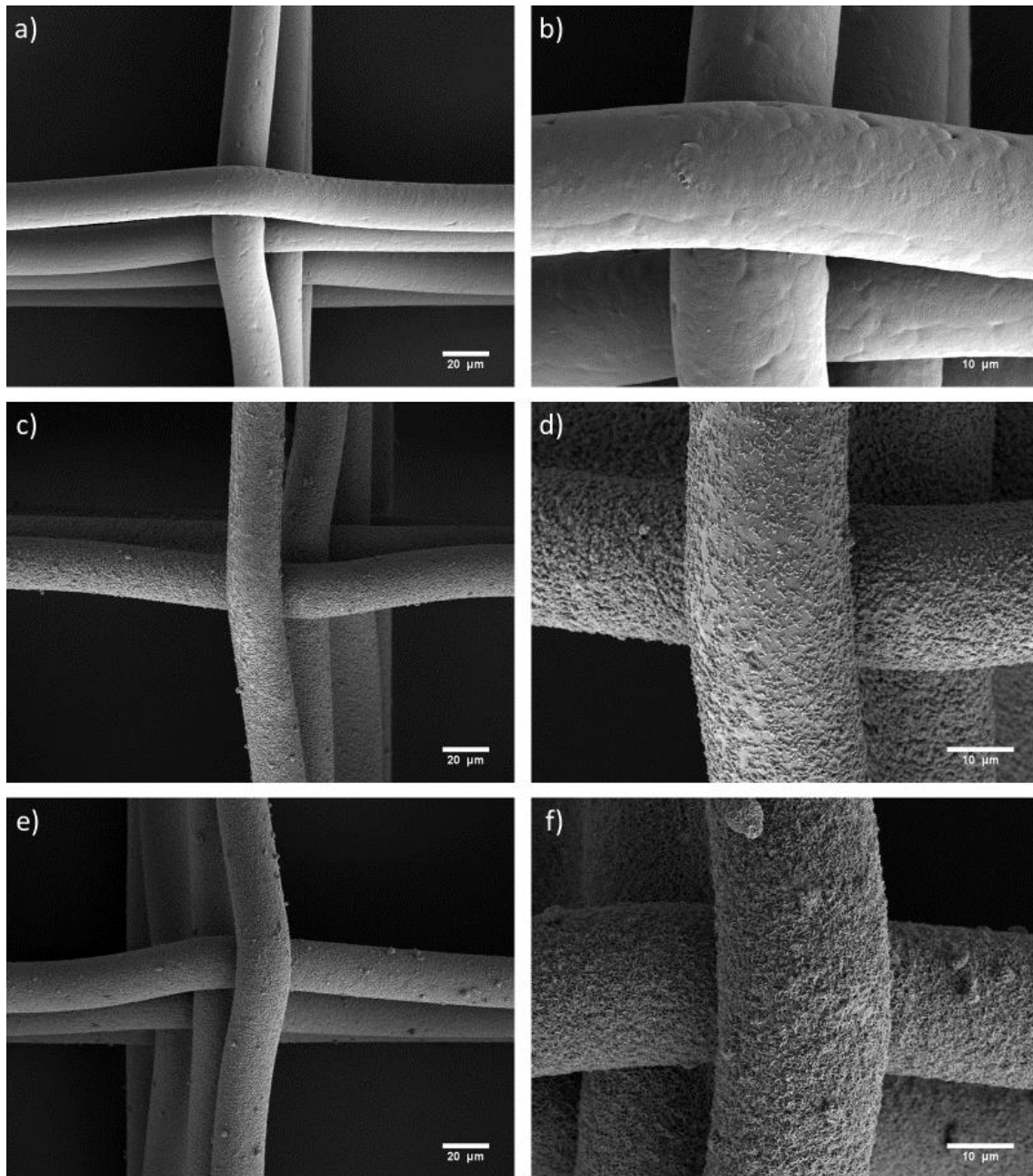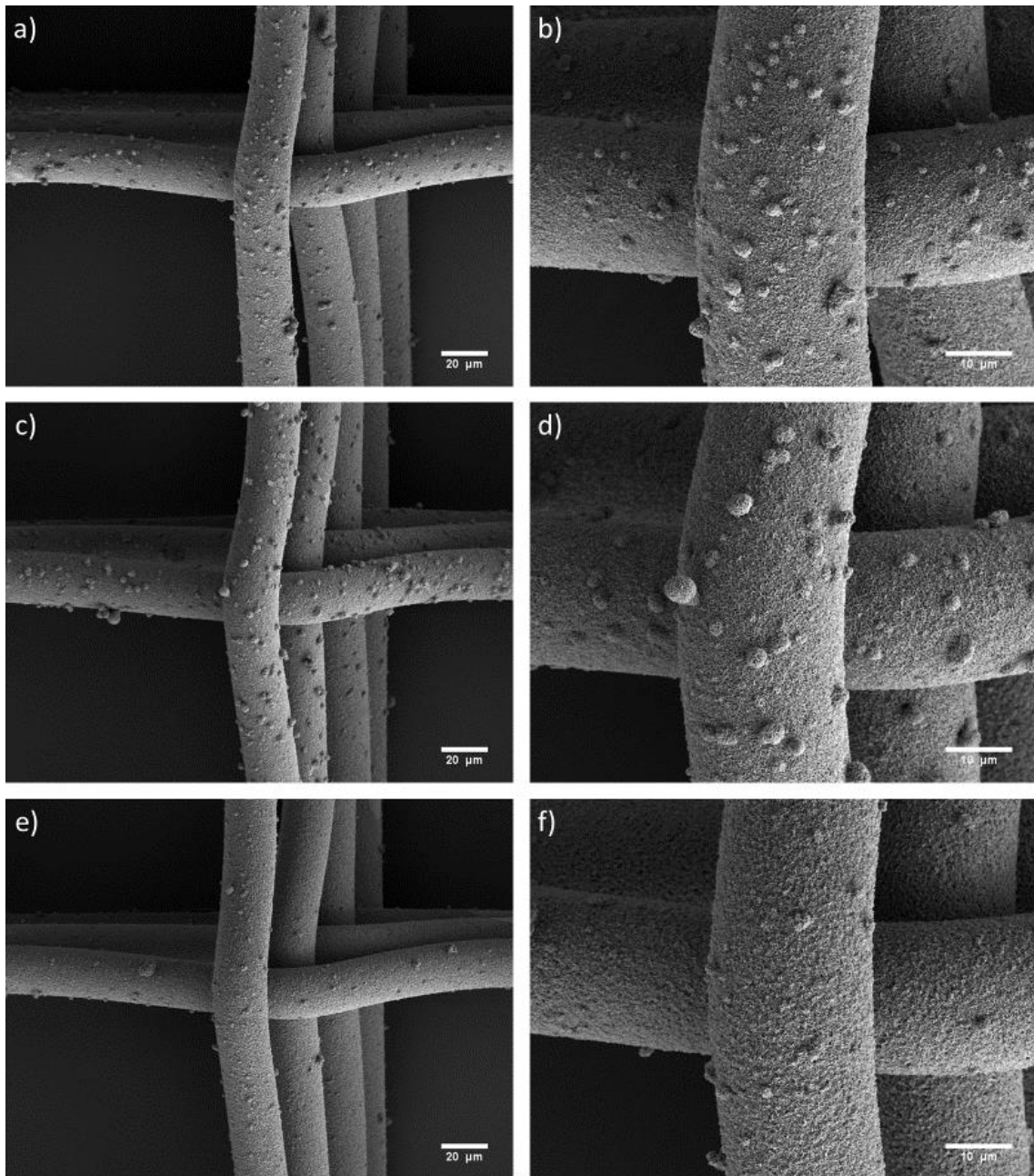
Figure 14: Group 3b (1%) (2.2.4 Group 3: Incubation of sPEG coated scaffolds in solutions of different 2-AEP concentrations; page 23); sample 1: a) 500x, b) 1500x; sample 2: c) 500x, d) 1500x; sample 3: e) 500x, f) 1500x

Figure 15: Group 3b (5%) (2.2.4 Group 3: Incubation of sPEG coated scaffolds in solutions of different 2-AEP concentrations; page 23); sample 1: a) 500x, b) 1500x; sample 2: c) 500x, d) 1500x; sample 3: e) 500x, f) 1500x

Figure 16: Group 3b (10%) (2.2.4 Group 3: Incubation of sPEG coated scaffolds in solutions of different 2-AEP concentrations; page 23); sample 1: a) 500x, b) 1500x; sample 2: c) 500x, d) 1500x; sample 3: e) 500x, f) 1500x

3.4 Group 4: Simultaneous incubation of sPEG/2-AEP followed by SBF 10x

3.4.1 Group 4a: PBS/water set to pH 8.1 before addition of AEPA

After pretreatment, samples were incubated with sPEG and 2-AEP simultaneously using either PBS or water as a solvent. Different ratios of sPEG and 2-AEP were investigated (1:1, 1:2, 1:3, 1:4, 1:6). The pH value of PBS/water was set to 8.1 before adding it to 2-AEP. For both, PBS and water, scaffolds were set up each time. The figures of this group show representable images of both samples.

Figure 17 represents group 4a(i). Each sample that was treated with PBS showed different results. The first sample (a) showed patchy deposits of CaP whose quantity occasionally allowed to be named a coating. The second one (b) was coated homogenously. It appeared to be a layer of hydrogel beneath the coating which was spanned inside the fiber boxes to some degree.
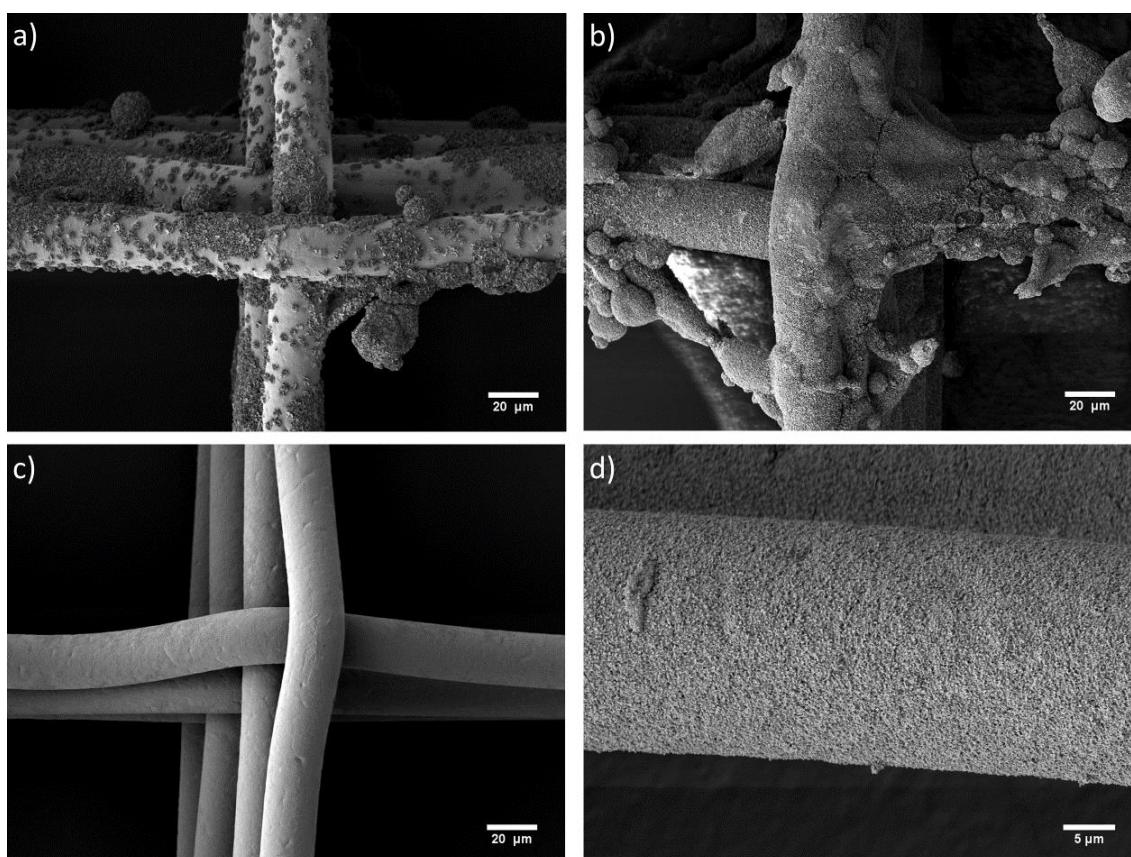
Figure 17: Group 4a(i) sPEG to 2-AEP ratio of 1:1, pH 7.3, (Group 4a: PBS/water set to pH 8.1 before addition of AEPA; page 25); a), b): PBS group at 500x magnification; c), d): H$_2$O group at 500x and 2000x magnification, respectively

Spherical structures were found on both samples. The crystals of the CaP coating appeared coralline and mature. Samples treated with water also showed differences. While one samples represented a thin, homogenous layer of grainy crystals across most of the scaffold (d) the other sample showed minimal amounts of crystals on its surface.
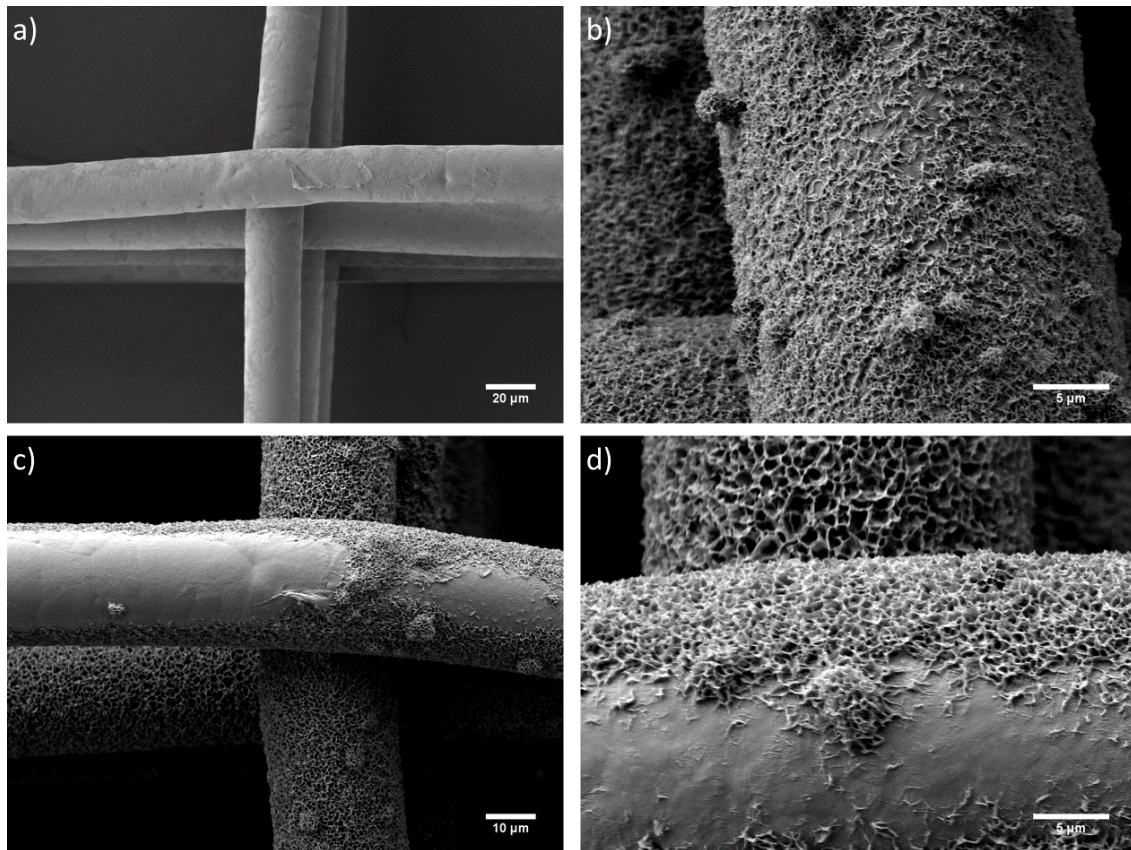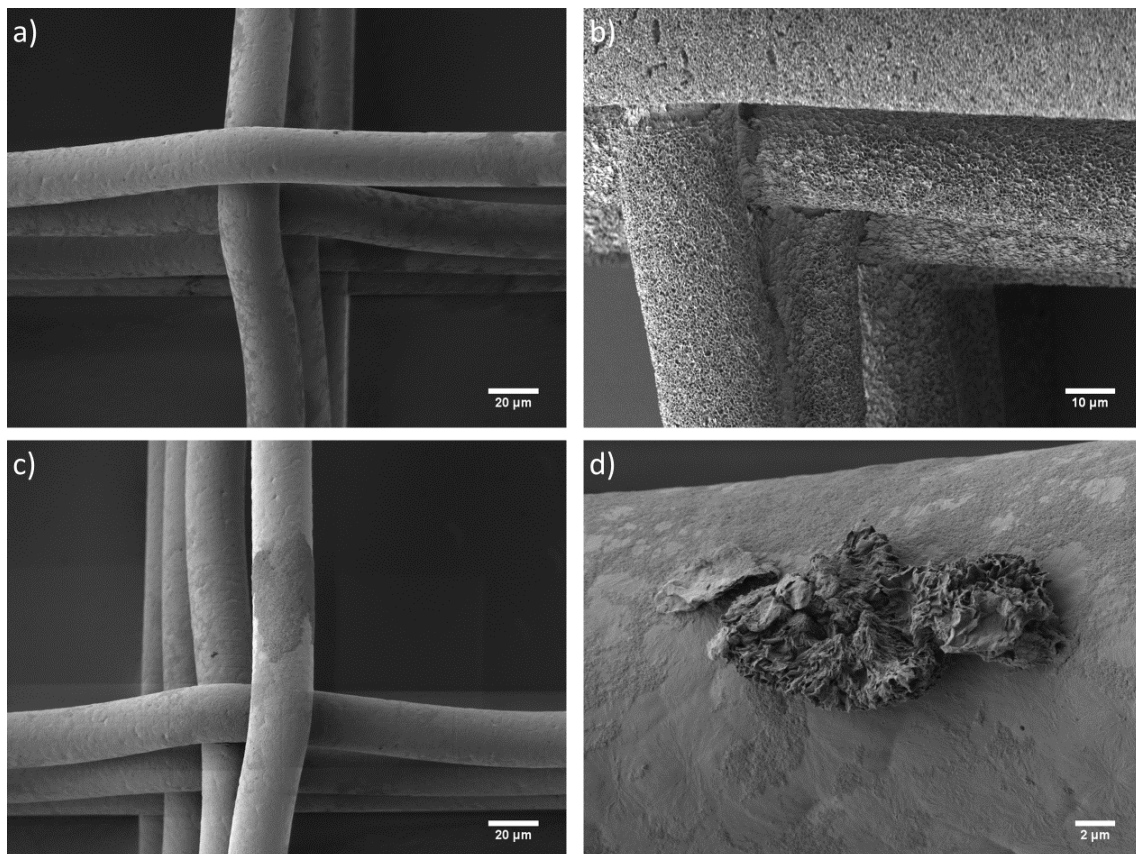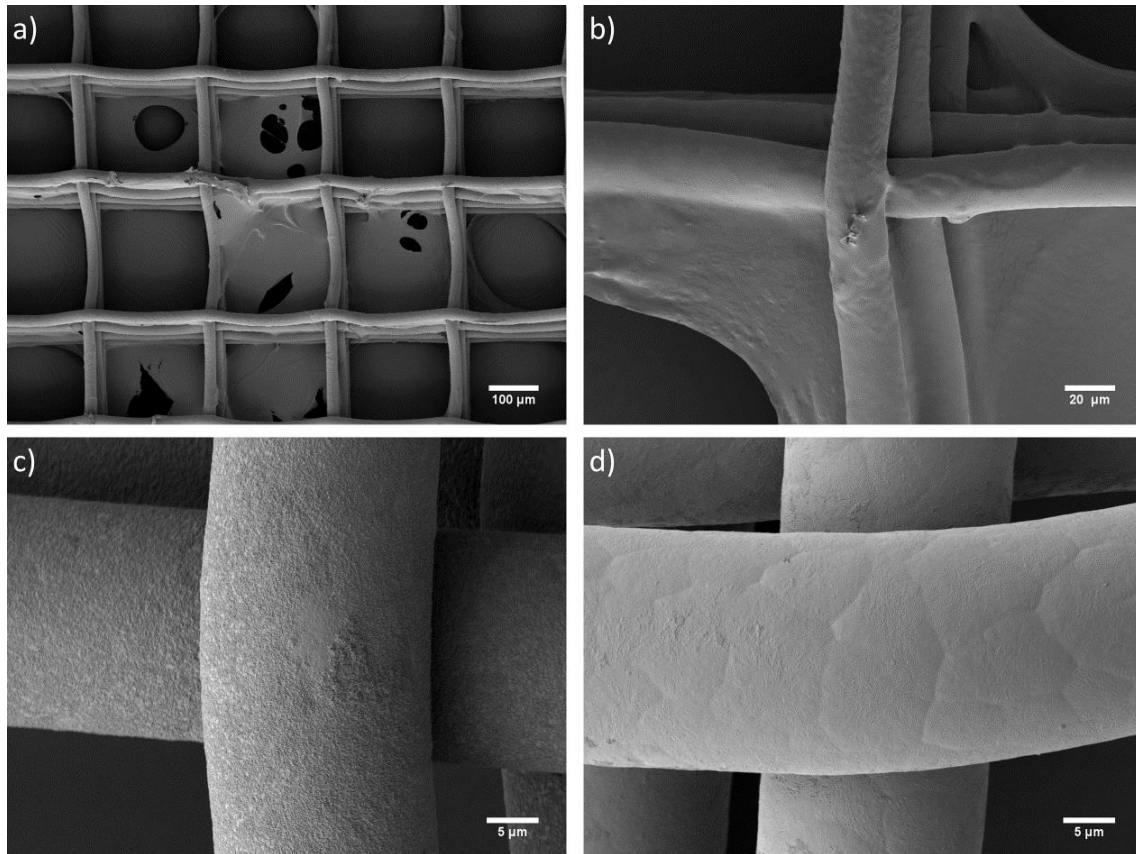

Figure 18: Group 4a(ii) sPEG to 2-AEP ratio of 1:2, pH 7, (Group 4a: PBS/water set to pH 8.1 before addition of AEPA; page 25); a), b): PBS group at 500x and 2000x magnification, respectively; c), d): H_2O group at 1000x and 2000x magnification, respectively

Pictures of group 4a(ii) are displayed in Figure 18. Again, the results in the PBS subgroup are diverse. One sample (a) presented itself as non-coated with very little signs of any CaP deposition. The other scaffold (b) showed a uniform CaP coating on top of the fiber surface, with a mature crystalline structure and nodular raisings. Samples from the water-subgroup both showed homogenously laminated fibers. Also, oval to longitudinal areas of uncoated fiber were present (c). These areas were exclusively observed on the outward site of the top fibers.

Figure 19 displays pictures referring to the experiments that used a sPEG

to 2-AEP ratio of 1:3. Samples treated with PBS showed different outcomes. The first sample (a) had occasional layers of flat, immature crystal deposits on the fibers. It can be labeled as non-coated. The second sample (b) appeared homogenously laminated with a thin CaP layer across the entire scaffold. Little cracks were found adjacent to fiber intersections. Close to no spherical elevations were found. Crystals were shaped coralline throughout the entire scaffold. Samples that were treated using water as a solvent for sPEG and 2-AEP both showed patches of flat laminations, similar to PBS a). Sporadically thick coating objects (d) were observed, also in form of flat sheets that were cracked or flaked off the fibers.
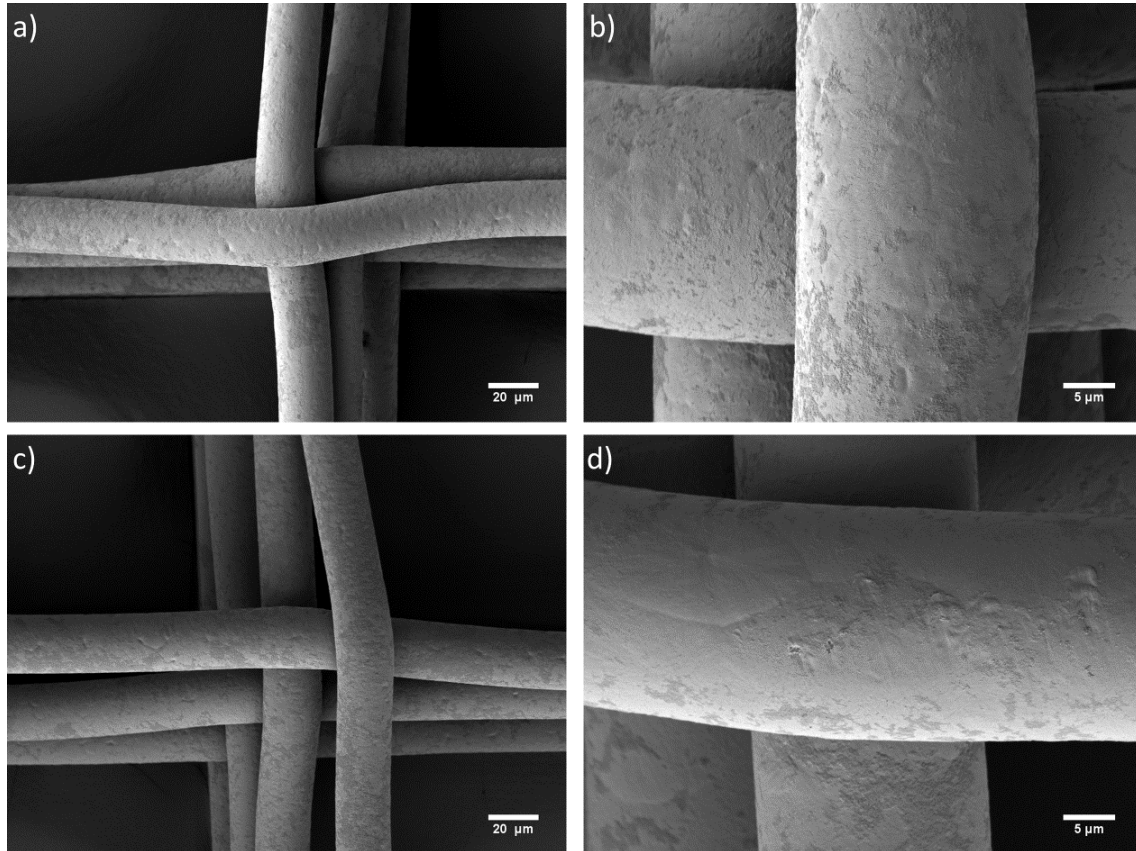

Figure 19: Group 4a(iii) sPEG to 2-AEP ratio of 1:3, pH 6.8, (Group 4a: PBS/water set to pH 8.1 before addition of AEPA; page 25); a), b): PBS group at 500x and 1000x magnification, respectively; c), d): H_2O group at 500x and 4000x magnification, respectively

Group 4a(iv) is represented by Figure 20. Scaffolds of the PBS-subgroup (a, b) presented large amounts of hydrogel, not only wrapped around the PCL fibers but also traversing scaffold boxes in form of thin sheets partially disrupted by holes and tears. The hydrogel is sprinkled with tiny CaP crystals. The water-

subgroup showed two distinct results. One sample (c) appears to be homogenously covered with grainy, sandy CaP crystals. Although homogenous, it was observed at higher magnifications that not all of the fibers' surface was covered within the lamination's structure. The thin CaP layer allowed for surface patterns of PCL fibers to gleam. The other sample (d) showed no signs of CaP coatings apart from patchy flat deposits.

Figure 20: Group 4a(iv) sPEG to 2-AEP ratio of 1:4, pH 6.6 (Group 4a: PBS/water set to pH 8.1 before addition of AEPA; page 25); a), b): PBS group at 100x and 500x magnification, respectively; c), d): H_2O group at 2000x magnification

Finally, Figure 21 represents group 4a(v). All samples treated with a sPEG to 2-AEP ratio of 1:6 showed patchy, flat deposits of CaP on the entire scaffold. Signs of a thick or homogenous coating were not found.

Figure 21: Group 4a(v) sPEG to 2-AEP ratio of 1:6, pH 6.4, (Group 4a: PBS/water set to pH 8.1 before addition of AEPA; page 25); a), b): PBS group at 500x and 2000x magnification, respectively; c), d): H_2O group at 500x and 2000x magnification, respectively

3.4.2 Group 4b: Different pH values of 2-AEP solutions

For group 4b 2-AEP was added to PBS before adjusting it to pH 7 (group 4b(i)), 7.5 (group 4b(ii)) or 8.1 (group 4b(iii)). This solution was then used to dissolve sPEG.

For group 4b(i) (Figure 22) SEM imaging displayed a shallow non-homogenous coating on all samples. Surface patterns of untreated PCL fibers can be seen. Spherical elevations are missing. CaP deposits on the fibers appear sandy and unevenly distributed.
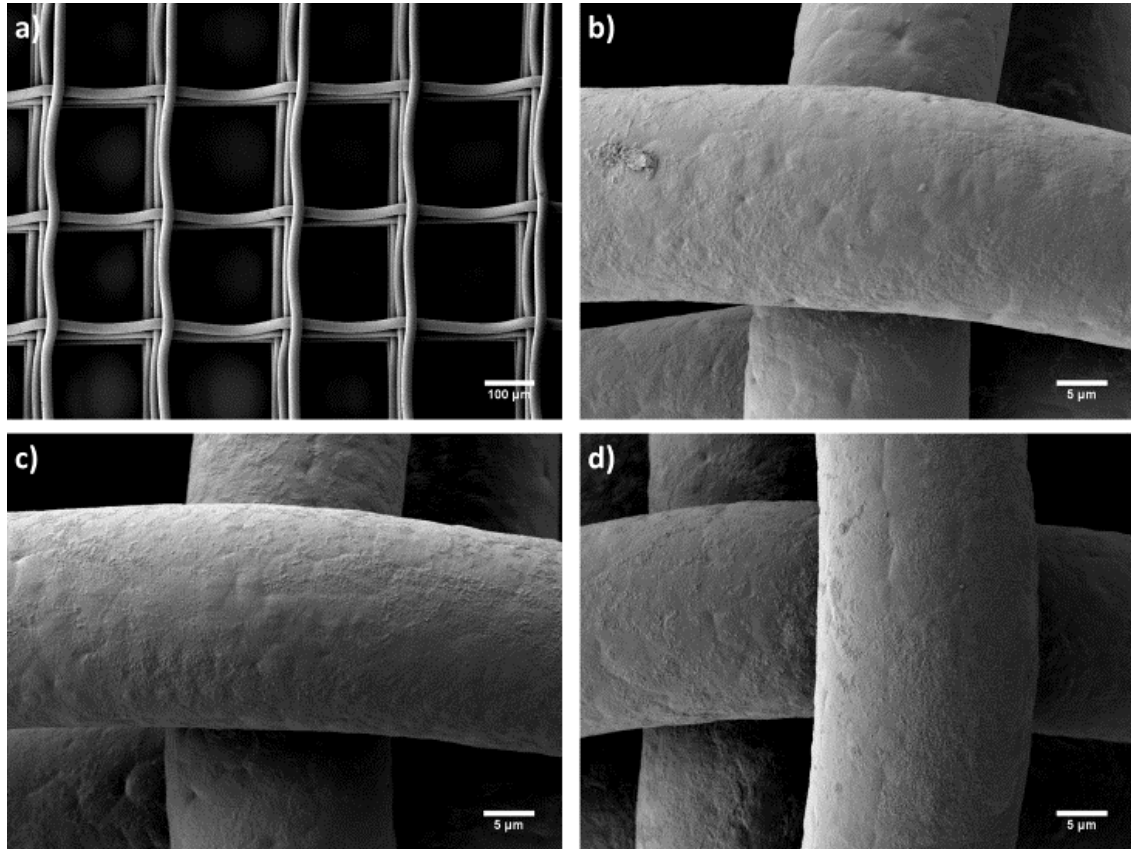
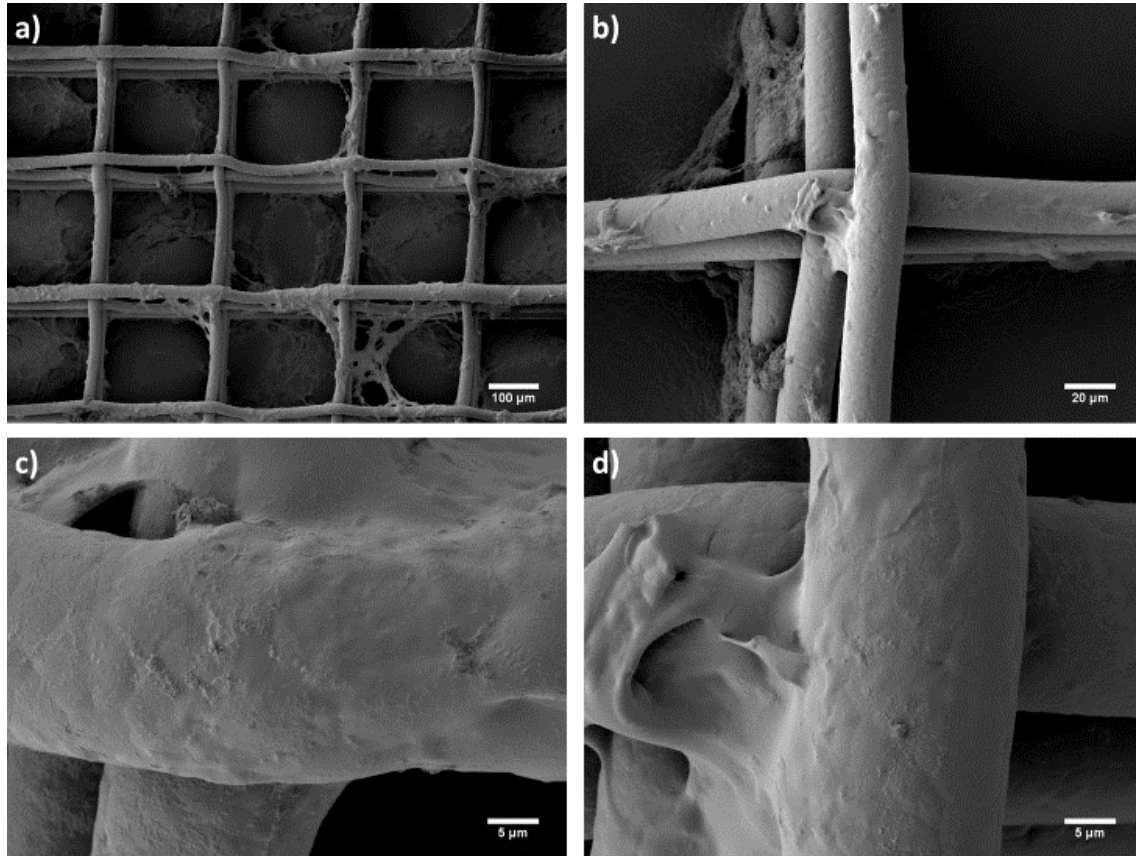*Figure 22: Group 4b(i) pH 7, (Group 4b: Different pH values of 2-AEP solutions; page 26); magnifications: a) 100x, b), c), d) 2000x*

Group 4b(ii) is represented by Figure 23. Fibers of all samples were laminated with a hydrogel that stretches at fiber intersections. Sample 2 (c, d) and 3 (e, f) also showed a CaP coating which appeared to be layered on top of the hydrogel. The CaP coating was thinner than in group 1. Patches of fiber-surface that were not coated with CaP were found on S 2 and S 3. Spherical CaP deposits often accumulated to give racemose objects. The crystal's structure appeared coralline and less dense than in group 1.
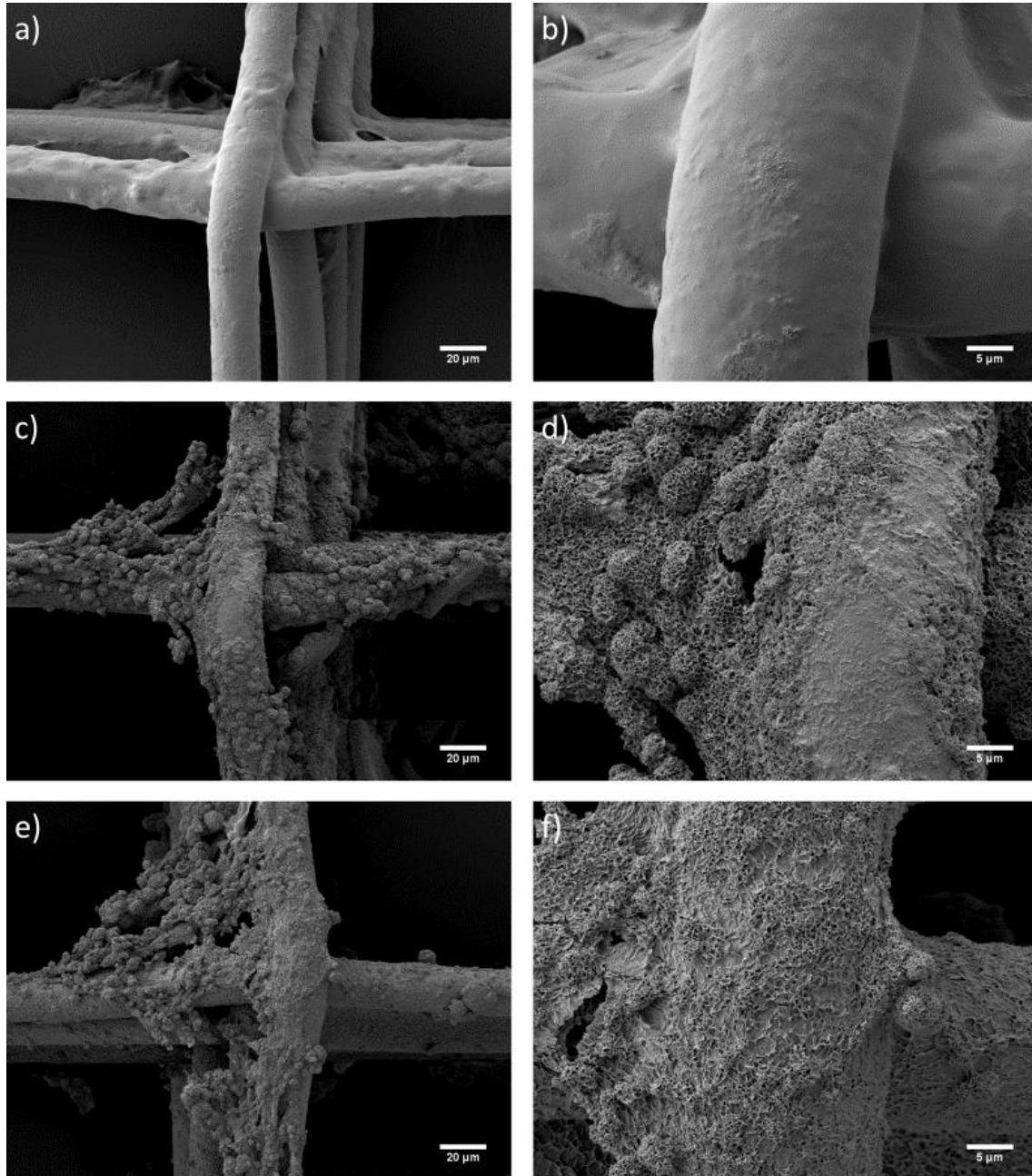
Figure 23: Group 4b(ii) pH 7.5, (Group 4b: Different pH values of 2-AEP solutions; page 26); sample 1: a) 500x, b) 2000x; sample 2: c) 500x, d) 2000x; sample 3: e) 500x, f) 2000x

Finally, Figure 24 displays SEM images from group 4b(iii). Scaffolds already showed macroscopic signs of hydrogel formation. SEM investigation confirmed this. PCL fibers are laminated with hydrogel. Strands of this hydrogel span between two sets of stacked fibers across the entire box size. Coating thickness appears to be variable as signs of untreated fiber patterns can be seen in c) and d). CaP deposits of variable sizes were found on all samples.

Figure 24: Group 4b(iii) pH 8.1, (Group 4b: Different pH values of 2-AEP solutions; page 26); magnifications: a) 100x, b) 500x, c), d) 2000x

3.4.3 Group 4c: Reduced dissolving and incubation time

For group 4c, sPEG was only allowed to dissolve for 2.5 minutes. Also, scaffolds were only incubated in sPEG-2-AEP solution for 3 minutes. sPEG and 2-AEP were weighed to give a molar ratio of 1:2. In all other aspects, the samples were treated as in group 4a.

Figure 25 shows representable pictures from group 4c. The samples appeared almost entirely sprinkled with very small crystal structures as can be seen in b). A thicker crystal structure was found in fragments (c-f). Also, crystal structures in the shape of flat sheets were observed, for example stuck between two layers of fiber (e).
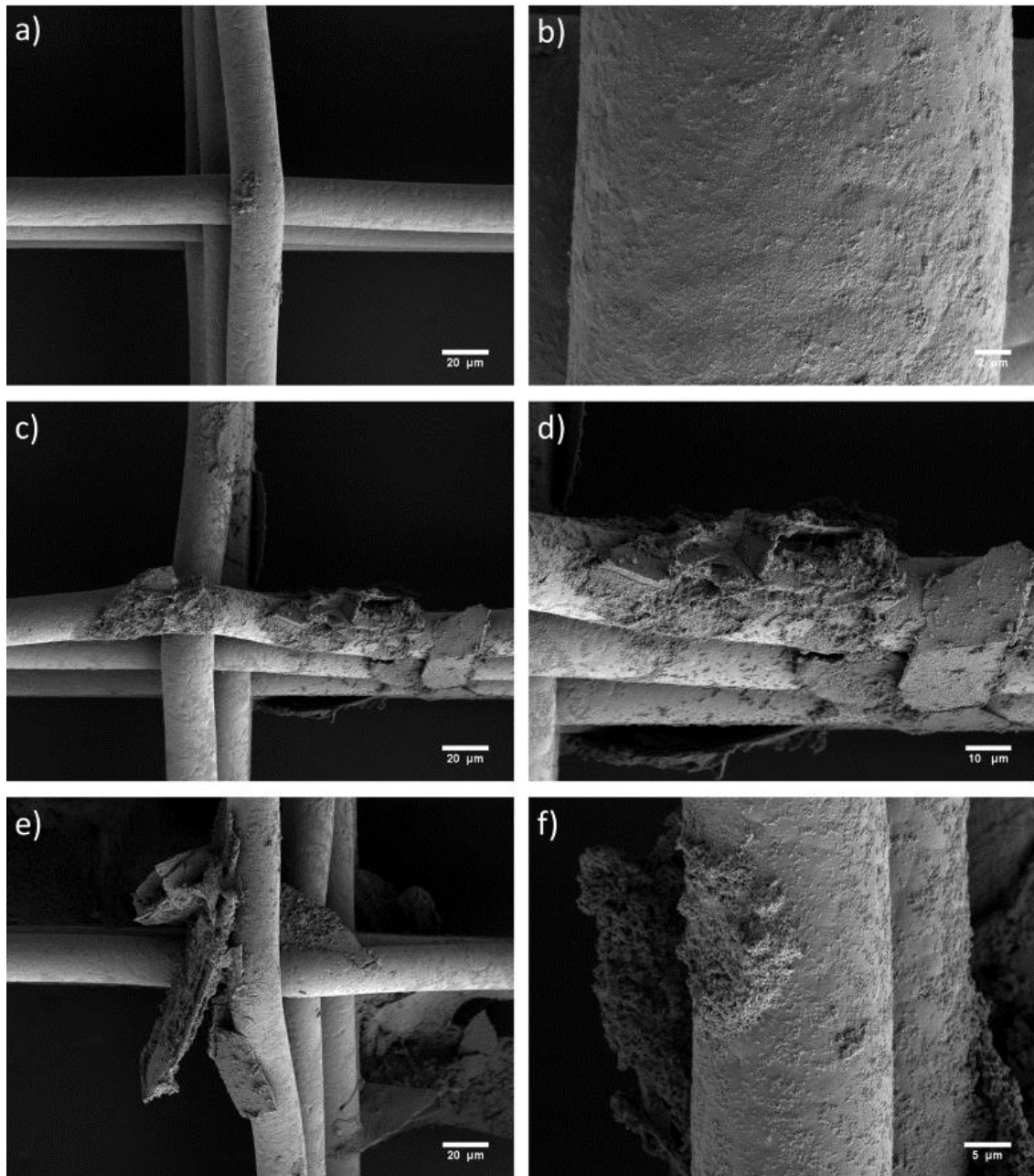
Figure 25: Group 4c (Group 4c: Reduced dissolving and incubation time; page 27); sample 1: a) 500x, b) 4000x; sample 2: c) 500x, d) 1000x; sample 3: e) 500x, f) 2000x

3.4.4 Group 4d: Samples left in water after sPEG incubation

Samples were treated as in group 4a with two differences: the dissolving time of sPEG was set to 2.5 minutes. Also, after the sPEG incubation and 2 x 30 seconds washing, the scaffolds were again put in 2 ml of water for 60 minutes.
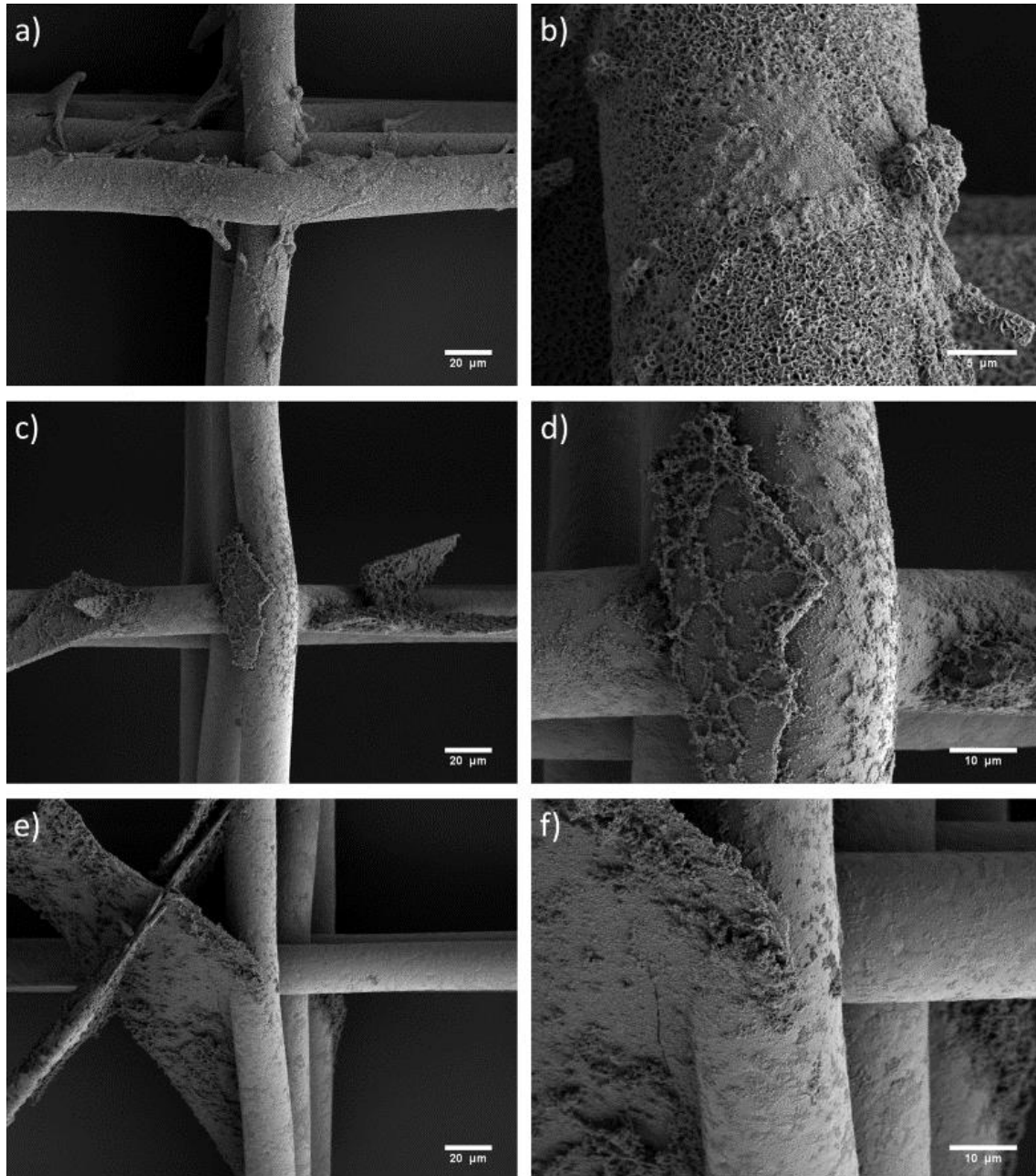

Figure 26: Group 4d (Group 4d: Samples left in water for 60 minutes after sPEG incubation; page 27); sample 1: a) 500x, b) 3000x; sample 2: c) 500x, d) 1500x; sample 3: e) 500x, f) 1500x

Pictures displaying sample 1 (Figure 26 a, b) show a completely homogenous CaP coating, which was observed among the entire scaffold

including all elevations that were not produced by PCL itself. The crystalline structure is coralline. Sample 2 (c, d) and 3 (e, f) do not show a proper coating quality. However, patchy deposits of CaP crystals were found among both scaffolds (Figure 26). Both also showed coating-fragments being present throughout the samples.

3.4.5 Group 4e: Effect of 0.5x PBS on CaP coating

Scaffolds were treated with sPEG, 2-AEP and SBF 10x as seen in the protocol from group 4a. In contrast to group 4a, 2-AEP and sPEG were dissolved in 0.5x PBS (50% PBS / 50% water). Dissolving time was reduced to 2.5 minutes. All other parameters were left untouched. The molar ratio of sPEG and 2-AEP was set 1:2.

Apart from inconsistent crystal deposits (Figure 27), sample 1 (a, b) can be classified as uncoated. Fibers of sample 3 (e, f) appear to have a basic non-crystalline, gelatinous lamination embedding tiny granular crystals which are evenly distributed. Picture e) displays shreds of the lamination at an intersection of fibers. Picture f) also shows a patch of uncoated fiber. Similar, however less homogenous, signs of this type of lamination are vaguely perceptible in sample 1 and 2.

3.4.6 Group 4f: Effect of self-made PBS on CaP coating

In this experiment scaffolds were etched, washed and then incubated with 2-AEP and sPEG. After a quick wash, SBF 10x treatment with subsequent post-treatment was performed. Unlike other groups, PBS used in group 4f was not purchased, but prepared in the lab beforehand. Dissolving time accounted for 2.5 minutes. The molar ratio of sPEG and 2-AEP was set 1:2.

Figure 28: Fibers of sample 1 (a, b) and 2 (c, d) appear to have a gelatinous coating, similar to sample 3 (e, f) of Figure 27. Patchy crystalline depositions were found superior to the coating. Sample 3 (e, f) of Figure 28 shows pictures of CaP coated fibers with small, round areas of non-lamination in patches which appear crateriform. On the contrary, half-spherical elevations can be observed on top of the basic coating. At higher magnification (f) the coating's crystalline structure
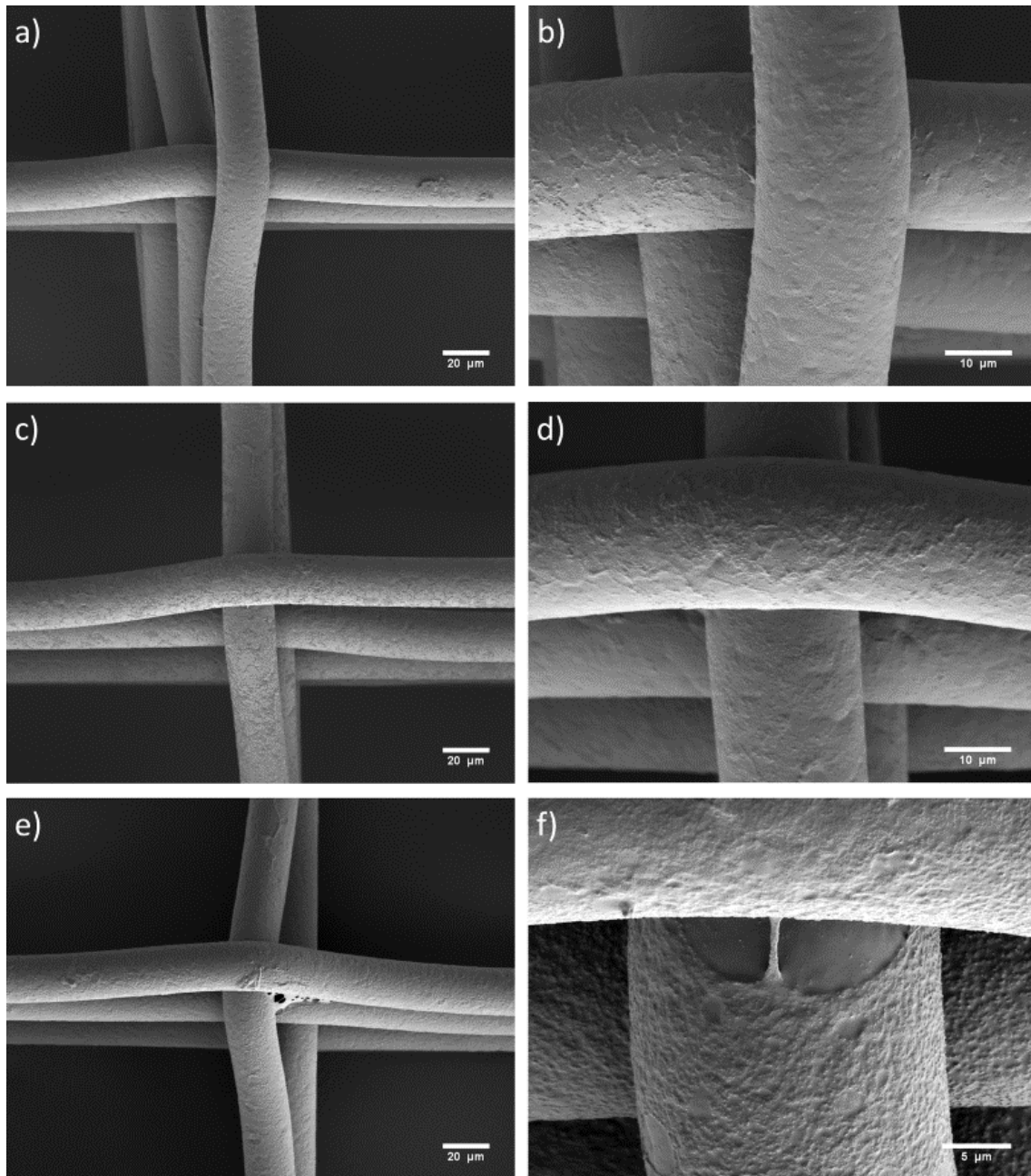
can be described as spiny-shaped.

Figure 27: Group 4e (Group 4e: Effect of 0.5x PBS on CaP coating; page 28); sample 1: a) 500x, b) 1500x; sample 2: c) 500x, d) 1500x; sample 3: e) 500x, f) 3000x
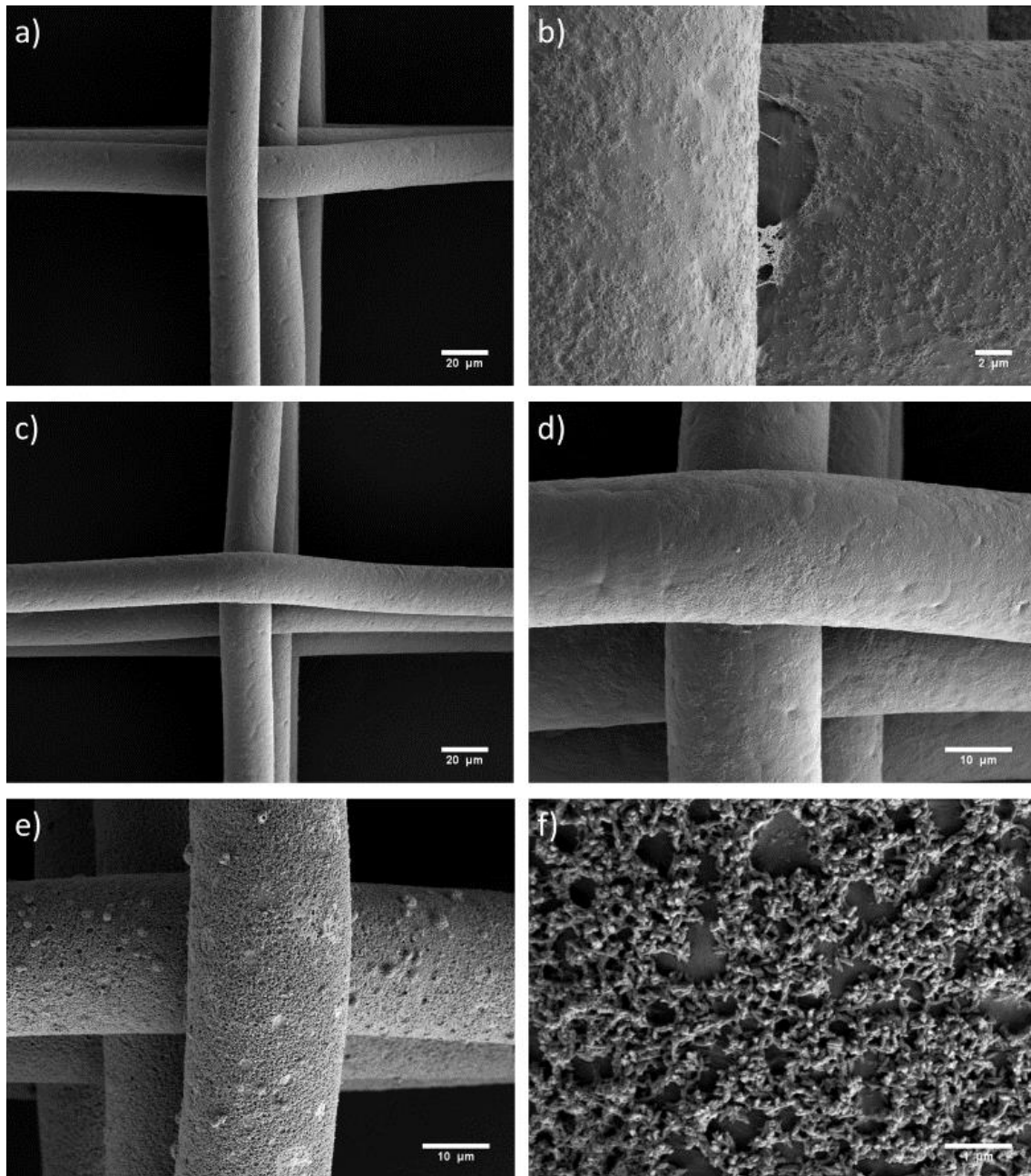
Figure 28: Group 4f (Group 4f: Effect of self-made PBS on CaP coating; page 28); sample 1: a) 500x, b) 4000x; sample 2: c) 500x, d) 1500x; sample 3: e) 500x, f) 15000x

3.5 Energy dispersive X-Ray spectroscopy

Initially, multiple samples were analyzed using EDX to provide evidence that the presented coatings actually consist of CaP. Exemplarily, Figure 29 and Figure 30 display the presence of calcium and phosphorus on coated fibers, following the coating's pattern and omitting its defect. In contrast, the defect shows presence of carbon which is not present on coated fibers. The platinum quantity is higher on coated fibers than within the defect.

When using $n = m / M_m$ to calculate the molar ratio of calcium and phosphorus, Figure 29 would give a value of 2.1, where n = moles, m = mass and M_m = molar mass. However, it can be seen in Figure 30 that lower fibers in the bottom right of the picture did not detect phosphorus, while calcium still was detected. Most other EDX measurements yielded values around 1.9 with the lowest value being 1.67.
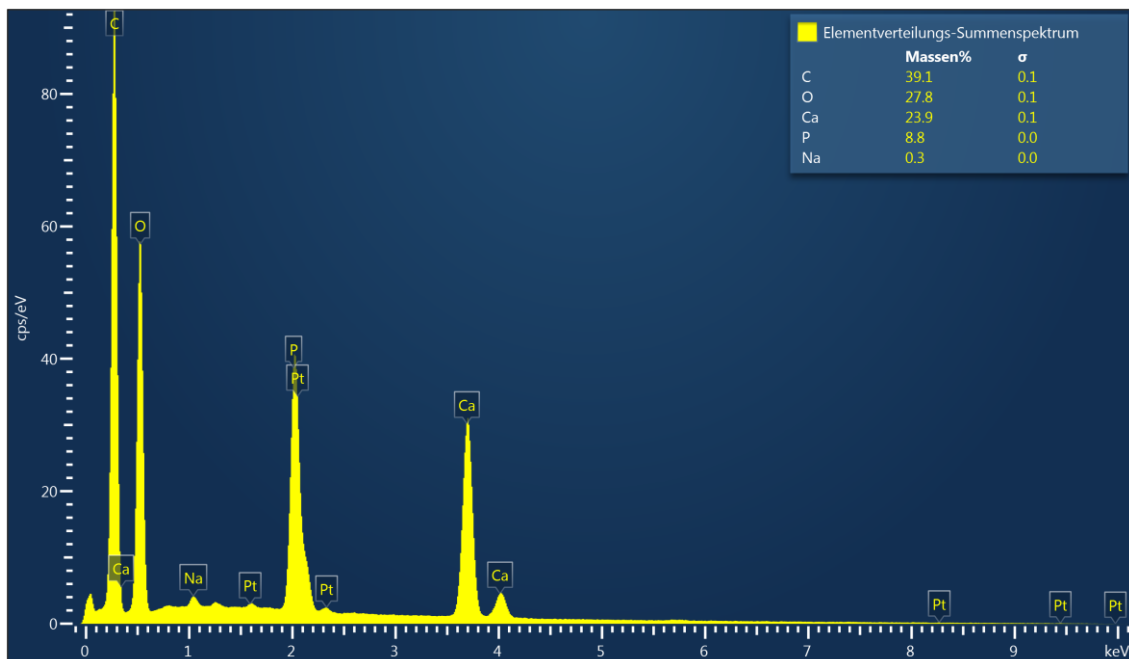

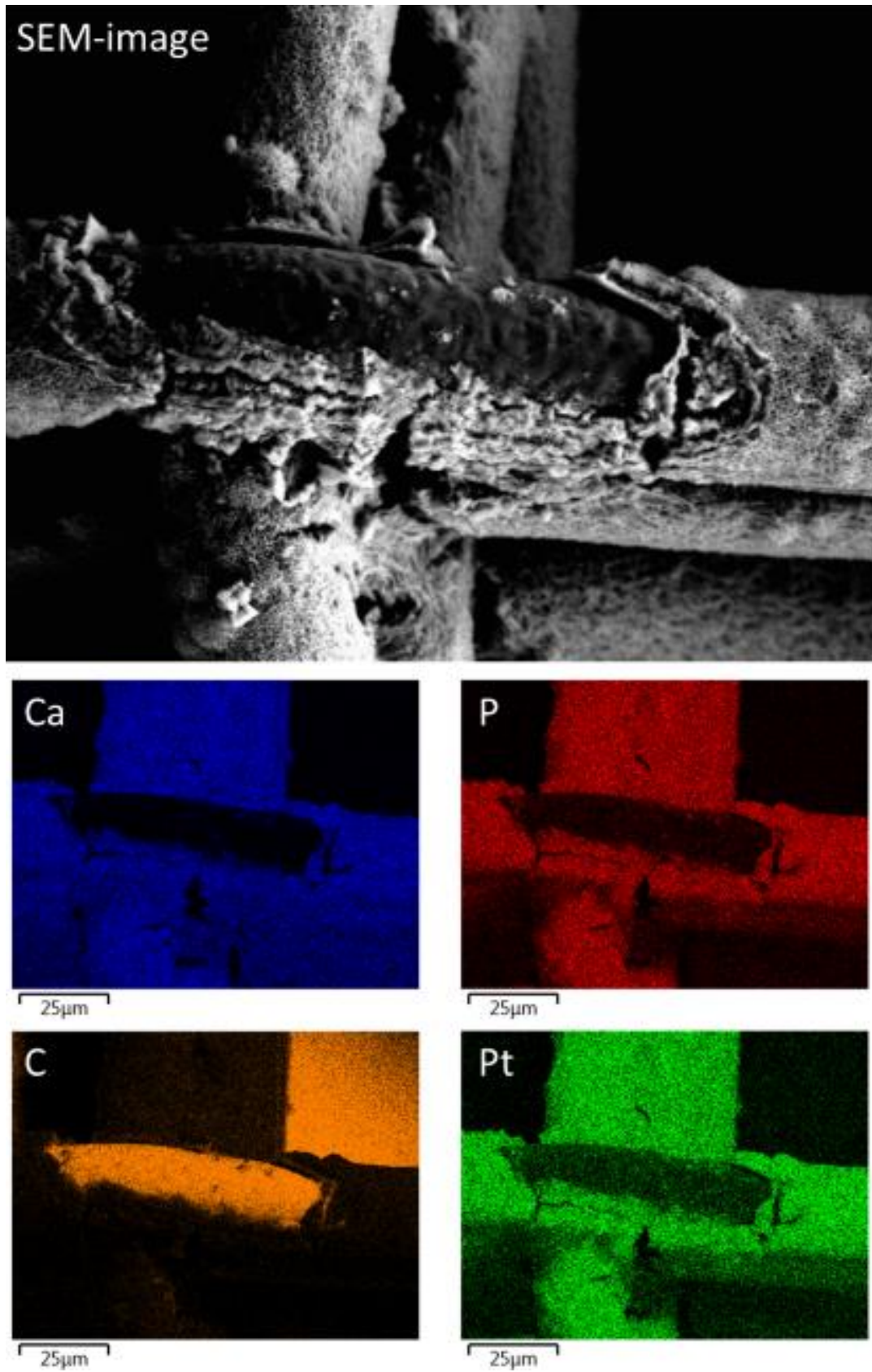*Figure 29: Total spectrum of elemental distribution relevant to Figure 30*

Figure 30: EDX-analyzation of partially fractured CaP coating: SEM image (top), analysis for Calcium (blue), Phosphorus (red), Carbon (orange) and Platinum (green)

3.6 Mechanical testing

All scaffolds were treated as described above (2.2.8 Mechanical testing; page 32) and as illustrated on pictures from Figure 4. Samples were examined afterwards. Focus was put on the comparison between before and after mechanical stress.

Figure 31 visualizes the differences before and after the test on an untreated scaffold. Pictures before the bending experiment (a, b) show fibers stacked more uniformly than afterwards. They also appear more linear and show no signs of external damage on their surface. After bending, the fibers appeared sporadically damaged. They also seem more undulating, especially the top layer.
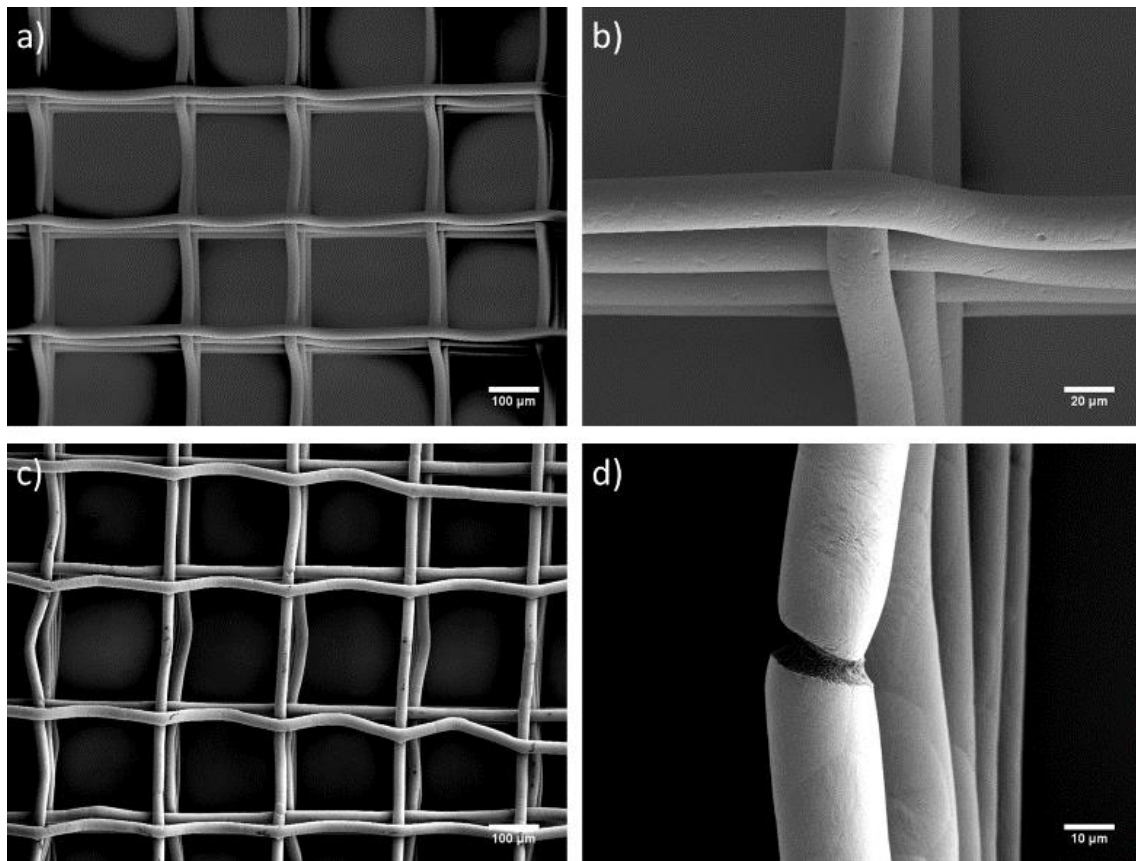
Figure 31: Untreated PCL-scaffold, mechanically stressed (2.2.8 Mechanical testing; page 32); before mechanical test: a) 100x, b) 500x; after mechanical test: c) 100x, d) 1000x

The sample from group 1a showed a homogenous CaP coating continuously traversed by cracks before stressing (Figure 32, a, b). Afterwards the stressed half of the samples was found unevenly damaged. While there were

areas that showed partially unlaminated fibers and flaked off coating fragments (c, d) there also were areas that showed less signs of damage (e). A few highly damaged bottom fibers that were out of position appeared partially coated (c).
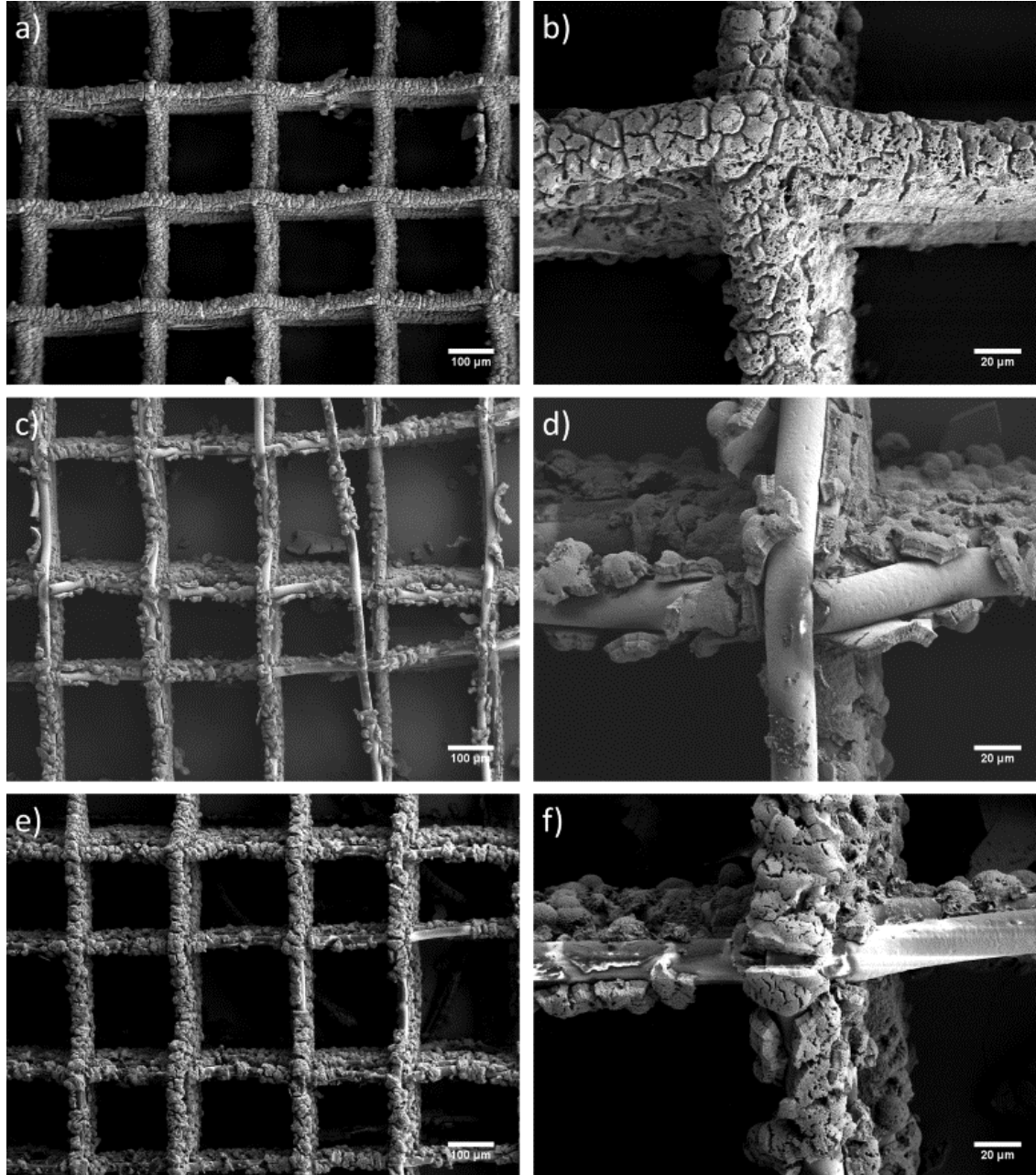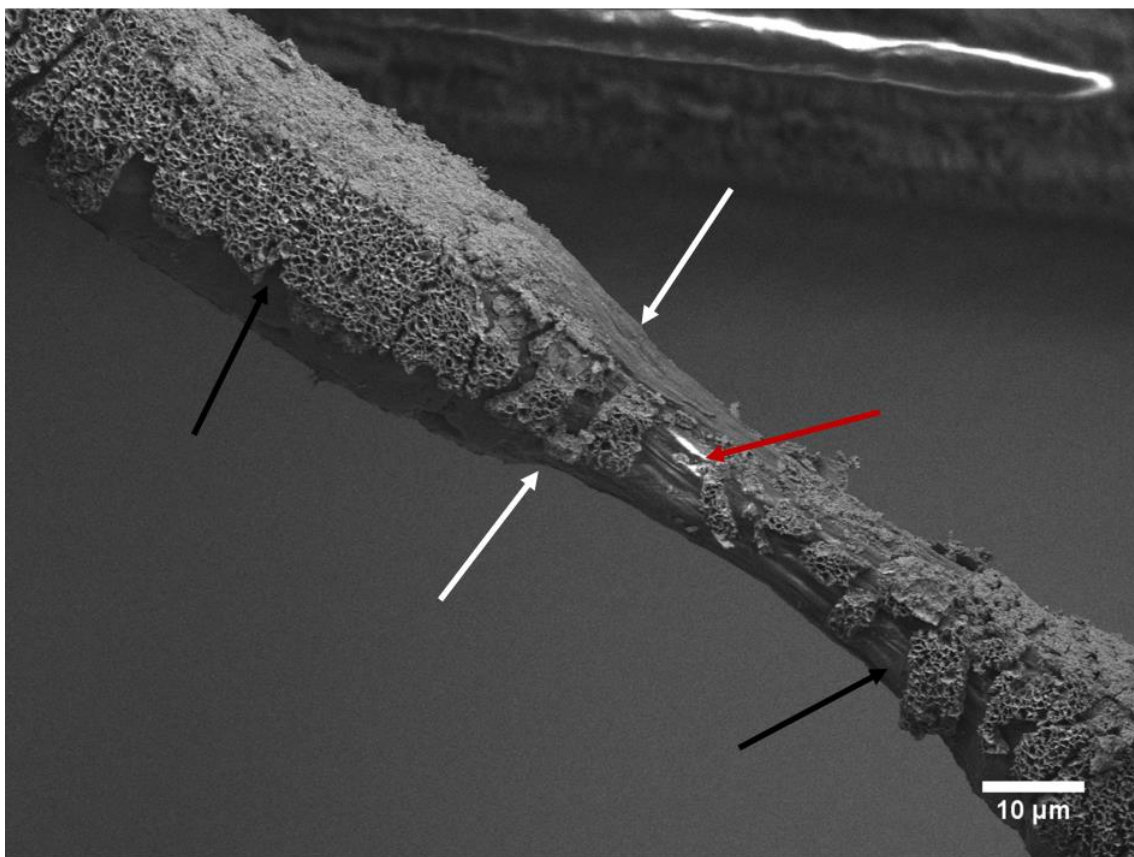

Figure 32: CaP-coated PCL-scaffold from group 1a, mechanically stressed (2.2.8 Mechanical testing; page 32); before mechanical test: a) 100x, b) 500x; after mechanical test: c) 100x, d) 500x, e) 100x, f) 500x

The sample utilizing sPEG and 2-AEP as well as SBF 10x to provide a homogenous coating is represented by Figure 33 and Figure 34. In Figure 34 a) and b) display a very even and uniformly coated scaffold before stressing. After mechanical strain (c-f), bottom fibers appeared highly damaged, out of position and partially delaminated. At higher magnifications, it was seen that the bottom fibers were highly stretched rather than being delaminated due to their visual decrease in diameter and surface appearance (e), f)). It must be stated here that it took more force to detach this sample from its mounted subsurface than for the previous two samples. Apart from the bottom fibers, the remaining sample appeared homogenously laminated with CaP. Cracks within the coating as seen in d) (Figure 34) were typically found halfway between fiber intersections all over the stressed part of the sample. Flaked off pieces of CaP coating were not found.

Figure 33: CaP coated PCL-fibers from group 4a, mechanically stressed; elongated PCL fiber partially covered with CaP; magnification: 1000x; Arrows: white: visual decrease in fiber diameter; black: fractured CaP coating due to damaged fibers still adhering to fiber's surface; red: charges due to insufficient platinum coverage
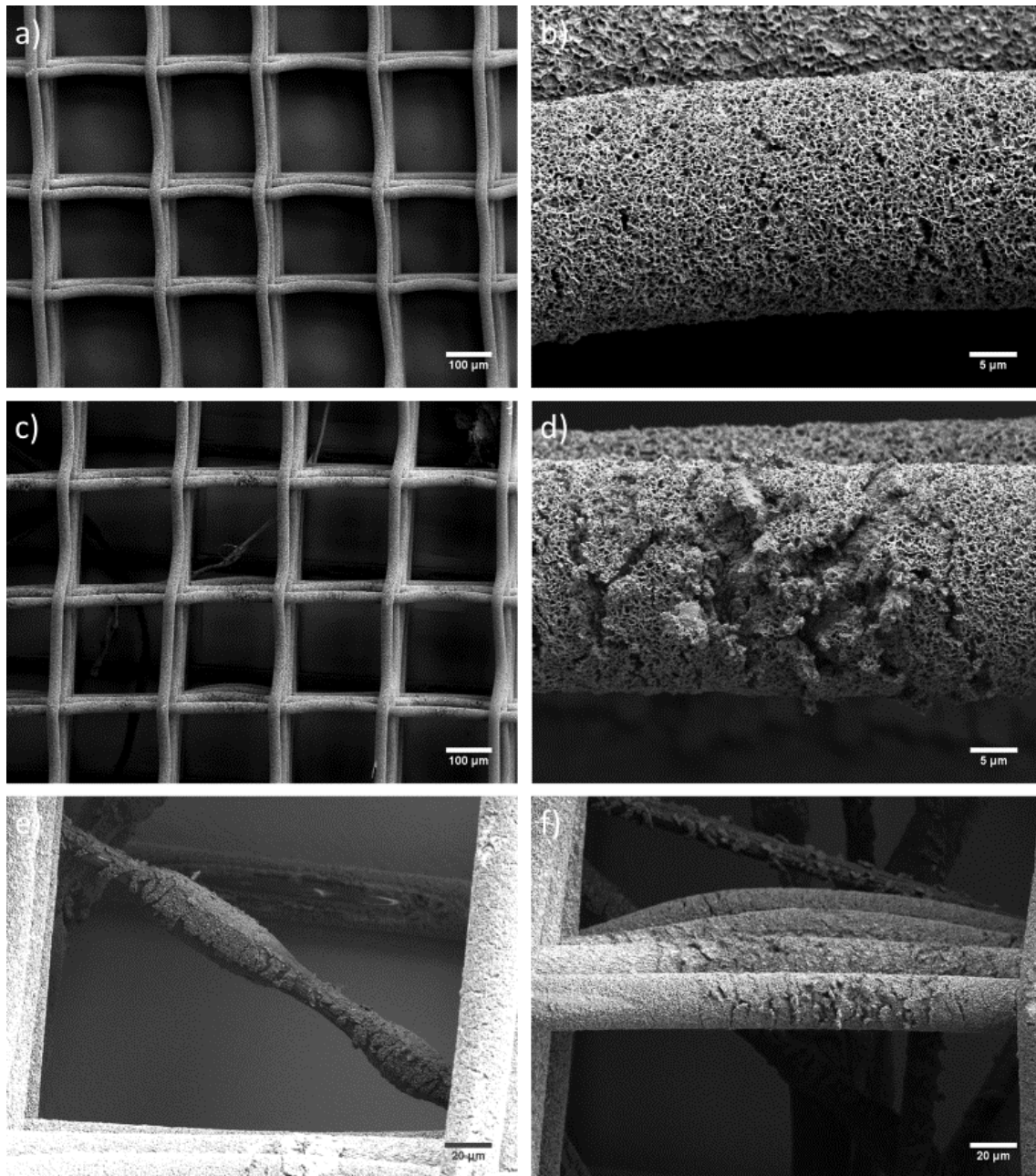
Figure 34: CaP coated PCL-scaffold from group 4a, mechanically stressed (2.2.8 Mechanical testing; page 32); before mechanical test: a) 100x, b) 2000x; after mechanical test: c) 100x, d) 2000x, e) 500x, f) 500x

4 Discussion

4.1 Biomimetic CaP coatings

Imitating the environment of the human body is an important principle of *in vitro* experiments. CaP coatings on 3D-printed PCL-scaffolds aim to mimic surface properties of the bone's trabecular network to stimulate osteogenic differentiation in multipotent cells [185, 186]. Initially, Vaquette's protocol [145] was performed to get a better experimental understanding of the SBF 10x treatment and to verify its feasibility.

Different etching parameters (group 1a-d) were tested with the purpose of further optimization. NaOH solution (2 M) was used as an etching agent to roughen and functionalize the surface of PCL-fibers by introducing hydroxyl and carboxylate groups onto PCL, which was described in the past [187, 188]. Results, however, show similar, reproducible outcomes within group 1a-d, indicating that the changes in etching duration and temperature were not significant to the experimental outcome. NaOH (0.5 M) was also used in a post-treatment step to remove highly soluble phase of di-calcium phosphate di-hydrate [145]. pH management seemed crucial for success as it enabled navigation of CaP crystal precipitation.

Furthermore, the necessity for three consecutive SBF 10x incubations was investigated in group 1e-g to try optimizing time management. Figure 9 () clearly reinforces this recommendation, as a sizable difference in coating quality can be seen between e, f and g.

4.2 Adding sPEG and 2-AEP into the equation

Although sPEG was mainly described as a substance that can provide protein non-adsorption to surfaces [121, 122], it was utilized as a chemical connector in this project. In contrast to Vaquette's protocol, molarity of NaOH and etching time were adjusted to those of the sPEG coating protocol provided by Ms Sarah Bertlein as sPEG was the first linking molecule to get in touch with PCL. Her work also confirmed the presence of sPEG on PCL-fibers utilizing fluorescent BSA which was very important for this thesis as SEM imaging did not show any

visual signs of sPEG coatings in group 2.

2-AEP should in theory act as the second linking molecule between PCL and CaP. It was chosen due to its small, simple molecular size and the two desired functional groups, amine and phosphate. In literature [189], it has already been used to bio-functionalize nano-particles.

Initially, scaffolds were incubated in sPEG and 2-AEP consecutively as described in group 3 to prove feasibility. Here, the lack of reproducibility became evident for the first time. This lack could have been partially due to the batch change of sPEG. However, this does not explain the diversity within subgroups on the same day. Also, the amounts of 2-AEP needed for these experiments were not economical as the most reproducible coating was produced with 10% 2-AEP concentrations (400 mg for 3 scaffolds) and 1 g of 2-AEP currently costs 159.50 € from Sigma-Aldrich (Germany). Hence, the need for a low-cost and more reproducible protocol is still required.

4.3 Parameter changes

For group 4, multiple parameters in the protocol were altered, mainly the fact that scaffolds were simultaneously incubated with sPEG and 2-AEP. This is due to the chemical properties of 2-AEP. It not only acts as a zwitterion (Figure 35) but also provides acidic conditions in aqueous solution causing its amine group to become protonated to give a quaternary ammonium cation (NH_3^+). These, however, are far less reactive than the original amine groups and would not easily react with the sPEG's isocyanate groups. Therefore, pH management became crucial in group 4 especially since group 4b) revealed an undesired hydrogel formation of sPEG in PBS at pH 7.5 and pH 8.1. Hence, the desired pH should be high enough to encourage the phosphoric acid group to become deprotonated at a sufficient rate but also low enough so that no hydrogel would form.
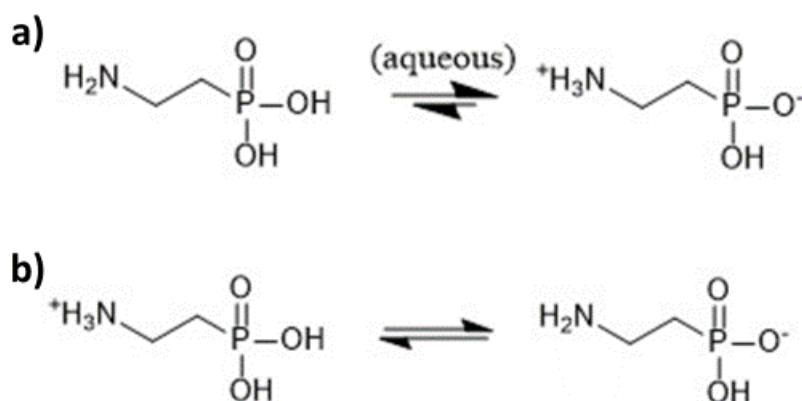
Figure 35: Zwitterion nature of 2-AEP; a) shows the zwitterion (right) which is only enabled when dissolved in aqueous solution; b) shows polarity changes in acidic (left) and basic (right) pH conditions

Another parameter that has changed was the use of PBS as a solvent. PBS's most important property was its buffer capacity, which not only partially buffers the acidic properties of 2-AEP but also enables more control over the pH value. Results of group 4a) show that coatings that utilized PBS as a solvent were superior for sPEG to 2-AEP ratios of 1:1 and 1:3, while water was superior for 1:2. Ratio 1:4 revealed a hydrogel formation of the PBS group due to preheated water of the sonication device caused by another laboratory worker. Ratio 1:6 did not show significant differences between PBS and water subgroups. However, a far larger sample pool is needed to give better evaluation. Also, each subgroup of group 4a had a different pH value as the amount of 2-AEP, that was added to pH-adjusted PBS, varied.

The next parameter change was ensuring that sPEG and 2-AEP incubation in group 4 took place simultaneously rather than as a two-staged process. The reason for this was to minimize the exposure of sPEG to water, thus preventing water from reacting with its isocyanate groups, which were desired to react with 2-AEP. By dissolving sPEG in 2-AEP solution, in theory, the two reagents should have formed a complex before adding it to the PCL-scaffolds. On paper, the optimal molar ratio of sPEG to 2-AEP ratio is 1:3, since sPEG is a star-polymer with six arms. This would mean that, on average, three arms would be occupied by 2-AEP molecules and the remaining three isocyanate groups would still be able to bind onto the functionalized PCL.

Groups 4c-f attempted to resolve reproducibility issues of group 4a. It was assumed that the time of contact between water and sPEG could still have been long enough to enable a significant reaction. Hence, the dissolving time was reduced for these groups as sPEG was able to be dissolved after 2.5 minutes. Also, the effect of a reduced incubation time (group 4c) was investigated. However, it resulted in undesirable, neglectable CaP deposits. This might have been due to the reduced dissolving time, which it was assumed is not the case. Reduced incubation time or reproducibility issues were thought to have been more likely to be responsible.

In contrast, group 4d was designed to make sure that no free isocyanate groups were present on the (hypothetical) PCL-sPEG-2-AEP complex. For this reason, samples were left in water for one hour after sPEG-2-AEP incubation. Data from Ms Sarah Bertlein indicated that all isocyanate groups of sPEG had reacted after a 60-minute water incubation. Results showed a vast difference in coating quality. Hence, the reproducibility issue was not resolved.

Group 4e investigated, whether the molarity of PBS could influence the final coating outcomes, or not. It was presumed that high PBS molarity might have had a negative effect. However, results do not support this hypothesis.

Finally, group 4f was designed to rule out the possibility of a faulty PBS compound, as it was purchased commercially. For this, PBS was produced in the lab following a standard protocol. Although one sample showed a homogenous coating, the other two showed far less satisfying results.

The aim of this thesis was to produce a CaP-coating which would be more resistant to flaking off and delamination than current standards. Initially, it was planned to produce such coatings and then compare them to the ones treated with Vaquette's protocol only (group 1) using a standardized mechanical test. Since it was not possible to ensure reproducibility, it would have not been clear whether a coating was initially present on the sample before stressing it, or not. Therefore, a compromise was made, for it was indeed known which samples presented a homogenous CaP coating after SEM analysis. Figure 34 (3.6 Mechanical testing) shows promising results as no flakes were found. It was

assumed that delamination of bottom fibers, which were torn out of position, were due to intense pulling causing elongated fibers.

4.4 Limitations

Despite the success in producing a homogenous coating using sPEG and 2-AEP, there were still multiple assumptions being made for which no evidence was provided. Also, other problems were encountered during the investigations.

First, it has to be pointed out that this thesis heavily focuses on sample quality rather than quantity, for it was a main aim to provide evidence on feasibility and show advantages of the new coating procedure. It was clear from the outset that further studies, utilizing larger sample pools, are needed in the future. However, the optimization of the protocol should be a priority before moving forward.

As already mentioned above, some surfaces that did not develop a CaP coating contrasted with many that did, and was a significant challenge during the investigations. The chemical interactions of sPEG, 2-AEP, PBS and SBF 10x seem to be a very sensitive environment regarding variances in coating quality as scaffolds, treated according to Vaquette's protocol only, did in fact show good reproducibility. Future work will have to focus on getting control over this with an expansion of possible parameter changes, and should be performed by a chemist. For instance, higher etching time, temperature or molarity of NaOH were not investigated. Also, the optimal pH value of 2-AEP solution could not be safely determined, although it is believed to be between 7 and 7.5.

Furthermore, the assumption of a chemical reaction between sPEG and 2-AEP during sPEG dissolvement was made. However, no evidence of the presence of 2-AEP onto PCL scaffolds was provided in this thesis. Therefore, it is still unclear whether sPEG and 2-AEP really formed a complex onto PCL or not. This question should be addressed in the future. Also, no control experiments were performed which would exclude either sPEG or 2-AEP incubation, to show that all of the here mentioned chemicals are needed for a succeeding outcome.

In the results, coralline crystals were described as mature. This adjective

has to be treated with caution as no measurements regarding crystal maturity were made, except EDX. Calcium to phosphorus ratio values obtained from EDX ranged from 1.67 to 2.1. Since hydroxyapatite is defined to have a Ca/P ratio of 1.67, it is possible that the coating's top layer presents mixed phases of CaP. Such bi- and triphasic CaP coatings have also been found to promote osteogenic differentiation and were even labeled as osteoinductive [190, 191]. This, however, is semi-correct since osteoinductivity requires the incorporation of an osteogenic agent, for example BMP-2 [192].

Once a protocol is established, which utilizes sPEG and 2-AEP to yield a reproducible, homogenous CaP coating, standardized tests can be used to determine its mechanical properties. The experiment in this thesis merely served the function to draw attention on the coating's seemingly improved properties. Also, a larger sample pool will be needed to confirm these results.

5 Conclusion

In conclusion, this thesis presents multiple protocols which have shown to produce a homogenous CaP coating onto 3D-printed PCL scaffolds using sPEG and 2-AEP. However, inconsistent results, even within groups treated with the exact same solutions, remain an issue. Also, categoric proof of either, sPEG – 2-AEP complexes on PCL fibers or the presence of covalent bonds, was not measurable using the techniques investigated. In comparison, Vaquette's protocol was revised and the resulting coatings show more reproducible outcomes on the one side, but also tends to crack and flake off on the other. Also, the necessity of three consecutive SBF 10x incubations was substantiated. Hydrogel formation of sPEG in PBS was observed due to either increase of pH (7.5 or higher) or increase of temperature during dissolvement. When comparing homogenous coatings from group 1 to the ones from group 3 and 4, a difference in coating thickness was seen. Adapting to the circumstances, a brief mechanical test was performed whose results indicated an improved adhesion of CaP to the PCL-scaffold.

All in all, this thesis is the necessary first step for establishing a new CaP coating protocol for 3D-printed PCL scaffolds providing improved coating adhesion. More investigations will be needed in the future to firstly give more evidence on the enhanced properties and then further optimize the parameters.

73

73

6 Future Recommendations

It would indeed be reasonable to invest further work into the investigation of a CaP coating protocol aided by sPEG and 2-AEP. The seemingly improved adhesion will need further evidence by the means of mechanical experiments. Since not all parameters were investigated, further steps are recommended

Future investigations by chemists could reveal a benefit of increasing etching time and temperature such as in group 1, while optimizing the chemical reactions required for modifying the surface. Apart from a potential thicker coating, it might also result in increased reproducibility. It would also be reasonable to further investigate the optimal ratio of sPEG to 2-AEP and the optimal pH value of 2-AEP solution that can be mixed with sPEG. The protocol on SBF 10x incubations should be of low priority as its effectiveness was seen in group 1. However, the findings here indicate that the CaP coating can be solidly bound to a 3D-printed PCL scaffold, so that when it is mechanically deformed, the coating is resistant to flaking.

7 Abstract

Biomimetic calcium phosphate (CaP) coatings imitate the trabecular bones surface structure and have shown to promote osteogenic differentiation in multipotent cells. The work of this thesis focused on the problem of former CaP coatings cracking and flaking off when being put on a bendable core structure like a 3D-printed poly (ε-caprolactone) (PCL) scaffold. The aim was to provide a chemical linkage between PCL and CaP using a star-shaped polymer (sPEG) and a phosphonate, 2-aminoethylphosphonic acid (2-AEP). First, a published CaP coating protocol was revised and investigated in terms of etching parameters for the PCL scaffold. Results presented reproducible thick coatings for all groups. The protocol was then broadened to include subsequent scaffold incubation in sPEG and 2-AEP solutions. Homogenous CaP coatings of decreased thickness presented themselves, proving feasibility. However, as is often found with physical CaP coating depositions, there were some irregular outcomes even during the same experimental group. A lower consumption of the chemical 2-AEP, for economic reasons, meant that the protocol was altered to simultaneously incubate scaffolds with sPEG and 2-AEP including preceding calculations for molar ratios. For ratios 1:1, 1:2 and 1:3, again a homogenous CaP coating was produced on most of the samples, although reproducibility issues maintained. However, the mechanical bending to induce surface cracking showed that the CaP did strongly bond to the sPEG/2-AEP, while the control CaP coating flaked off the surface in large pieces. This research demonstrates that chemically-bound CaP coatings resist flaking off the fiber surface. Future investigations should focus on the mechanisms of CaP crystallization, to improve reproducibility.

Biomimetische Calciumphosphat (CaP) - Beschichtungen imitieren die oberflächliche Struktur des spongiösen Knochens und wirkten sich bereits begünstigend auf die osteogene Differenzierung von multipotenten Zellen aus. Diese Dissertation konzentriert sich auf das Problem des Reißens und Abplatzens bisheriger CaP-Beschichtungen, wenn diese sich auf einem biegsamen Kern-Gerüst, wie einem 3D-gedruckten Polycaprolacton (PCL)-Konstrukt befanden. Das Ziel war, durch den Gebrauch eines sternförmigen Polymers (sPEG) und eines Phosphonates, 2-Aminoethylphosphonsäure (2-AEP), eine chemische Verknüpfung zwischen PCL und CaP herzustellen. Zuerst wurde ein bereits publiziertes CaP-Beschichtungs-Protokoll nachgestellt und verschiedene Ätzungsparameter untersucht. Die Ergebnisse zeigten reproduzierbare, dicke Beschichtungen in allen Gruppen. Danach wurde dieses Protokoll erweitert, indem es nun nacheinander gestellte Inkubationen in sPEG- und 2-AEP-Lösungen mit einbezog. Dünnere, homogene Beschichtungen waren das Ergebnis, was beweist, dass die Hypothese realisierbar ist. Jedoch zeigten die Ergebnisse nicht reproduzierbare Resultate. Desweiteren, war der 2-AEP Verbrauch nicht wirtschaftlich. Daher wurde das Protokoll weiterentwickelt, indem die Proben, nach vorherigen Berechnungen zu den molaren Verhältnissen, simultan mit sPEG und 2-AEP inkubiert wurden. Für die Verhältnisse 1:1, 1:2 und 1:3 wurden wiederum homogene CaP-Beschichtungen produziert. Mit der Absicht Reproduzierbarkeit zu erzielen, wurden weitere Parameter untersucht. Dies blieb jedoch erfolglos. Zuletzt wurde ein mechanischer Test durchgeführt, welcher eine verbesserte CaP-Adhäsion zu den PCL-Fasern nahelegt, wenn diese zuvor mit sPEG und 2-AEP inkubiert wurden. Zukünftige Untersuchungen werden jedoch von Nöten sein, um Daten zur Oberflächenanalyse und von weiteren mechanischen Tests bereitzustellen und um das Protokoll in Bezug auf die Reproduzierbarkeit zu verbessern.

8 References

1. Nau, C, Henrich, D, Seebach, C*, et al.* (2016) Treatment of Large Bone Defects with a Vascularized Periosteal Flap in Combination with Biodegradable Scaffold Seeded with Bone Marrow-Derived Mononuclear Cells: An Experimental Study in Rats*. Tissue Eng Part A*, **22**(1-2): 133-41.

2. Lethaus, B, Ter Laak, MP, Laeven, P*, et al.* (2011) A treatment algorithm for patients with large skull bone defects and first results*. J Craniomaxillofac Surg*, **39**(6): 435-40.

3. Zeng, JJ, Guo, P, Zhou, N*, et al.* (2016) Treatment of large bone defects with a novel biological transport disc in non-vascular transport distraction osteogenesis*. Int J Oral Surg,* **45**(5): 670-677.

4. Calori, GM, Mazza, E, Colombo, M*, et al.* (2011) The use of bone-graft substitutes in large bone defects: Any specific needs? *Injury*, **42 Suppl 2**, 56-63.

5. Schrag, C, Chang, YM, Tsai, CY*, et al.* (2006) Complete rehabilitation of the mandible following segmental resection*. J Surg Oncol*, **94**(6): 538-45.

6. Fritz, JM and Mcdonald, JR (2008) Osteomyelitis: approach to diagnosis and treatment*. Phys Sportsmed*, **36**(1): nihpa116823.

7. Lee, EA (2017) Subperiosteal Minimally Invasive Aesthetic Ridge Augmentation Technique (SMART): A New Standard for Bone Reconstruction of the Jaws*. Int J Periodontics Restorative Dent*, **37**(2): 165-173.

8. Jauhar, P, Handley, T, and Hammersley, N (2016) A Pathological Fracture of the Mandible due to Osteomyelitis following a Full Dental Clearance*. Dent Update*, **43**(2): 168-70, 173, 175.

9. Abbaszadeh, H and Sheibani, MS (2016) Actinomycotic Osteomyelitis of Mandible*. J Craniofac Surg*, **27**(5): e452-4.

10. Fritz, JM and Mcdonald, JR (2008) Osteomyelitis: Approach to Diagnosis and Treatment*. Phys Sportsmed*, **36**(1): 50-54.

11. Lew, DP and Waldvogel, FA (2004) Osteomyelitis*. Lancet*, **364**(9431): 369-79.

12. Nezafati, S, Ghavimi, MA, and Yavari, AS (2009) Localized Osteomyelitis of the Mandible Secondary to Dental Treatment: Report of a Case*. J Dent Res Dent Clin Dent Prospects*, **3**(2): 67-69.

13. Berchtold, P and Seitz, M (1996) [Immunosuppression--a tightrope walk between iatrogenic harm and therapy]*. Schweiz Med Wochenschr Suppl*, **126**(38): 1603-9.

14. Hoefert, S, Schmitz, I, Weichert, F*, et al.* (2015) Macrophages and bisphosphonate-related osteonecrosis of the jaw (BRONJ): evidence of local immunosuppression of macrophages in contrast to other infectious jaw diseases*. Clin Oral Investig,* **19**(2): 497-508.

15. Singh, S, Graham, ME, Bullock, M*, et al.* (2015) Chronic Sclerosing Osteomyelitis of the Mandible Treated with Hemimandibulectomy and Fibular Free Flap Reconstruction*. Plast Reconstr Surg Glob Open*, **3**(12): e580.

16. Agarwal, A, Kumar, N, Tyagi, A*, et al.* (2014) Primary chronic osteomyelitis in the mandible: a conservative approach*. BMJ Case Rep*, *2014*, bcr2013202448. doi:10.1136/bcr-2013-202448.

17. Welter, S, Theegarten, D, Trarbach, T*, et al.* (2011) Safety distance in the resection of colorectal lung metastases: a prospective evaluation of satellite tumor cells with immunohistochemistry*. J Thorac Cardiovasc Surg*, **141**(5): 1218-22.

18. Lewandrowski, K-U, D. Gresser, J, Wise, DL*, et al.* (2000) Bioresorbable bone graft substitutes of different osteoconductivities: a histologic evaluation of osteointegration of poly(propylene glycol-co-fumaric acid)-based cement

implants in rats. *Biomaterials*, **21**(8): 757-764.

19. Damien, CJ and Parsons, JR (1991) Bone graft and bone graft substitutes: A review of current technology and applications. *J Appl Biomater*, **2**(3): 187-208.

20. Kerwin, SC, Lewis, DD, Elkins, AD*, et al.* (1996) Deep-frozen allogeneic cancellous bone grafts in 10 dogs: a case series. *Vet Surg*, **25**(1): 18-28.

21. Giannoudis, PV, Dinopoulos, H, and Tsiridis, E (2005) Bone substitutes: an update. *Injury*, **36 Suppl 3**: 20-27.

22. Urist, MR, Silverman, BF, Buring, K*, et al.* (1967) The bone induction principle. *Clin Orthop Relat Res*, **1967**(53): 243-83.

23. Urist, MR (1965) Bone: formation by autoinduction. *Science*, **150**(3698): 893-9.

24. Legeros, RZ (2002) Properties of osteoconductive biomaterials: calcium phosphates. *Clin Orthop Relat Res*, **2002**(395): 81-98.

25. Kim, H, Camata, RP, Vohra, YK*, et al.* (2005) Control of phase composition in hydroxyapatite/tetracalcium phosphate biphasic thin coatings for biomedical applications. *J Mater Sci Mater Med*, **16**(10): 961-6.

26. Saju, KK, Reshmi, R, Jayadas, NH*, et al.* (2009) Polycrystalline coating of hydroxyapatite on TiAl6V4 implant material grown at lower substrate temperatures by hydrothermal annealing after pulsed laser deposition. *Proc Inst Mech Eng H*, **223**(8): 1049-57.

27. Ghaffari, M, Moztarzadeh, F, Sepahvandi, A*, et al.* (2013) How bone marrow-derived human mesenchymal stem cells respond to poorly crystalline apatite coated orthopedic and dental titanium implants. *Ceram Int*, **39**(7): 7793-7802.

28. Silva, MA, Gomes, PS, Vila, M*, et al.* (2010) New titanium and titanium/hydroxyapatite coatings on ultra-high-molecular-weight polyethylene-in vitro osteoblastic performance. *Biomed Mater*, **5**(3): 35014.

29. Moses, O, Nemcovsky, CE, Langer, Y*, et al.* (2007) Severely resorbed mandible treated with iliac crest autogenous bone graft and dental implants: 17-year follow-up. *Int J Oral Maxillofac Implants*, **22**(6): 1017-21.

30. Leong, DJ, Oh, TJ, Benavides, E*, et al.* (2015) Comparison between sandwich bone augmentation and allogenic block graft for vertical ridge augmentation in the posterior mandible. *Implant Dent*, **24**(1): 4-12.

31. Al-Asfour, A, Andersson, L, Kamal, M*, et al.* (2013) New bone formation around xenogenic dentin grafts to rabbit tibia marrow. *Dent Traumatol*, **29**(6): 455-60.

32. Kubosch, EJ, Bernstein, A, Wolf, L*, et al.* (2016) Clinical trial and in-vitro study comparing the efficacy of treating bony lesions with allografts versus synthetic or highly-processed xenogeneic bone grafts. *BMC Musculoskelet Disord*, **17**: 77.

33. Issa, JP, Gonzaga, M, Kotake, BG*, et al.* (2016) Bone repair of critical size defects treated with autogenic, allogenic, or xenogenic bone grafts alone or in combination with rhBMP-2. *Clin Oral Implants Res*, **27**(5): 558-66.

34. Cheng, CW, Solorio, LD, and Alsberg, E (2014) Decellularized Tissue and Cell-Derived Extracellular Matrices as Scaffolds for Orthopaedic Tissue Engineering. *Biotechnol Adv*, **32**(2): 462-484.

35. Tanase, A, Colita, A, Ianosi, G*, et al.* (2016) Rare case of disseminated fusariosis in a young patient with graft vs. host disease following an allogeneic transplant. *Exp Ther Med*, **12**(4): 2078-2082.

36. Assi, MA, Pulido, JS, Peters, SG*, et al.* (2007) Graft-vs.-host disease in lung and other solid organ transplant recipients. *Clin Transplant*, **21**(1): 1-6.

37. Buck, BE, Malinin, TI, and Brown, MD (1989) Bone transplantation and human immunodeficiency virus. An estimate of risk of acquired immunodeficiency syndrome (AIDS). *Clin Orthop Relat Res*, **1989**(240): 129-36.

38. Naughton, GK, Tolbert, WR, and Grillot, TM (1995) Emerging developments in tissue engineering and cell technology. *Tissue Eng*, **1**(2): 211-9.

39. Shanbhag, S, Pandis, N, Mustafa, K*, et al.* (2016) Alveolar bone tissue

engineering in critical-size defects of experimental animal models: a systematic review and meta-analysis. *J Tissue Eng Regen Med*, **12**(1):e336-e349

40. Marsell, R and Einhorn, TA (2011) The biology of fracture healing. *Injury*, **42**(6): 551-5.

41. Epari, DR, Duda, GN, and Thompson, MS (2010) Mechanobiology of bone healing and regeneration: in vivo models. *Proc Inst Mech Eng H*, **224**(12): 1543-53.

42. Shapiro, F (1988) Cortical bone repair. The relationship of the lacunar-canalicular system and intercellular gap junctions to the repair process. *J Bone Joint Surg Am*, **70**(7): 1067-1081.

43. Dimitriou, R, Tsiridis, E, and Giannoudis, PV (2005) Current concepts of molecular aspects of bone healing. *Injury*, **36**(12): 1392-1404.

44. Gerstenfeld, LC, Alkhiary, YM, Krall, EA*, et al.* (2006) Three-dimensional Reconstruction of Fracture Callus Morphogenesis. *J Histochem Cytochem*, **54**(11): 1215-1228.

45. Wang, HL and Boyapati, L (2006) "PASS" principles for predictable bone regeneration. *Implant Dent*, **15**(1): 8-17.

46. Dahlin, C, Linde, A, Gottlow, J*, et al.* (1988) Healing of bone defects by guided tissue regeneration. *Plast Reconstr Surg*, **81**(5): 672-6.

47. Liu, J and Kerns, DG (2014) Mechanisms of guided bone regeneration: a review. *Open Dent J*, **8**: 56-65.

48. Granero-Moltó, F, Weis, JA, Miga, MI*, et al.* (2009) Regenerative Effects of Transplanted Mesenchymal Stem Cells in Fracture Healing. *Stem Cells*, **27**(8): 1887-1898.

49. Lekovic, V, Camargo, PM, Klokkevold, PR*, et al.* (1998) Preservation of alveolar bone in extraction sockets using bioabsorbable membranes. *J Periodontol*, **69**(9): 1044-9.

50. Schenk, RK, Buser, D, Hardwick, WR*, et al.* (1994) Healing pattern of bone regeneration in membrane-protected defects: a histologic study in the canine mandible. *Int J Oral Maxillofac Implants*, **9**(1): 13-29.

51. Javed, A, Chen, H, and Ghori, FY (2010) Genetic and transcriptional control of bone formation. *Oral Maxillofac Surg Clin North Am*, **22**(3): 283-93.

52. Grandin, HM, Gemperli, AC, and Dard, M (2012) Enamel matrix derivative: a review of cellular effects in vitro and a model of molecular arrangement and functioning. *Tissue Eng Part B Rev*, **18**(3): 181-202.

53. Nikkhah, M, Edalat, F, Manoucheri, S*, et al.* (2012) Engineering microscale topographies to control the cell–substrate interface. *Biomaterials*, **33**(21): 5230-5246.

54. Titushkin, IA, Shin, J, and Cho, M (2010) A new perspective for stem-cell mechanobiology: biomechanical control of stem-cell behavior and fate. *Crit Rev Biomed Eng*, **38**(5): 393-433.

55. Scaglione, S, Ilengo, C, Fato, M*, et al.* (2009) Hydroxyapatite-coated polycaprolacton wide mesh as a model of open structure for bone regeneration. *Tissue Eng Part A*, **15**(1): 155-63.

56. Vacanti, CA (2006) History of tissue engineering and a glimpse into its future. *Tissue Eng*, **12**(5): 1137-42.

57. Berthiaume, F, Maguire, TJ, and Yarmush, ML (2011) Tissue engineering and regenerative medicine: history, progress, and challenges. *Annu Rev Chem Biomol Eng*, **2**: 403-30.

58. Angammana, CJ and Jayaram, SH (2016) Fundamentals of electrospinning and processing technologies. *Particul Sci Technol*, **34**(1): 72-82.

59. Healy, K and Guldberg, R (2007) Bone tissue engineering. *J Musculoskelet Neuronal Interact*, **7**(4): 328.

60. Gomes, ME and Reis, RL (2004) Tissue Engineering: Key Elements and Some Trends. *Macromol Biosci*, **4**(8): 737-742.
61. Thomson, RC, Yaszemski, MJ, Powers, JM*, et al.* (1996) Fabrication of biodegradable polymer scaffolds to engineer trabecular bone. *J Biomater Sci Polym Ed*, **7**(1): 23-38.
62. Minuth, WW, Sittinger, M, and Kloth, S (1997) Tissue engineering: generation of differentiated artificial tissues for biomedical applications. *Cell Tissue Res*, **291**(1): 1-11.
63. Zadpoor, AA (2015) Bone tissue regeneration: the role of scaffold geometry. *Biomater Sci*, **3**(2): 231-45.
64. Joly, P, Duda, GN, Schone, M*, et al.* (2013) Geometry-driven cell organization determines tissue growths in scaffold pores: consequences for fibronectin organization. *PLoS One*, **8**(9): e73545.
65. Costa, PF, Vaquette, C, Zhang, Q*, et al.* (2014) Advanced tissue engineering scaffold design for regeneration of the complex hierarchical periodontal structure. *J Clin Periodontol*, **41**(3): 283-94.
66. Holzapfel, BM, Hutmacher, DW, Nowlan, B*, et al.* (2015) Tissue engineered humanized bone supports human hematopoiesis in vivo. *Biomaterials*, **61**: 103-14.
67. Jank, BJ, Xiong, L, Moser, PT*, et al.* (2015) Engineered composite tissue as a bioartificial limb graft. *Biomaterials*, **61**: 246-256.
68. Takahashi, K and Yamanaka, S (2006) Induction of pluripotent stem cells from mouse embryonic and adult fibroblast cultures by defined factors. *Cell*, **126**(4): 663-76.
69. Wobma, H and Vunjak-Novakovic, G (2016) Tissue Engineering and Regenerative Medicine 2015: A Year in Review. *Tissue Eng Part B Rev*, **22**(2): 101-13.
70. Zacharias, DG, Nelson, TJ, Mueller, PS*, et al.* (2011) The science and ethics of induced pluripotency: what will become of embryonic stem cells? *Mayo Clin Proc*, **86**(7): 634-40.
71. Narsinh, KH, Plews, J, and Wu, JC (2011) Comparison of Human Induced Pluripotent and Embryonic Stem Cells: Fraternal or Identical Twins? *Mol Ther*, **19**(4): 635-638.
72. Sheikh, Z, Qureshi, J, Alshahrani, AM*, et al.* (2016) Collagen based barrier membranes for periodontal guided bone regeneration applications. *Odontology*, **105**(1): 1-12.
73. Vaquette, C and Cooper-White, JJ (2011) Increasing electrospun scaffold pore size with tailored collectors for improved cell penetration. *Acta Biomater*, **7**(6): 2544-2557.
74. Brown, TD, Dalton, PD, and Hutmacher, DW (2016) Melt electrospinning today: An opportune time for an emerging polymer process. *Prog Polym Sci,* **56**: 116-166.
75. Hartman, RPA, Brunner, DJ, Camelot, DMA*, et al.* (1999) Electrohydrodynamic atomization in the cone-jet mode physical modeling of the liquid cone and jet. *J Aerosol Sci*, **30**(7): 823-849.
76. Brown, TD, Daltona, PD, and Hutmacher, DW (2016) Melt electrospinning today: An opportune time for an emerging polymer process. *Prog Polym Sci*, **56**: 116-166.
77. Li, D and Xia, YN (2004) Electrospinning of nanofibers: Reinventing the wheel? *Adv Mater*, **16**(14): 1151-1170.
78. Hutmacher, DW and Dalton, PD (2011) Melt electrospinning. *Chem Asian J*, **6**(1): 44-56.
79. Wei, C and Dong, JY (2013) Direct fabrication of high-resolution three-

dimensional polymeric scaffolds using electrohydrodynamic hot jet plotting. *J Micromech Microeng*, **23**(2) 025017.

80. Dalton, PD, Grafahrend, D, Klinkhammer, K*, et al.* (2007) Electrospinning of polymer melts: Phenomenological observations. *Polymer*, **48**(23): 6823-6833.

81. Brown, TD, Dalton, PD, and Hutmacher, DW (2011) Direct writing by way of melt electrospinning. *Adv Mater*, **23**(47): 5651-5657.

82. Brown, TD, Slotosch, A, Thibaudeau, L*, et al.* (2012) Design and fabrication of tubular scaffolds via direct writing in a melt electrospinning mode. *Biointerphases*, **7**(1-4): 13.

83. Ogata, N, Yamaguchi, S, Shimada, N*, et al.* (2007) Poly(lactide) nanofibers produced by a melt-electrospinning system with a laser melting device. *J Appl Polym Sci*, **104**(3): 1640-1645.

84. Tian, S, Ogata, N, Shimada, N*, et al.* (2009) Melt Electrospinning from Poly(L-lactide) Rods Coated with Poly(ethylene-co-vinyl alcohol). *J Appl Polym Sci*, **113**(2): 1282-1288.

85. Muerza-Cascante, ML, Haylock, D, Hutmacher, DW*, et al.* (2015) Melt electrospinning and its technologization in tissue engineering. *Tissue Eng Part B Rev*, **21**(2): 187-202.

86. Park, SJ, Lee, BK, Na, MH*, et al.* (2013) Melt-spun shaped fibers with enhanced surface effects: fiber fabrication, characterization and application to woven scaffolds. *Acta Biomater*, **9**(8): 7719-26.

87. Lyons, J, Li, C, and Ko, F (2004) Melt-electrospinning part I: processing parameters and geometric properties. *Polymer*, **45**(22): 7597-7603.

88. Zhou, HJ, Green, TB, and Joo, YL (2006) The thermal effects on electrospinning of polylactic acid melts. *Polymer*, **47**(21): 7497-7505.

89. Huang, C, Niu, HT, Wu, JL*, et al.* (2012) Needleless Electrospinning of Polystyrene Fibers with an Oriented Surface Line Texture. *J Nanomater,* **2012**: 473872.

90. Niu, HT and Lin, T (2012) Fiber Generators in Needleless Electrospinning. *J Nanomater,* **2012**: 725950.

91. Zhou, FL, Gong, RH, and Porat, I (2009) Mass production of nanofibre assemblies by electrostatic spinning. *Polym Int*, **58**(4): 331-342.

92. Niu, HT, Wang, XG, and Lin, T (2012) Upward Needleless Electrospinning of Nanofibers. *J Eng Fiber Fabr*, **7**: 17-22.

93. Lowery, JL, Datta, N, and Rutledge, GC (2010) Effect of fiber diameter, pore size and seeding method on growth of human dermal fibroblasts in electrospun poly(epsilon-caprolactone) fibrous mats. *Biomaterials*, **31**(3): 491-504.

94. Venugopal, J, Low, S, Choon, AT*, et al.* (2008) Interaction of cells and nanofiber scaffolds in tissue engineering. *J Biomed Mater Res B Appl Biomater*, **84**(1): 34-48.

95. Szot, CS, Buchanan, CF, Gatenholm, P*, et al.* (2011) Investigation of cancer cell behavior on nanofibrous scaffolds. *Mater Sci Eng C Mater Biol Appl*, **31**(1): 37-42.

96. Hakkarainen, M and Albertsson, A-C (2002) Heterogeneous biodegradation of polycaprolactone – low molecular weight products and surface changes. *Macromol Chem Phys*, **203**(10-11): 1357-1363.

97. Balmayor, ER, Tuzlakoglu, K, Azevedo, HS*, et al.* (2009) Preparation and characterization of starch-poly-ε-caprolactone microparticles incorporating bioactive agents for drug delivery and tissue engineering applications. *Acta Biomater*, **5**(4): 1035-1045.

98. Sankavarapu, V and Aukunuru, J (2010) Development and evaluation of zero order sustained release matrix type transdermal films of ibuprofen. *J Global Pharm Technol*, **2**(2): 51-58.

99. Kalambur, S and Rizvi, SSH (2006) Rheological behavior of starch-polycaprolactone (PCL) nanocomposite melts synthesized by reactive extrusion. *Polym Eng Sci*, **46**(5): 650-658.

100. Mundargi, RC, Srirangarajan, S, Agnihotri, SA*, et al.* (2007) Development and evaluation of novel biodegradable microspheres based on poly(d,l-lactide-co-glycolide) and poly(ε-caprolactone) for controlled delivery of doxycycline in the treatment of human periodontal pocket: In vitro and in vivo studies. *J Control Release*, **119**(1): 59-68.

101. Martina, M and Hutmacher, DW (2007) Biodegradable polymers applied in tissue engineering research: a review. *Polym Int*, **56**(2): 145-157.

102. Woodruff, MA and Hutmacher, DW (2010) The return of a forgotten polymer—Polycaprolactone in the 21st century. *Prog Polym Sci*, **35**(10): 1217-1256.

103. Abedalwafa, M, Wang, FJ, Wang, L*, et al.* (2013) Biodegradable Poly-Epsilon-Caprolactone (Pcl) for Tissue Engineering Applications: A Review. *Rev Adv Mater Sci*, **34**(2): 123-140.

104. Mikos, AG and Temenoff, JS (2000) Formation of highly porous biodegradable scaffolds for tissue engineering. *Electron J Biotechnol*, **3**: 23-24.

105. You, Y, Min, B-M, Lee, SJ*, et al.* (2005) In vitro degradation behavior of electrospun polyglycolide, polylactide, and poly(lactide-co-glycolide). *J Appl Polym Sci*, **95**(2): 193-200.

106. Sinha, VR, Bansal, K, Kaushik, R*, et al.* (2004) Poly-ε-caprolactone microspheres and nanospheres: an overview. *Int J Pharm*, **278**(1): 1-23.

107. Jenkins, MJ and Harrison, KL (2006) The effect of molecular weight on the crystallization kinetics of polycaprolactone. *Polym Adv Technol*, **17**(6): 474-478.

108. Chen, DR, Bei, JZ, and Wang, SG (2000) Polycaprolactone microparticles and their biodegradation. *Polym Degrad Stab*, **67**(3): 455-459.

109. Liu, CB, Gong, CY, Huang, MJ*, et al.* (2008) Thermoreversible gel-sol behavior of biodegradable PCL-PEG-PCL triblock copolymer in aqueous solutions. *J Biomed Mater Res B Appl Biomater*, **84**(1): 165-75.

110. Detta, N, Brown, TD, Edin, FK*, et al.* (2010) Melt electrospinning of polycaprolactone and its blends with poly(ethylene glycol). *Polym Int*, **59**(11): 1558-1562.

111. Wan, Y, Lu, X, Dalai, S*, et al.* (2009) Thermophysical properties of polycaprolactone/chitosan blend membranes. *Thermochim Acta*, **487**(1–2): 33-38.

112. Sheikh, FA, Barakat, NaM, Kanjwal, MA*, et al.* (2009) Novel self-assembled amphiphilic poly(ε-caprolactone)-grafted- poly(vinyl alcohol) nanoparticles: Hydrophobic and hydrophilic drugs carrier nanoparticles. *J Mater Sci Mater Med*, **20**(3): 821-831.

113. Chern, M-J, Yang, L-Y, Shen, Y-K*, et al.* (2013) 3D scaffold with PCL combined biomedical ceramic materials for bone tissue regeneration. *Int J Precis Eng Man*, **14**(12): 2201-2207.

114. Doustgani, A and Ahmadi, E (2015) Melt electrospinning process optimization of polylactic acid nanofibers. *J Ind Text,* **45**(4): 626-634.

115. Yoon, YI, Park, KE, Lee, SJ*, et al.* (2013) Fabrication of Microfibrous and Nano-/Microfibrous Scaffolds: Melt and Hybrid Electrospinning and Surface Modification of Poly(L-lactic acid) with Plasticizer. *BioMed Res Int*, **2013**: 309048.

116. Larrondo, L and St. John Manley, R (1981) Electrostatic fiber spinning from polymer melts. I. Experimental observations on fiber formation and properties. *J Polym Sci B Polym Phys*, **19**(6): 909-920.

117. Shimada, N, Tsutsumi, H, Nakane, K*, et al.* (2010) Poly(ethylene-co-vinyl alcohol) and Nylon 6/12 nanofibers produced by melt electrospinning system equipped with a line-like laser beam melting device. *J Appl Polym Sci*, **116**(5): 2998-3004.

118. Wang, X-F and Huang, Z-M (2009) Melt-electrospinning of PMMA. *Chin J Polym Sci*, **28**(1): 45-53.

119. Groll, J and Möller, M (2015) Star Polymers as Biofunctional Coatings. In: Kobayashi, S and Müllen, K, (editors) *Encyclopedia of Polymeric Nanomaterials*,. 2015, Springer Berlin Heidelberg: 2237-2243.

120. Harris, Z and Zalipsky, S, (1997) Poly(ethylene Glycol). *ACS Symp Ser* **680**.

121. Sofia, SJ, Premnath, V, and Merrill, EW (1998) Poly (ethylene oxide) grafted to silicon surfaces: grafting density and protein adsorption. *Macromolecules*, **31**(15): 5059-5070.

122. Szleifer, I and Carignano, MA (2000) Tethered polymer layers: phase transitions and reduction of protein adsorption. *Macromol Rapid Commun*, **21**(8): 423-448.

123. Irvine, DJ, Mayes, AM, Satija, SK*, et al.* (1998) Comparison of tethered star and linear poly(ethylene oxide) for control of biomaterials surface properties. *J Biomed Mater Res*, **40**(3): 498-509.

124. Shimizu, H, Kakimoto, Y, Nakajima, T*, et al.* (1965) Isolation and identification of 2-aminoethylphosphonic acid from bovine brain. *Nature*, **207**(5002): 1197-8.

125. Itasaka, O, Hori, T, and Sugita, M (1969) Biochemistry of shellfish lipids. XI. Incorporation of [32P]orthophosphate into ceramide ciliatine (2-aminoethylphosphonic acid) of the fresh-water mussel, Hyriopsis schlegelii. *Biochim Biophys Acta*, **176**(4): 783-8.

126. Alhadeff, JA and Daves, GD, Jr. (1970) Occurrence of 2-aminoethylphosphonic acid in human brain. *Biochemistry*, **9**(25): 4866-9.

127. De Koning, AJ (1970) Detection of 2-aminoethylphosphonic acid in the phospholipids of the crab (Cyclograpsus punctatus). *Biochim Biophys Acta*, **202**(1): 187-8.

128. Alhadeff, JA and Daves, GD, Jr. (1971) 2-Aminoethylphosphonic acid: distribution in human tissues. *Biochim Biophys Acta*, **244**(1): 211-3.

129. Czerkawski, JW (1974) Methods for determining 2-6-diaminopimelic acid and 2-aminoethylphosphonic acid in gut contents. *J Sci Food Agric*, **25**(1): 45-55.

130. Joseph, JC and Henderson, TO (1977) 2-Aminoethylphosphonic acid metabolism in the rat. *Lipids*, **12**(1): 75-84.

131. Tan, SA and Tan, LG (1989) Distribution of ciliatine (2-aminoethylphosphonic acid) and phosphonoalanine (2-amino-3-phosphonopropionic acid) in human tissues. *Clin Physiol Biochem*, **7**(6): 303-9.

132. Kafarski, P and Lejczak, B (2001) Aminophosphonic Acids of Potential Medical Importance. *Curr Med Chem Anticancer Agents*, **1**(3): 301-312.

133. Feng, B, Weng, J, Yang, BC*, et al.* (2004) Characterization of titanium surfaces with calcium and phosphate and osteoblast adhesion. *Biomaterials*, **25**(17): 3421-8.

134. Yang, S-P, Yang, C-Y, Lee, T-M*, et al.* (2012) Effects of calcium-phosphate topography on osteoblast mechanobiology determined using a cytodetacher. *Mater Sci Eng C Mater Biol Appl*, **32**(2): 254-262.

135. Massaro, C, Baker, MA, Cosentino, F*, et al.* (2001) Surface and biological evaluation of hydroxyapatite-based coatings on titanium deposited by different techniques. *J Biomed Mater Res*, **58**(6): 651-657.

136. He, J, Huang, T, Gan, L*, et al.* (2012) Collagen-infiltrated porous hydroxyapatite coating and its osteogenic properties: in vitro and in vivo study. *J Biomed Mater Res A*, **100**(7): 1706-15.

137. Meirelles, L, Arvidsson, A, Andersson, M*, et al.* (2008) Nano hydroxyapatite structures influence early bone formation. *J Biomed Mater Res A*, **87**(2): 299-307.

138. Tan, F, Naciri, M, Dowling, D*, et al.* (2012) In vitro and in vivo bioactivity of CoBlast hydroxyapatite coating and the effect of impaction on its osteoconductivity. *Biotechnol Adv*, **30**(1): 352-62.

139. Surmenev, RA, Surmeneva, MA, and Ivanova, AA (2014) Significance of calcium phosphate coatings for the enhancement of new bone osteogenesis--a review. *Acta Biomater*, **10**(2): 557-79.

140. ASTM, (2014) Standard Specification for Composition of Hydroxylapatite for Surgical Implants. *ASTM Int.* p. 10.1520/f1185-03r14.

141. Hacking, SA, Tanzer, M, Harvey, EJ*, et al.* (2002) Relative contributions of chemistry and topography to the osseointegration of hydroxyapatite coatings. *Clin Orthop Relat Res*, **2002**(405): 24-38.

142. Oyane, A, Wang, X, Sogo, Y*, et al.* (2012) Calcium phosphate composite layers for surface-mediated gene transfer. *Acta Biomater*, **8**(6): 2034-2046.

143. Kokubo, T, Kushitani, H, Sakka, S*, et al.* (1990) Solutions able to reproduce in vivo surface-structure changes in bioactive glass-ceramic A-W. *J Biomed Mater Res*, **24**(6): 721-34.

144. Yang, F, Wolke, JGC, and Jansen, JA (2008) Biomimetic calcium phosphate coating on electrospun poly (epsilon-caprolactone) scaffolds for bone tissue engineering. *Chem Eng J*, **137**(1): 154-161.

145. Vaquette, C, Ivanovski, S, Hamlet, SM*, et al.* (2013) Effect of culture conditions and calcium phosphate coating on ectopic bone formation. *Biomaterials*, **34**(22): 5538-51.

146. Hagi, TT, Enggist, L, Michel, D*, et al.* (2010) Mechanical insertion properties of calcium-phosphate implant coatings. *Clin Oral Implants Res*, **21**(11): 1214-22.

147. Hunziker, EB, Enggist, L, Küffer, A*, et al.* (2012) Osseointegration: The slow delivery of BMP-2 enhances osteoinductivity. *Bone*, **51**(1): 98-106.

148. Ciobanu, G and Ciobanu, O (2013) Investigation on the effect of collagen and vitamins on biomimetic hydroxyapatite coating formation on titanium surfaces. *Mater Sci Eng C Mater Biol Appl*, **33**(3): 1683-1688.

149. Luong, LN, Mcfalls, KM, and Kohn, DH (2009) Gene delivery via DNA incorporation within a biomimetic apatite coating. *Biomaterials*, **30**(36): 6996-7004.

150. Yu, X, Wang, L, Jiang, X*, et al.* (2012) Biomimetic CaP coating incorporated with parathyroid hormone improves the osseointegration of titanium implant. *J Mater Sci Mater Med*, **23**(9): 2177-86.

151. Zhao, L, Chu, PK, Zhang, Y*, et al.* (2009) Antibacterial coatings on titanium implants. *J Biomed Mater Res B Appl Biomater*, **91**(1): 470-80.

152. Forsgren, J, Brohede, U, Piskounova, S*, et al.* (2011) In Vivo Evaluation of Functionalized Biomimetic Hydroxyapatite for Local Delivery of Active Agents. *J Biomater Nanobiotechnol*, **2**(2): 6.

153. Kokubo, T, Kim, H-M, and Kawashita, M (2003) Novel bioactive materials with different mechanical properties. *Biomaterials*, **24**(13): 2161-2175.

154. Kawai, T, Ohtsuki, C, Kamitakahara, M*, et al.* (2004) Coating of an apatite layer on polyamide films containing sulfonic groups by a biomimetic process. *Biomaterials*, **25**(19): 4529-4534.

155. Coelho, PG, Cardaropoli, G, Suzuki, M*, et al.* (2009) Histomorphometric evaluation of a nanothickness bioceramic deposition on endosseous implants: a study in dogs. *Clin Implant Dent Relat Res*, **11**(4): 292-302.

156. Rahbek, O, Overgaard, S, Lind, M*, et al.* (2001) Sealing effect of hydroxyapatite coating on peri-implant migration of particles. An experimental study in dogs. *J Bone Joint Surg Br*, **83**(3): 441-7.

157. Habibovic, P, Barrère, F, Van Blitterswijk, CA*, et al.* (2002) Biomimetic Hydroxyapatite Coating on Metal Implants. *J Am Ceram Soc*, **85**(3): 517-522.

158. Junker, R, Dimakis, A, Thoneick, M*, et al.* (2009) Effects of implant surface coatings and composition on bone integration: a systematic review. *Clin Oral Implants Res*, **20 Suppl 4**: 185-206.

159. Cunningham, BW, Hu, N, Zorn, CM*, et al.* (2009) Bioactive titanium calcium phosphate coating for disc arthroplasty: analysis of 58 vertebral end plates after 6- to 12-month implantation*. Spine J*, **9**(10): 836-845.

160. Rad, AT, Novin, M, Solati-Hashjin, M*, et al.* (2013) The effect of crystallographic orientation of titanium substrate on the structure and bioperformance of hydroxyapatite coatings*. Colloids Surf B Biointerfaces*, **103**: 200-208.

161. Yan, Y, Wolke, JG, De Ruijter, A*, et al.* (2006) Growth behavior of rat bone marrow cells on RF magnetron sputtered hydroxyapatite and dicalcium pyrophosphate coatings*. J Biomed Mater Res A*, **78**(1): 42-9.

162. Ueda, K, Narushima, T, Goto, T*, et al.* (2007) Fabrication of calcium phosphate films for coating on titanium substrates heated up to 773 K by RF magnetron sputtering and their evaluations*. Biomed Mater*, **2**(3): 160-6.

163. Jayakumar, P and Di Silvio, L (2010) Osteoblasts in bone tissue engineering*. Proc Inst Mech Eng H*, **224**(12): 1415-40.

164. Jimbo, R, Coelho, PG, Bryington, M*, et al.* (2012) Nano hydroxyapatite-coated implants improve bone nanomechanical properties*. J Dent Res*, **91**(12): 1172-7.

165. Eom, TG, Jeon, GR, Jeong, CM*, et al.* (2012) Experimental study of bone response to hydroxyapatite coating implants: bone-implant contact and removal torque test*. Oral Surg Oral Med Oral Pathol Oral Radiol*, **114**(4): 411-8.

166. Yin, K, Wang, Z, Fan, X*, et al.* (2012) The experimental research on two-generation BLB dental implants - part I: surface modification and osseointegration*. Clin Oral Implants Res*, **23**(7): 846-52.

167. Kim, YH, Kim, JS, Joo, JH*, et al.* (2012) Is hydroxyapatite coating necessary to improve survivorship of porous-coated titanium femoral stem? *J Arthroplasty*, **27**(4): 559-63.

168. Lazarinis, S, Kärrholm, J, and Hailer, NP (2010) Increased risk of revision of acetabular cups coated with hydroxyapatite: A Swedish Hip Arthroplasty Register study involving 8,043 total hip replacements. *Acta Orthop*, **81**(1): 53-59.

169. De Wilde, EA, Jimbo, R, Wennerberg, A*, et al.* (2015) The soft tissue immunologic response to hydroxyapatite-coated transmucosal implant surfaces: a study in humans*. Clin Implant Dent Relat Res*, **17 Suppl 1**: e65-74.

170. Camazzola, D, Hammond, T, Gandhi, R*, et al.* (2009) A randomized trial of hydroxyapatite-coated femoral stems in total hip arthroplasty: a 13-year follow-up*. J Arthroplasty*, **24**(1): 33-7.

171. Lu, X and Leng, Y (2009) Comparison of the osteoblast and myoblast behavior on hydroxyapatite microgrooves*. J Biomed Mater Res B Appl Biomater*, **90**(1): 438-45.

172. Novaes, AB, Jr., De Souza, SL, De Barros, RR*, et al.* (2010) Influence of implant surfaces on osseointegration*. Braz Dent J*, **21**(6): 471-81.

173. Lu, HH, Pollack, SR, and Ducheyne, P (2000) Temporal zeta potential variations of 45S5 bioactive glass immersed in an electrolyte solution*. J Biomed Mater Res*, **51**(1): 80-7.

174. Hu, Q, Tan, Z, Liu, Y*, et al.* (2007) Effect of crystallinity of calcium phosphate nanoparticles on adhesion, proliferation, and differentiation of bone marrow mesenchymal stem cells*. J Mater Chem*, **17**(44): 4690-4698.

175. Xue, W, Liu, X, Zheng, X*, et al.* (2005) Effect of hydroxyapatite coating crystallinity on dissolution and osseointegration in vivo*. J Biomed Mater Res A*, **74**(4): 553-61.

176. Lee, JA and Lee, W-K (2013) Calcium phosphate-mediated surface modification of titanium oxide and its effects on surface potential and fibrinogen adsorption*. J Ind Eng Chem*, **19**(5): 1448-1456.

177. Cairns, ML, Meenan, BJ, Burke, GA*, et al.* (2010) Influence of surface topography on osteoblast response to fibronectin coated calcium phosphate thin films*.

Colloids and Surf B: Biointerfaces, **78**(2): 283-290.

178. Wang, X, Yu, L, Li, C*, et al.* (2003) Competitive adsorption behavior of human serum albumin and fibrinogen on titanium oxide films coated on LTI-carbon by IBED*. Colloids and Surf B: Biointerfaces*, **30**(1–2): 111-121.

179. Boyd, AR, Burke, GA, Duffy, H*, et al.* (2011) Sputter deposited bioceramic coatings: surface characterisation and initial protein adsorption studies using surface-MALDI-MS*. J Mater Sci Mater Med*, **22**(1): 71-84.

180. Radin, SR and Ducheyne, P (1992) Plasma spraying induced changes of calcium phosphate ceramic characteristics and the effect onin vitro stability*. J Mater Sci Mater Med*, **3**(1): 33-42.

181. Nguyen, HQ, Deporter, DA, Pilliar, RM*, et al.* (2004) The effect of sol–gel-formed calcium phosphate coatings on bone ingrowth and osteoconductivity of porous-surfaced Ti alloy implants*. Biomaterials*, **25**(5): 865-876.

182. Barrere, F, Snel, MME, Van Blitterswijk, CA*, et al.* (2004) Nano-scale study of the nucleation and growth of calcium phosphate coating on titanium implants*. Biomaterials*, **25**(14): 2901-2910.

183. Hochleitner, G, Youssef, A, Hrynevich, A*, et al.* (2016) Fibre pulsing during melt electrospinning writing*. BioNanoMaterials*, **17**(3-4): 159.

184. Götz, H, Beginn, U, Bartelink, CF*, et al.* (2002) Preparation of Isophorone Diisocyanate Terminated Star Polyethers*. Macromol Mater Eng*, **287**(4): 223-230.

185. Yu, HS, Jang, JH, Kim, TI*, et al.* (2009) Apatite-mineralized polycaprolactone nanofibrous web as a bone tissue regeneration substrate*. J Biomed Mater Res A* , **88**(3): 747-54.

186. Oyane, A, Uchida, M, Choong, C*, et al.* (2005) Simple surface modification of poly(epsilon-caprolactone) for apatite deposition from simulated body fluid*. Biomaterials*, **26**(15): 2407-13.

187. Lam, CXF, Teoh, SH, and Hutmacher, DW (2007) Comparison of the degradation of polycaprolactone and polycaprolactone–(β-tricalcium phosphate) scaffolds in alkaline medium*. Polym Int*, **56**(6): 718-728.

188. Lam, CX, Savalani, MM, Teoh, SH*, et al.* (2008) Dynamics of in vitro polymer degradation of polycaprolactone-based scaffolds: accelerated versus simulated physiological conditions*. Biomed Mater*, **3**(3): 034108.

189. Das, M, Mishra, D, Maiti, TK*, et al.* (2008) Bio-functionalization of magnetite nanoparticles using an aminophosphonic acid coupling agent: new, ultradispersed, iron-oxide folate nanoconjugates for cancer-specific targeting*. Nanotechnology*, **19**(41): 415101.

190. Shin, HI, Kim, KH, Kang, IK*, et al.* (2005) Successful osteoinduction by cell-macroporous biphasic HA-TCP ceramic matrix*. Key Eng Mat*, **288-289**: 245-248.

191. Ye, F, Lu, X, Lu, B*, et al.* (2007) A long-term evaluation of osteoinductive HA/β-TCP ceramics in vivo: 4.5 years study in pigs*. J Mater Sci Mater Med* , **18**(11): 2173-2178.

192. Lin, X, De Groot, K, Wang, D*, et al.* (2015) A review paper on biomimetic calcium phosphate coatings*. Open Biomed Eng J*, **9**: 56-64.

List of figures

Acknowledgements

Zuallererst möchte ich meiner Mutter und meiner Oma dafür danken, dass sie mir diese Chance überhaupt erst ermöglicht und mir immer den Rücken freigehalten haben, nicht nur während der Promotionsarbeit, sondern auch während des gesamten Studiums. Ihr habt mich stets unterstützt und wart immer zur Stelle, wenn ich euch gebraucht habe. Das ist nicht selbstverständlich und dafür möchte ich euch an dieser Stelle Danke sagen.

Furthermore, I am very grateful to Mr Moataz Youssef for his dedication to initially get me in touch with real science and for being a great advisor throughout the work of my thesis. You were always calm and collected and a reliable contact person with an open door. Thank you very much!

Of course, none of this work could have been done without the opportunity of work itself. I would like to thank my Doktorvater Paul Dalton Ph.D. for including me into his department and for this unique window of opportunity that he has provided me with. Thank you also for all the meetings we held to keep my experiments on track, they were of great help!

Special thanks are due to Ph.D. Jürgen Groll who provided us with great chemical insights during our meetings. They were very constructive and highly important for keeping us on track.

I would also very much like to send my warmest thanks to Carina Blum and Judith Friedlein who patiently spent a lot of long hours helping me with the SEM imaging.

Last but not least, I would like to thank the entire FMZ team, especially the ones around me in the office for establishing such a great family-like atmosphere. For all the lunches we had, for all the coffees we drank together. I believe that these kinds of interpersonal relationships are very important and highly beneficial for a workgroup to compensate for work and to keep motivation up high.

Curriculum Vitae

Persönliche Daten:

Name:	Jean Nicolas Behets
Geburtsdatum:	20.04.1992
Geburtsort:	Düren-Birkesdorf
Wohnort:	Nörvenich, Deutschland
Nationalität:	deutsch

Ausbildung:

2016	Abschluss des zahnmedizinischen Staatsexamens an der Julius-Maximillians Universität und Erhalt der Approbation
2011 - 2016	Absolvierung des Studiums der Zahnmedizin einschließlich 10 Fachsemester in Regelstudienzeit
2010	Abschluss des Abiturs an der Strathallan School in Forgandenny, Schottland

Würzburg den

_____

(Jean Nicolas Behets)